



**Università degli Studi del Piemonte Orientale**

**“Amedeo Avogadro”**

**Department of Health Sciences**

**PhD Course in “Food, Health and Longevity”**

**Curriculum: Food, microbiota, and disease**

**Cycle XXXV (2019-2022)**

**The Role of ICOS/OPN/ICOSL System in Wound Healing, Sepsis and  
Cancer.**

SSD: MED/04

Candidate: Ian Stoppa

Coordinator: Prof. Antonia Follenzi

Tutor: Prof. Marisa Gariglio

Correlator: Prof. Umberto Dianzani

# Index

<b>Summary</b> .....	<b>1</b>
<i>Summary (english)</i> .....	1
<i>Sommario (italiano)</i> .....	2
<i>References</i> .....	4
<b>Introduction</b> .....	<b>5</b>
<i>ICOS/OPN/ICOSL System</i> .....	5
<i>Multiple Myeloma</i> .....	6
<i>Melanoma</i> .....	6
<i>Wound Healing</i> .....	7
<i>Sepsis</i> .....	8
<i>Aim of the Thesis</i> .....	8
<i>References</i> .....	9
<b>Publications</b> .....	<b>13</b>
<i>Inducible T-cell co-stimulator (ICOS) and ICOS ligand are novel players in the multiple-myeloma microenvironment</i> .....	13
<i>Parenteral Nanoemulsions Loaded with Combined Immuno- and Chemo-Therapy for Melanoma Treatment</i> .....	25
<i>ICOSL Stimulation by ICOS-Fc Accelerates Cutaneous Wound Healing In Vivo</i> .....	43
<i>ICOS-Fc as innovative immunomodulatory approach to counteract inflammation and organ injury in sepsis</i> .....	55
<b>Conclusions</b> .....	<b>68</b>
<i>Future perspectives</i> .....	70
<i>References</i> .....	71
<i>Acknowledgements</i> .....	72

# Summary

## Summary (English)

ICOS (also known as CD278) is a T cell co-stimulatory molecule, a member of the CD28 family [1]. It was originally identified on activated T cells, but it has been recently detected also in dendritic cells and macrophages [2,3,4].

ICOS binds ICOSL (or B7h), a member of the B7 family. ICOSL is expressed by multiple cell types, such as antigen presenting cells (APC), endothelial cells, epithelial cells, fibroblasts and several types of neoplastic cells [5,6]. The interaction of ICOSL and ICOS can induce the transmission of “reverse signals” in the cell that expresses ICOSL [7]. Moreover, recent data showed that also OPN (Osteopontin) binds ICOSL using a different binding site than that used by ICOS and elicits different, often opposite, effects [8] in the immune response, tumor development, and bone metabolism. In particular, ICOSL triggering using a recombinant soluble form of ICOS (ICOS-Fc) inhibits tumor cell migration, tumor angiogenesis, and tumor growth, which are increased by OPN. Moreover, ICOS-Fc inhibits bone resorption mediated by osteoclasts, whereas OPN is involved in bone deposition.

Aim of this thesis was to assess the role of the ICOS/ICOSL interaction in tumor development, working on multiple myeloma and melanoma; and the relative role in the inflammatory and repair phases of inflammation, working in skin wound healing and sepsis.

1) Multiple myeloma was chosen because it is a bone tumor in which the ICOS/ICOSL interaction may influence both the tumor growth and the osteolytic lesions. Results show that that multiple myeloma cells express high levels of ICOSL and low levels of ICOS, and patients with multiple myeloma display increased serum levels of soluble forms of both molecules correlating with known parameters of tumor burden. Moreover, treatment of mice with ICOS-Fc loaded in biocompatible biodegradable PLGA nanoparticles inhibits the growth of myeloma cells *in vivo*, exerting a predominant anti-angiogenic effect.

2) Melanoma was chosen because previous data showed that treatment of mice with ICOS-Fc loaded on PLGA or cyclodextrin nanoparticles strongly inhibits tumor growth and metastatization, and exerts anti-angiogenic effects. Using the B16 mouse melanoma model, we investigated the possibility of using ICOS-Fc in a combination therapy where ICOS-Fc was loaded in Intralipid® nanoemulsions together with the targeted drug sorafenib, and the chemotherapeutic drug temozolomide. Results show that the combination therapy strongly inhibits the tumor growth and angiogenesis, and a key role is played by ICOS-Fc.

3) Skin wound healing was chosen because it is a physiologic process in which the inflammatory and the repair phases of inflammation can be easily monitored in mice. Results show that local treatment with ICOS-Fc improves wound healing, promotes angiogenesis, preceded by upregulation of IL-6 and VEGF expression; increases the number of fibroblasts and T cells, whereas it reduces that of neutrophils; and increases the number of M2 vs. M1 macrophages.

4) Sepsis was chosen because it is a pathologic process due to excessive and uncoordinated development of the inflammatory and the repair phase of inflammation. Results show that, in sepsis induced by cecal ligation and puncture (CLP) in mice, treatment with ICOS-Fc reduces the clinical severity score, plasma cytokines, liver injury, and kidney dysfunction.

These data suggest that ICOS-mediated triggering of ICOSL may play a key role in the repair phase of inflammation, and short circuits of this interaction may be involved in tumor development.

### **Riassunto (Italiano)**

ICOS (noto anche come CD278) è una molecola co-stimolatrice espressa dalle cellule T; è un membro della famiglia CD28 [1], originariamente identificato sulle cellule T attivate, ma recentemente rilevato anche nelle cellule dendritiche e nei macrofagi [2,3,4].

ICOS lega ICOSL (o B7h), un membro della famiglia B7. ICOSL è espresso da più tipi di cellule, come cellule presentanti l'antigene (APC), cellule endoteliali, cellule epiteliali, fibroblasti e vari tipi di cellule neoplastiche [5,6]. L'interazione tra ICOSL e ICOS può indurre la trasmissione di “segnali inversi” nella cellula che esprime ICOSL [7]. Inoltre dati recenti hanno mostrato che anche OPN (Osteopontina) lega ICOSL, utilizzando un sito di legame diverso da quello utilizzato da ICOS e inducendo effetti diversi, spesso opposti [8] sulla risposta immunitaria, sullo sviluppo dei tumori e sul metabolismo osseo. In particolare, l'attivazione di ICOSL mediata da una forma solubile ricombinante di ICOS (ICOS-Fc) inibisce la migrazione, l'angiogenesi e la crescita nei tumori, che risultano invece aumentate da OPN. Inoltre ICOS-Fc inibisce il riassorbimento osseo mediato dagli osteoclasti, mentre OPN è coinvolta nella deposizione di nuova matrice ossea.

Lo scopo di questa tesi è stato quello di valutare il ruolo dell'interazione tra ICOS/ICOSL sullo sviluppo tumorale, focalizzando l'attenzione su mieloma multiplo e melanoma; e sulle fasi

infiammatoria e riparativa dell'infiammazione, focalizzando l'attenzione sulla guarigione delle ferite cutanee e sulla sepsi.

1) Il mieloma multiplo è stato scelto perché è un tumore osseo in cui l'interazione tra ICOS/ICOSL può influenzare sia la crescita tumorale sia le lesioni osteolitiche. Abbiamo osservato che le cellule di mieloma multiplo esprimono alti livelli di ICOSL e bassi livelli di ICOS, e i pazienti con mieloma multiplo mostrano livelli sierici aumentati di forme solubili di entrambe le molecole, correlati a noti marcatori di massa tumorale. Inoltre il trattamento di topi con ICOS-Fc caricato in nanoparticelle biocompatibili e biodegradabili di PLGA inibisce la crescita delle cellule di mieloma *in vivo*, esercitando in modo predominante un effetto anti-angiogenico.

2) Il melanoma è stato scelto perché dati precedenti hanno mostrato che, nel topo, il trattamento con ICOS-Fc caricato su nanoparticelle di PLGA o ciclodestrine inibisce la crescita e la metastatizzazione del tumore ed esercita effetti anti-angiogenici. Utilizzando un modello di melanoma (B16) nel topo, abbiamo studiato la possibilità di utilizzare ICOS-Fc in una terapia di combinazione in cui ICOS-Fc è stato caricato in Intralipid® (nanoemulsioni) insieme al farmaco “mirato” sorafenib e al chemioterapico temozolomide. I risultati hanno mostrato che questa terapia di combinazione inibisce in modo sostanziale la crescita tumorale e l'angiogenesi, e che ICOS-Fc svolge un ruolo chiave.

3) La riparazione delle ferite cutanee è stata scelta perché è un processo fisiologico in cui le fasi infiammatoria e di riparazione dell'infiammazione possono essere facilmente monitorate nel topo. I risultati hanno mostrato che il trattamento locale con ICOS-Fc migliora la guarigione delle ferite, promuovendo l'angiogenesi, preceduta dall'aumento dell'espressione di IL-6 e VEGF; aumentando il numero dei fibroblasti e dei linfociti T, mentre riduce quello dei neutrofili; e aumentando il numero di macrofagi M2 rispetto ai macrofagi M1.

4) La sepsi è stata scelta perché è un processo patologico dovuto una infiammazione esagerata con scoordinamento della infiammatoria e di riparazione. I risultati hanno dimostrato che nella sepsi indotta da legatura e puntura cecale (CLP) nel topo, il trattamento con ICOS-Fc riduce la gravità clinica della malattia, le citochine plasmatiche, il danno epatico e la disfunzione renale.

Questi dati suggeriscono che l'attivazione di ICOSL mediata da ICOS può svolgere un ruolo chiave nella fase di risoluzione dell'infiammazione e che un cortocircuito funzionale di questa interazione può essere coinvolto nello sviluppo dei tumori.

## References

- 1- Aicher, A.; Hayden-Ledbetter, M.; Brady, W. A.; Pezzutto, A.; Richter, G.; Magaletti, D.; Buckwalter, S.; Ledbetter, J. A.; Clark E. A. Characterization of human inducible costimulator ligand expression and function. *J. Immunol.*, **2000**, 164, 4689-96.
- 2- Hedl, M.; Lahiri, A.; Ning, K.; Cho, J.H.; Abraham, C. Pattern recognition receptor signaling in human dendritic cells is enhanced by ICOS ligand and modulated by the Crohn's disease ICOSLG risk allele. *Immunity*, **2014**, 15;40(5):734-46.
- 3- Buonfiglio, D.; Bragardo, M.; Bonisconi, S.; Redoglia, V.; Cauda, R.; Zupo, S.; Burgio, V.L.; Wolff, H.; Franssila, K.; Gaidano, G.; Carbone, A.; Janeway, C.A. Jr; Dianzani, U. Characterization of a novel human surface molecule selectively expressed by mature thymocytes, activated T cells and subsets of T cell lymphomas. *Eur J Immunol*, **1999**, 29(9):2863-74.
- 4- Buonfiglio, D; Bragardo, M.; Redoglia, V.; Vaschetto, R.; Bottarel, F.; Bonisconi, S.; Bensi, T.; Mezzatesta, C.; Janeway C.A. Jr.; Dianzani, U. The T cell activation molecule H4 and the CD28-like molecule ICOS are identical. *Eur J Immunol*, **2000**, 30(12):3463-7.
- 5- Yoshinaga, S.K.; Whoriskey, J.S.; Khare, S.D.; Sarmiento, U.; Guo, J.; Horan, T.; Shih, G.; Zhang, M.; Coccia, M.A.; Kohno, T.; et al. T-cell co-stimulation through B7RP-1 and ICOS. *Nature* **1999**, 402, 827–832.
- 6- Sharpe, A.H.; Freeman, G.J. The B7-CD28 superfamily. *Nat. Rev. Immunol.* **2002**, 2, 116–126.
- 7- Tang, G.; Qin, Q.; Zhang, P.; Wang, G.; Liu, M.; Ding, Q.; Qin, Y.; Shen, Q. Reverse signaling using an inducible costimulator to enhance immunogenic function of dendritic cells. *Cell. Mol. Life Sci.* **2009**, 66, 3067–3080.
- 8- Raineri, D.; Dianzani, C.; Cappellano, G.; Maione, F.; Baldanzi, G.; Iacobucci, I.; Clemente, N.; Baldone, G.; Boggio, E.; Gigliotti, C.L.; et al. Osteopontin binds ICOSL promoting tumor metastasis. *Commun. Biol.* **2020**, 3, 615.

# Introduction

## *ICOS/OPN/ICOSL System*

ICOS (CD278) is a T cell co-stimulatory receptor, member of the CD28 family [1], mainly expressed on activated T-cells. ICOS binds ICOSL (CD275, also called B7h, GL50, B7H2), a member of the B7 family. ICOS triggering in T cells promotes not only the activation of effector T cells in peripheral tissues but also the development of regulatory T cells [2]. ICOSL is expressed on multiple cell types, including antigen presenting cells (APCs), activated endothelial cells (EC), epithelial cells, fibroblasts, and keratinocytes [3,4]. ICOSL triggering mediated by ICOS drives a “reverse signal” that inhibits the migration of endothelial, dendritic, and tumor cells, modulates cytokine secretion while promoting antigen cross-presentation in dendritic cells, and inhibits osteoclast differentiation and functions [5-9]. It has been recently shown that ICOSL also binds osteopontin (OPN) [10] a protein that can act both as an ECM component and a soluble cytokine involved in inflammation and angiogenesis [11,12] and known to bind several ligands, including several integrins and CD44, using different binding sites. OPN binds ICOSL using a different binding site than that used by ICOS and elicits different, often opposite, effects [10]. In particular, ICOSL triggering by ICOS inhibits tumor cell migration, tumor angiogenesis, and tumor growth, which are increased by OPN. Moreover, ICOSL triggering by ICOS inhibits bone resorption mediated by osteoclasts, whereas OPN is involved in bone deposition [10].

In the tumor microenvironment, ICOS-L is expressed by several types of immune cells, EC, and often tumor cells themselves, whereas ICOS is expressed by infiltrating T cells. It has been recently shown that the growth of established mouse melanoma is inhibited by treatment with ICOS-Fc, a recombinant water-soluble ICOS protein, when it is loaded into either biocompatible poly(lactic-co-glycolic acid) (PLGA) or cyclodextrin nanoparticles, capable to target the drug into the tumor mass [13]. The main effect of ICOS-Fc is the inhibition of tumor angiogenesis, which is accompanied by variable immuno-regulatory activities and direct effects on the tumor cells, which are mainly detectable in vitro.

### *Multiple Myeloma*

Multiple myeloma (MM) is a plasma cell neoplasia resulting from monoclonal expansion of long-lived myeloma cells in the bone marrow, leading to production of monoclonal immunoglobulins (M protein), mostly IgG or IgA. MM tends to develop from premalignant monoclonal gammopathy of undetermined significance (MGUS), possibly going through a stage known as asymptomatic smouldering multiple myeloma (SMM) [14-17]. Both MGUS and SMM do not display the end organ damage typical of MM, consisting of osteolytic lesions, anaemia, hypercalcaemia, and renal failure, which constitutes the classical CRAB clinical presentation (hyperCalcaemia, Renal failure, Anaemia, Bone disease) [17,18]. In MM, active osteolytic lesions are promoted by osteoclasts stimulated by high levels of receptor activator of nuclear factor kappa-B ligand (RANKL) expressed on the surface of myeloma cells, bone marrow stromal cells, T helper (Th) cells (mainly Th-17 cells), and soluble RANKL (sRANKL) in the serum [19,16,20]. Two aspects of the ICOS/ICOSL system are relevant for MM. First, ICOSL is expressed on OC, and ICOS-Fc inhibits RANKL-driven maturation and osteolytic activity of these cells in vitro, and the development of RANKL-induced osteoporosis in vivo [9]. Second, ICOSL is also bound by OPN, involved in bone formation. OPN is also expressed by myeloma cells where it regulates a number of functions, including adhesion to the extracellular matrix and angiogenesis. ICOS and ICOSL can also be secreted as soluble forms — namely sICOS and sICOSL — which may derive from alternative transcription of the gene, alternative splicing of the mRNA, or proteolytic cleavage of the membrane form [21,22]. Of note, the serum levels of sICOS and sICOSL are increased in some autoimmune diseases that are often associated with osteoporosis due to unbalance between bone resorption mediated by OC and bone deposition mediated by osteoblasts [23-27].

### *Melanoma*

Therapeutic options for melanoma depend upon disease staging. The surgical removal of a primary tumor is normally practiced in the case of early-stage disease (0–IIA). In stage IIB/C (tumor thickness > 2.0 mm) and stage III, adjuvant chemotherapies are practiced following surgery. Dacarbazine, the standard chemotherapy for stage IV (metastatic) melanoma up to 2011, is simply a palliative care treatment [28]. Temozolomide (TMZ) is an alternative treatment as it can reach the central nervous system (CNS) to treat brain metastases [29]. New pharmacological agents have recently been approved. Since half of the total melanomas show the V-raf murine sarcoma viral oncogene homolog B1 (BRAF) mutation, they may respond to targeted therapies with inhibitors of BRAF (vemurafenib, dabrafenib, encorafenib) and/or



mitogen-activated protein kinase (MEK) (trametinib, cobimetinib, binimetinib). Moreover, melanomas respond to immunotherapy with monoclonal antibodies that block the immune checkpoint receptors cytotoxic T-lymphocyte antigen 4 (CTLA4), such as ipilimumab, and programmed cell death protein 1 (PD1), such as pembrolizumab and nivolumab [28]. Indeed, melanoma is one of the most immunogenic tumors and its relationship with the host immune system is currently under investigation [30]. Besides immunotherapy with CTLA4 and PD1 inhibitors, it has been recently reported the efficacy of targeting the inducible T-cell co-stimulator (ICOS)/ICOS ligand (ICOSL) dyad in mouse models of melanoma [13]. Nonetheless, despite significant therapeutic advancements, malignant melanoma remains an aggressive and resistant tumor with unpredictable responses to chemotherapy, making it a major health challenge [28]. Targeted therapies are hampered by chemoresistance [31], while the response to immunotherapy strictly correlates to the tumor-mutation burden [32-34]. Therefore, a multi-pronged approach that can target melanoma proliferation, angiogenesis, and chemoresistance should be practiced, concurrently to immunotherapy, to improve therapeutic efficacy.

Combinations of drugs against melanoma can be loaded into nanoemulsions for total parenteral nutrition, namely Intralipid® 10% (IL), and have been found to be effective in an *in vivo* mouse model of melanoma [35]. Specifically, a combination of drugs targeting tumor proliferation (temozolomide), angiogenesis (bevacizumab), and mTOR (rapamycin), was loaded into IL and tested in mice. Despite the promising results obtained, a strong dependence on the rapamycin dose was observed as the relevant *in vivo* tumor inhibition was only achieved at a high dose of this drug. This poses a concern for human translation since the rationale for anti-cancer drug combinations focuses on reducing the dose of each component to prevent side effects.

### *Wound Healing*

Skin wound healing starts immediately after injury and evolves in three phases. The first one is an inflammatory phase during which platelets tend to aggregate, while inflammatory cells are recruited to the wound site. The second proliferative phase is characterized by the formation of granulation tissue and re-epithelialization due to the migration and proliferation of keratinocytes, fibroblasts, and ECs, and by ECM deposition. The last one is the so-called remodeling phase during which the regenerative process comes to an end and the wound becomes avascular and acellular, thereby allowing the reorganization of the connective tissue to promote scar formation [36,37]. The formal demonstration of a functional role of the ICOS/ICOSL pathway in wound healing comes from the observation that ICOS<sup>-/-</sup>, ICOSL<sup>-/-</sup>,

and ICOS/ICOSL<sup>-/-</sup> mice show delayed wound healing [38] likely due to decreased production of IL-6 [39]. In good agreement with a role of the ICOS/ICOSL dyad in normal tissue repair, it has been recently shown that CCl<sub>4</sub>-induced liver damage, which is dependent on massive recruitment of blood-derived monocytes/macrophages, is dramatically worsened in both ICOS<sup>-/-</sup> and ICOSL<sup>-/-</sup> mice [40]. Interestingly, this impairment has been rescued by treating mice with ICOS-Fc.

### *Sepsis*

Sepsis is a life-threatening medical emergency characterized by a complex interplay of exaggerated pro- and anti-inflammatory host responses, resulting in multiple organ dysfunction that can ultimately lead to death [41]. Currently, deaths from sepsis correspond to nearly 20% of all deaths worldwide, and there is still no specific treatment available [42]. Given the fact that both animals and septic patients have an increased percentage of circulating Treg cells [43-45], it is suggestive that ICOS triggering may play a role in the septic immunosuppressive status. On the other hand, ICOSL triggering by ICOS may exert anti-inflammatory effects via responses by modulating the maturation and migration of macrophage and dendritic cells and the endothelial cell adhesiveness [8]. Nevertheless, little is known about the ICOSL-involvement in the inflammatory response.

### *Aim of the Thesis*

Aim of this thesis was to assess the role of the ICOS/ICOSL interaction in tumor development, working on multiple myeloma and melanoma; and the relative role in the inflammatory and repair phases of inflammation, working in skin wound healing and sepsis.

1) Multiple myeloma was chosen to assess whether the ICOS/ICOSL interaction may influence the tumor growth and the osteolytic activity. Results show that multiple myeloma cells express high levels of ICOSL and low levels of ICOS, and patients with multiple myeloma display increased serum levels of soluble forms of both molecules correlating with known parameters of tumor burden. Moreover, treatment with ICOS-Fc loaded in biocompatible biodegradable PLGA nanoparticles inhibits the growth of myeloma cells in an *in vivo* model in mice, exerting a predominant anti-angiogenic effect.

2) Melanoma was chosen to assess whether the anti-tumor activity of ICOS-Fc may be exploited in combination therapies starting from the previous work using temozolomide, bevacizumab, and rapamycin loaded in intralipid nanoemulsions. Results show that Intralipid nanoemulsions

loaded with ICOS-Fc, sorafenib, and temozolomide strongly inhibits the tumor growth and angiogenesis, and a key role is played by ICOS-Fc.

3) Skin wound healing was chosen because it is a physiologic process in which inflammatory and the repair phases of inflammation can be easily followed up in mice. Results show that local treatment with ICOS-Fc improves wound healing, promotes angiogenesis, preceded by upregulation of IL-6 and VEGF expression; increases the number of fibroblasts and T cells, whereas it reduces that of neutrophils; and increases the number of M2 vs. M1 macrophages.

4) Sepsis was chosen because it is a pathologic process due to excessive and uncoordinated development of the inflammatory and the repair phase of inflammation. Results show that, in sepsis induced by cecal ligation and puncture (CLP) in mice, treatment with ICOS-Fc reduces the clinical severity score, plasma cytokines, liver injury, and kidney dysfunction.

Altogether, these data suggest that ICOS-mediated triggering of ICOSL may play a key role in the repair phase of inflammation, and short circuits of this interaction may be involved in tumor development.

## References



- 1- Aicher, A.; Hayden-Ledbetter, M.; Brady, W.A.; Pezzutto, A.; Richter, G.; Magaletti, D.; Buckwalter, S.; Ledbetter, J.A.; Clark, E.A. Characterization of human inducible costimulator ligand expression and function. *J. Immunol.* **2000**, 164, 4689–4696
- 2- Li, D.; Xiong, X. ICOS<sup>+</sup> Tregs: A Functional Subset of Tregs in Immune Diseases. *Front. Immunol.* **2020**, 11, 2104, Correction in *Front. Immunol.* **2021**, 12, 701515
- 3- Yoshinaga, S.K.; Whoriskey, J.S.; Khare, S.D.; Sarmiento, U.; Guo, J.; Horan, T.; Shih, G.; Zhang, M.; Coccia, M.A.; Kohno, T.; et al. T-cell co-stimulation through B7RP-1 and ICOS. *Nature* **1999**, 402, 827–832.
- 4- Sharpe, A.H.; Freeman, G.J. The B7-CD28 superfamily. *Nat. Rev. Immunol.* **2002**, 2, 116–126.
- 5- Tang, G.; Qin, Q.; Zhang, P.; Wang, G.; Liu, M.; Ding, Q.; Qin, Y.; Shen, Q. Reverse signaling using an inducible costimulator to enhance immunogenic function of dendritic cells. *Cell. Mol. Life Sci.* **2009**, 66, 3067–3080.
- 6- Dianzani, C.; Minelli, R.; Mesturini, R.; Chiocchetti, A.; Barrera, G.; Boscolo, S.; Sarasso, C.; Gigliotti, C.L.; Sblattero, D.; Yagi, J.; et al. B7h triggering inhibits umbilical vascular endothelial cell adhesiveness to tumor cell lines and polymorphonuclear cells. *J. Immunol.* **2010**, 185, 3970–3979.
- 7- Dianzani, C.; Minelli, R.; Gigliotti, C.L.; Occhipinti, S.; Giovarelli, M.; Conti, L.; Boggio, E.; Shivakumar, Y.; Baldanzi, G.; Malacarne, V.; et al. B7h triggering inhibits the migration of tumor cell lines. *J. Immunol.* **2014**, 192, 4921–4931.

- 8- Occhipinti, S.; Dianzani, C.; Chiocchetti, A.; Boggio, E.; Clemente, N.; Gigliotti, C.L.; Soluri, M.F.; Minelli, R.; Fantozzi, R.; Yagi, J.; et al. Triggering of B7h by the ICOS modulates maturation and migration of monocyte-derived dendritic cells. *J. Immunol.* **2013**, 190, 1125–1134.
- 9- Gigliotti, C.L.; Boggio, E.; Clemente, N.; Shivakumar, Y.; Toth, E.; Sblattero, D.; D'Amelio, P.; Isaia, G.C.; Dianzani, C.; Yagi, J.; et al. ICOS-Ligand Triggering Impairs Osteoclast Differentiation and Function In Vitro and In Vivo. *J. Immunol.* **2016**, 197, 3905–3916.
- 10- Raineri, D.; Dianzani, C.; Cappellano, G.; Maione, F.; Baldanzi, G.; Iacobucci, I.; Clemente, N.; Baldone, G.; Boggio, E.; Gigliotti, C.L.; et al. Osteopontin binds ICOSL promoting tumor metastasis. *Commun. Biol.* **2020**, 3, 615.
- 11- Weber, C.E.; Li, N.Y.; Wai, P.Y.; Kuo, P.C. Epithelial-mesenchymal transition, TGF- $\beta$ , and osteopontin in wound healing and tissue remodeling after injury. *J. Burn Care Res.* **2012**, 33, 311–318.
- 12- Mori, R.; Shaw, T.J.; Martin, P. Molecular mechanisms linking wound inflammation and fibrosis: Knockdown of osteopontin leads to rapid repair and reduced scarring. *J. Exp. Med.* **2008**, 205, 43–51.
- 13- Clemente, N.; Boggio, E.; Gigliotti, L.C.; Raineri, D.; Ferrara, B.; Miglio, G.; Argenziano, M.; Chiocchetti, A.; Cappellano, G.; Trotta, F.; et al. Immunotherapy of experimental melanoma with ICOS-Fc loaded in biocompatible and biodegradable nanoparticles. *J. Control. Release* **2020**, 320, 112–124.
- 14- Rollig, C.; Knop, S.; Bornhauser, M. Multiple multiple myeloma. *Lancet*, **2015**, 385(9983):2197–208.
- 15- Michels, T.C.; Petersen, K.E. Multiple myeloma: diagnosis and treatment. *Am Fam Physician*, **2017**, 95(6):373–83.
- 16- Terpos, E.; Christoulas, D.; Gavriatopoulou, M.; Dimopoulos, M.A. Mechanisms of bone destruction in multiple myeloma. *Eur J Cancer Care (Engl)*, **2017**, 26(6):e12761.
- 17- Tomasson, M.; Ali, M.; De Oliveira, V.; Xiao, Q.; Jethava, Y.; Zhan, F.; Fitzsimmons, A.M.; Bates, M.L. Prevention is the best treatment: the case for understanding the transition from monoclonal gammopathy of undetermined significance to myeloma. *Int J Mol Sci*, **2018**, 19(11):1–19.
- 18- Fairfield, H.; Falank, C.; Avery, L.; Reagan, M.R. Multiple myeloma in the marrow: pathogenesis and treatments. *Ann N Y Acad Sci*, **2016**, 1364(1):32–51.
- 19- Tikhonova, A.N.; Dolgalev, I.; Hu, H.; Sivaraj, K.K.; Hoxha, E.; Cuesta-Domínguez, A.; Akhmetzyanova, I.; Gao, J.; Witkowski, M.; Giullamot, M.; et al. The bone marrow microenvironment at single-cell resolution. *Nature*, **2019**, 569(7755):222–8.
- 20- Buckle, C.H.; de Leenheer, E.; Lawson, M.A. Soluble rank ligand produced by myeloma cells causes generalised bone loss in multiple myeloma. *PLoS One*, **2012**, 7(8):e41127.
- 21- Lownik, J.C.; Luker, A.J.; Damle, S.R.; Cooley, L.F.; El Sayed, R.; Hutloff, A.; Pitzalis, C.; Martin, K.R.; El Shikh, M.E.; Conrad, D.H. ADAM10-mediated ICOSL shedding on B cells is necessary for proper T cell ICOS regulation and TFH responses. *J Immunol.* **2017**, 199(7), 2305–15.
- 22- Lownik, J.C.; Wimberly, J.L.; Conrad, D.H.; Martin, R.K. B cell ADAM10 controls murine lupus progression through regulation of the ICOS:ICOSL axis. *J Immunol*, **2019**, 202(3):664–74.
- 23- Iwai, H.; Abe, M.; Hirose, S.; Tsushima, F.; Tezuka, K.; Akiba, H.; Yagita, H.; Okumura, K.; Kohosaka, H.; Miyasaka, N.; Azuma, M. Involvement of inducible costimulator-B7 homologous protein costimulatory pathway in murine lupus nephritis. *J Immunol.* **2003**, 171(6), 2848–54.

- 24- Her, M.; Kim, D.; Oh, M.; Jeong, H.; Choi, I. Increased expression of soluble inducible costimulator ligand (ICOSL) in patients with systemic lupus erythematosus. *Lupus*, **2009**, 18(6):501–7.
- 25- Yu, H.; Zou, X.; Peng, L.; Wang, Y.; Zhang, C.; Chen, B.; Zou, Y. Effect of soluble inducible costimulator level and its polymorphisms on age-related macular degeneration. *DNA Cell Biol*, **2013**, 32(12), 717–21.
- 26- Wang, D.; Zhou, D.; Du, Q.; Liang, Q.I.; Wang, Q.; Fang, L.; Wang, G.; Fan, Q.; Liu, B.; Zhou, J.; et al. Aberrant production of soluble inducible T-cell co-stimulator (sICOS) and soluble programmed cell death protein 1 (sPD-1) in patients with chronic hepatitis C. *Mol Med Rep*. **2013**, 7(4), 1197–202.
- 27- Yanaba, K.; Asano, Y.; Noda, S.; Akamata, K.; Aozasa, N.; Taniguchi, T.; Takahashi, T.; Ichimura, Y.; Toyama, T.; Sumida, H. Increased production of soluble inducible costimulator in patients with diffuse cutaneous systemic sclerosis. *Arch Dermatol Res*, **2013**, 305(1):17–23.
- 28- Battaglia, L.; Scomparin, A.; Dianzani, C.; Milla, P.; Muntoni, E.; Arpicco, S.; Cavalli, R. Nanotechnology Addressing Cutaneous Melanoma: The Italian Landscape. *Pharmaceutics* **2021**, 13, 1617.
- 29- Velho, T.R. Metastatic Melanoma—A Review of Current and Future Drugs. *Drugs Context* **2012**, 2012, 212242.
- 30- Passarelli, A.; Tucci, M.; Mannavola, F.; Felici, C.; Silvestris, F. The metabolic milieu in melanoma: Role of immune suppression by CD73/adenosine. *Tumour Biol*. **2019**, 41, 1010428319837138.
- 31- Sun, J.; Carr, M.J.; Khushalani, N.I. Principles of Targeted Therapy for Melanoma. *Surg. Clin. N. Am.* **2020**, 100, 175–188.
- 32- Snyder, A.; Makarov, V.; Merghoub, T.; Yuan, J.; Zaretsky, J.M.; Desrichard, A.; Walsh, L.A.; Postow, M.A.; Wong, P.; Ho, T.S.; et al. Genetic Basis for Clinical Response to CTLA-4 Blockade in Melanoma. *N. Engl. J. Med.* **2014**, 371, 2189–2199.
- 33- Hugo, W.; Zaretsky, J.M.; Sun, L.; Song, C.; Moreno, B.H.; Hu-Lieskovan, S.; Berent-Maoz, B.; Pang, J.; Chmielowski, B.; Cherry, G.; et al. Genomic and Transcriptomic Features of Response to Anti-PD-1 Therapy in Metastatic Melanoma. *Cell* **2016**, 165, 35–44.
- 34- Riaz, N.; Havel, J.J.; Makarov, V.; Desrichard, A.; Urba, W.J.; Sims, J.S.; Hodi, F.S.; Martín-Algarra, S.; Mandal, R.; Sharfman, W.H.; et al. Tumour and Microenvironment Evolution during Immunotherapy with Nivolumab. *Cell* **2017**, 171, 934–949.
- 35- Dianzani, C.; Monge, C.; Miglio, G.; Serpe, L.; Martina, K.; Cangemi, L.; Ferraris, C.; Mioletti, S.; Osella, S.; Gigliotti, C.L.; et al. Nanoemulsions as Delivery Systems for Poly-Chemotherapy Aiming at Melanoma Treatment. *Cancers* **2020**, 12, 1198.
- 36- Singer, A.J.; Clark, R.A. Cutaneous wound healing. *N. Engl. J. Med.* **1999**, 341, 738–746.
- 37- Singampalli, K.L.; Balaji, S.; Wang, X.; Parikh, U.M.; Kaul, A.; Gilley, J.; Birla, R.K.; Bollyky, P.L.; Keswani, S.G. The Role of an IL-10/Hyaluronan Axis in Dermal Wound Healing. *Front. Cell Dev. Biol.* **2020**, 8, 636.
- 38- Maeda, S.; Fujimoto, M.; Matsushita, T.; Hamaguchi, Y.; Takehara, K.; Hasegawa, M. Inducible costimulator (ICOS) and ICOS ligand signaling has pivotal roles in skin wound healing via cytokine production. *Am. J. Pathol.* **2011**, 179, 2360–2369.

- 39-** Johnson, B.Z.; Stevenson, A.W.; Prêle, C.M.; Fear, M.W.; Wood, F.M. The Role of IL-6 in Skin Fibrosis and Cutaneous Wound Healing. *Biomedicines* **2020**, *8*, 101.
- 40-** Ramavath, N.N.; Gadipudi, L.L.; Provera, A.; Gigliotti, L.C.; Boggio, E.; Bozzola, C.; Albano, E.; Dianzani, U.; Sutti, S. Inducible T-Cell Costimulator Mediates Lymphocyte/Macrophage Interactions During Liver Repair. *Front. Immunol.* **2021**, *12*, 786680.
- 41-** Hotchkiss, R.S.; Monneret, G.; Payen, D. Sepsis-induced immunosuppression: From cellular dysfunctions to immunotherapy. *Nat Rev Immunol*, **2013**, *13*:862–74.
- 42-** Rudd, K.E.; Johnson, S.C.; Agesa, K.M.; Shackelford, K.A.; Tsoi, D.; Kievlan, D.R.; Colombara, D.V.; Ikuta, K.S.; Kisson, N.; Finfer, S.; et al. Global, regional, and national sepsis incidence and mortality, 1990 – 2017 : analysis for the global burden of disease study. *Lancet*, **2020**, *395*:200–11.
- 43-** Luan, Y.; Yin, C.; Qin, Q.; Dong, N.; Zhu, X.; Sheng, Z. Effect of regulatory T cells on promoting apoptosis of T lymphocyte and its regulatory mechanism in sepsis. *J Interf Cytokine Res*, **2015**, *35*:969–80.
- 44-** Saito, K.; Wagatsuma, T.; Toyama, H.; Ejima, Y.; Hoshi, K.; Shibusawa, M.; Kato, M.; Kurosawa, S. Sepsis is characterized by the increases in percentages of circulating CD4 + CD25 + regulatory T cells and plasma levels of soluble CD25. *J Exp Med*, **2008**, *216*:61–8.
- 45-** Leng, F.; Liu, J.; Liu, Z.; Yin, J.; Qu, H.P. Increased proportion of CD4 d CD25 d Foxp3 d regulatory T cells during early-stage sepsis in ICU patients. *J Microbiol Immunol Infect*, **2013**, *46*:338–44.

# Inducible T-cell co-stimulator (ICOS) and ICOS ligand are novel players in the multiple-myeloma microenvironment

Elena Boggio,<sup>1,\*</sup>  Casimiro Luca Gigliotti,<sup>1,\*</sup> Riccardo Moia,<sup>2,3,\*</sup>  Annamaria Scotta,<sup>3</sup> Ilaria Crespi,<sup>3</sup> Paola Boggione,<sup>2,3</sup> Lorenzo De Paoli,<sup>2,3</sup> Clara Deambroggi,<sup>2,3</sup> Massimiliano Garzaro,<sup>1</sup> Matteo Vidali,<sup>3</sup> Annalisa Chiocchetti,<sup>1</sup> Ian Stoppa,<sup>1</sup> Roberta Rolla,<sup>1,3</sup> Chiara Dianzani,<sup>4</sup> Chiara Monge,<sup>4</sup> Nausicaa Clemente,<sup>1</sup> Gianluca Gaidano,<sup>2,3</sup> and Umberto Dianzani<sup>1,3</sup>

<sup>1</sup>Department of Health Sciences and Interdisciplinary Research Center of Autoimmune Diseases (IRCAD), Università del Piemonte Orientale, <sup>2</sup>Division of Hematology, Department of Translational Medicine, Università del Piemonte Orientale, <sup>3</sup>Maggiore della Carità University Hospital, Novara, and <sup>4</sup>Department of Scienza e Tecnologia del Farmaco, University of Turin, Turin, Italy

Received 29 September 2021; accepted for publication 9 November 2021

Correspondence: Umberto Dianzani, Department of Health Sciences, Interdisciplinary Research Center of Autoimmune Diseases, University of Piemonte Orientale, Via Solaroli 17, 28100 Novara, Italy. E-mail: umberto.dianzani@uniupo.it

\*These authors contributed equally.

## Introduction

Multiple myeloma (MM) is a plasma cell neoplasia resulting from monoclonal expansion of long-lived myeloma cells in the bone marrow (BM), leading to production of monoclonal immunoglobulins (M protein), mostly IgG or IgA.

Multiple myeloma tends to develop from premalignant monoclonal gammopathy of undetermined significance (MGUS), possibly going through a stage known as asymptomatic smouldering multiple myeloma (SMM).<sup>1–4</sup> Both MGUS and SMM do not display the end organ damage typical of MM, consisting of osteolytic lesions, anaemia,

## Summary

The inducible T-cell co-stimulator (ICOS) is a T-cell receptor that, once bound to ICOS ligand (ICOSL) expressed on several cell types including the B-cell lineage, plays a decisive role in adaptive immunity by regulating the interplay between B and T cells. In addition to its immunomodulatory functions, we have shown that ICOS/ICOSL signalling can inhibit the activity of osteoclasts, unveiling a novel mechanism of lymphocyte–bone cells interactions. ICOS and ICOSL can also be found as soluble forms, namely sICOS and sICOSL. Here we show that: (i) levels of sICOS and sICOSL are increased in multiple myeloma (MM) compared to monoclonal gammopathy of undetermined significance and smouldering MM; (ii) levels of sICOS and sICOSL variably correlate with several markers of tumour burden; and (iii) sICOS levels tend to be higher in Durie–Salmon stage II/III versus stage I MM and correlate with overall survival as an independent variable. Moreover, surface ICOS and ICOSL are expressed in both myeloma cells and normal plasma cells, where they probably regulate different functional stages. Finally, ICOSL triggering inhibits the migration of myeloma cell lines *in vitro* and the growth of ICOSL<sup>+</sup> MOPC-21 myeloma cells *in vivo*. These results suggest that ICOS and ICOSL represent novel markers and therapeutic targets for MM.

**Keywords:** inducible T-cell co-stimulator (ICOS)/ICOS ligand (ICOSL) system, multiple myeloma, sICOS and sICOSL.

hypercalcaemia, and renal failure, which constitutes the classical CRAB clinical presentation (hypercalcaemia, Renal failure, Anaemia, Bone disease).<sup>4,5</sup>

In MM, active osteolytic lesions are promoted by osteoclasts (OC) stimulated by high levels of receptor activator of nuclear factor kappa-B ligand (RANKL) expressed on the surface of myeloma cells, BM stromal cells, T helper (Th) cells (mainly Th-17 cells), and soluble RANKL (sRANKL) in the serum.<sup>6–8</sup>

We have recently shown that novel players in bone metabolism are the inducible T-cell co-stimulator (ICOS) and its ligand (ICOSL), both with a well-established role in activation of Th cells and T-/B-cell interaction.<sup>9</sup> ICOS (CD278)

belongs to the CD28 family and binds ICOSL (also known as B7h, CD275, B7H2, B7-RP1, or GL50), a member of the B7 family.<sup>10–12</sup> ICOS is mainly expressed on activated T cells, but weak levels have been detected also on dendritic cells (DC).<sup>13</sup> ICOSL is expressed not only on a wide variety of cell types, including B cells, macrophages, and DC, but also on non-haematopoietic cells, such as vascular endothelial cells, epithelial cells, fibroblasts, and many cancer cell types.<sup>14–17</sup>

The main biological function of ICOSL is triggering ICOS, which acts as a costimulatory molecule for activated Th cells by modulating their cytokine secretion.<sup>18–21</sup> Moreover, the ICOS/ICOSL axis can elicit a bidirectional signal acting on ICOSL-expressing cells.<sup>22,23</sup> In DC, ICOSL triggering by ICOS-Fc, a recombinant soluble form of ICOS composed of the extra-cellular portion of ICOS fused to the IgG<sub>1</sub> Fc portion, modulates cytokine secretion, potentiates cross-presentation of endocytosed antigens on class I MHC molecules, and inhibits cell adhesiveness and migration. Moreover, ICOS-Fc inhibits adhesiveness and migration of endothelial cells and tumour cell lines *in vitro* as well as metastatic dissemination of tumour cells *in vivo*.<sup>24–26</sup> Recently, we have shown that ICOS-Fc encapsulated in bio-compatible and biodegradable nanoparticles inhibits the growth of established B16-F10 melanoma by decreasing tumour vascularization and inhibiting regulatory T cells.<sup>27</sup>

Two aspects of the ICOS/ICOSL system are relevant for MM. First, ICOSL is expressed on OC, and ICOS-Fc inhibits RANKL-driven maturation and osteolytic activity of these cells *in vitro*, and the development of RANKL-induced osteoporosis *in vivo*.<sup>9</sup> Second, ICOSL is also bound by osteopontin (OPN), involved in bone formation. OPN is also expressed by myeloma cells where it regulates a number of functions, including adhesion to the extra-cellular matrix and angiogenesis. OPN and ICOS form a complex with ICOSL through different binding sites and elicit different, often opposite, functional effects.<sup>28–30</sup>

ICOS and ICOSL can also be secreted as soluble forms — namely sICOS and sICOSL — which may derive from alternative transcription of the gene, alternative splicing of the mRNA, or proteolytic cleavage of the membrane form.<sup>31,32</sup> Of note, the serum levels of sICOS and sICOSL are increased in some autoimmune diseases.<sup>33–37</sup>

The aim of this study was to assess the expression of ICOS and ICOSL in plasma cell dyscrasias to investigate the role of this receptor system in malignant progression and end organ damages.

## Materials and methods

### Patients

The study enrolled 204 patients with plasma cell dyscrasias referred to the Hematology Division of the “AOU Maggiore della Carità”, Novara, Italy between November 2016 and March 2021. They were grouped in MGUS, SMM, and MM

according to the 2017 updated ESMO guidelines, referring to International Myeloma Working Group (IMWG) diagnostic criteria (Table I).<sup>38</sup> All MM patients received therapy, including immunomodulatory agents, proteasome inhibitors, monoclonal antibodies, and chemotherapy. At the time of sampling, the median number of previous lines of therapy was 1 (0–6). Fifty-nine healthy controls (HCs) were matched for gender and age. The protocol was approved by the local Ethics Committee (No. CE 33/17), and all subjects signed an informed consent.

### ICOS/ICOSL analysis

Serum levels of sICOS, sICOSL and sRANKL were assessed by enzyme-linked immunosorbent assay (Cloud Clone Corporation, Katy, TX, USA). In two samples, sICOS and sICOSL levels were also measured after ultracentrifugation for 1 h at 4°C at 100.000 g in both the supernatant and the extra-cellular vesicle (EV) pellet.

Surface expression of ICOS and ICOSL was evaluated by flow cytometry (Attune NxT, Thermo-Fisher, Waltham, MA, USA) using fluorescein isothiocyanate (FITC)-conjugated anti-CD38 (eBioscience, San Diego, CA, USA), PE-conjugated anti-ICOS (R&D System, Minneapolis, MN, USA), PE-Cyanine (Cy) 7-conjugated anti-ICOSL (BioLegend, San Diego, CA, USA), PE- or APC-Cy7-conjugated anti-CD45 (eBioscience), and APC-conjugated anti-CD56 (eBioscience) mAb.<sup>39–42</sup>

### Cell migration assay

MOPC-21 cells (mouse myeloma) were a gift from Monash University (Clayton, Australia); RPMI-8226 cells (human myeloma) were purchased from ATCC (Manassas, VA, USA). MOPC-21<sup>ICOSL</sup> cells were MOPC-21 cells that were transfected with 2.5 µg of plasmid DNA coding for mouse ICOSL, as previously reported.<sup>30</sup>

In transwell plates (Corning Inc., Corning, NY, USA), 1.9 × 10<sup>6</sup> cells were plated onto the upper side of each well in serum-free medium with or without 2 µg/ml of ICOS-Fc

Table I. Patients' characteristics.

		MGUS	SMM	MM	Total
Patients	<i>n</i> (%)	36 (17.6)	97 (47.5)	71 (34.8)	204
Gender	Female	14 (38.9)	38 (39.2)	36 (50.7)	88 (43.2)
	Male	22 (61.1)	59 (60.8)	35 (49.3)	116 (56.8)
Age (years)	Median	69	72	71	71
	Min	32	38	40	32
	Max	83	90	84	90
	Mean	65.2	69.9	69.6	68.9
	SD	11	11.5	8.3	10.5

MM, multiple myeloma; MGUS, monoclonal gammopathy of undetermined significance; SD, standard deviation; SMM, smouldering multiple myeloma.



(human or murine), that is an agonist of ICOSL, or  $F^{1195}$ ICOS-Fc (human). Twenty percent fetal bovine serum (FBS) was used as a chemoattractant. After 18 h, the cells migrated to the lower chamber were counted with an inverted microscope (magnification 9100).

### *In vivo experiments*

Eight-week-old female NOD-SCID-IL2Rc-null mice (NSG) (Charles River Laboratories, Wilmington, MA, USA) were injected subcutaneously with  $2.9 \times 10^6$  MOPC-21<sup>ICOSL</sup> cells. When tumours were palpable, mice were treated every four days by intraperitoneal injection of murine ICOS-Fc loaded in poly(lactic-co-glycolic acid) (PLGA) nanoparticles (ICOS/PLGA, 100 Ig) or empty PLGA or saline. The tumour size was measured every four days and mice were sacrificed after 20 days.<sup>27</sup>

Mice were bred under pathogen-free conditions in the animal facility of the Department of Health Sciences. The study was approved by Ministero della Salute, Rome (No. 477/2016-PR and No. 849/2016 PR).

Staining of CD31 and Ki67, and tumour microvessel density measurements were performed on tissue sections as previously described.<sup>27,43</sup>

### *Statistical analyses*

Correlations were determined using Spearman's non-parametric test. Comparisons were performed using the Mann-Whitney test, Wilcoxon test, and paired *t*-test. Survival analysis was performed by the Kaplan-Meier method and compared between strata using the log-rank test. The adjusted association between exposure variables and overall survival (OS) was estimated by Cox regression.

## **Results**

### *Serum levels of sICOS and sICOSL in patients with plasma cell dyscrasias*

Serum levels of sICOS and sICOSL were measured in a cohort of plasma cell dyscrasia patients ( $n = 204$ ) (Table 1), and in 59 HCs. MM patients displayed higher sICOS and sICOSL serum levels than those found in MGUS and SMM patients (Fig 1A,B). Of note, the serum levels of sICOS and sICOSL in MGUS and SMM patients were not statistically different from those present in HCs (Fig 1A,B). Stratification of MM patients according to the Durie-Salmon staging system (DS; DS-I:  $n = 16$ ; DS-II:  $n = 39$ ; DS-III:  $n = 16$ ) revealed that sICOS serum concentration was higher in DS-II and DS-III compared to DS-I (Fig 1C,D), whereas no difference was found for sICOSL.

### *Correlations with disease markers*

Spearman's Rho test was performed to evaluate any correlations between sICOSL or sICOS serum levels and other known serum disease markers. These included *i*) the tumour burden markers  $\beta$ 2-microglobulin (B2M), M protein, BM plasma cells, and haemoglobin (Hb); *ii*) the bone metabolism markers calcium, sRANKL, and OPN.

Analysis of the tumour burden markers showed that, in all patients, sICOS correlated directly with B2M, total M protein, BM plasma cells and inversely with Hb (Fig 2A-D). On the other hand, sICOSL correlated directly with B2M and total M protein (Fig 2E-F). sICOS also showed a positive correlation with BM plasma cells among MM and MGUS patients ( $r = 0.731$ ,  $P = 0.02$ ), whereas sICOSL correlated with total M protein in MM patients ( $r = 0.478$ ,  $P = 0.0002$ ) (data not shown).

Analysis of bone metabolism and kidney injury markers revealed a direct correlation between sICOSL and sRANKL (Fig 2G).

Since MM patients display decreased levels of polyclonal Ig, we also analyzed the correlation of serum sICOS and sICOSL with polyclonal IgM and IgA in 50 MM patients producing IgG M protein (IgG/MM). We found that sICOS, but not sICOSL (data not shown), negatively correlated with polyclonal IgA and IgM (Fig 2H-I).

After a median follow-up period of 37.6 months, 40 patients died, and the 36-month OS was 78.7%. As expected, patients with MM had a worse OS than those with SMM or MGUS. Stratification of all patients for the median value of serum concentration of sICOS (27.9 pg/ml), sICOSL (994.7 pg/ml), or sRANKL (1024.3 pg/ml) showed that patients with sICOS levels above the median value had a worse OS than those below this value (OS-36: 70.1% vs 89.2%,  $P = 0.002$ ). By contrast, levels of sICOSL and sRANKL did not correlate with OS (Figure S1). An optimized sICOS threshold of 40 pg/ml was the best cut-off for OS, which was 67.2% for patients above this cut-off and 89.2% for those below ( $P = 0.00017$ ) (Fig 3A). Multivariate analysis showed that sICOS levels above 40 pg/ml maintained an independent association with an increased risk of death (HR 2.78, 95% CI 1.07-7.2,  $P = 0.035$ ) when adjusted for Durie-Salmon staging. The clinical impact of sICOS was detected in MM, but not in SMM and MGUS (Fig 3B-D).

### *Surface expression of ICOS and ICOSL*

Since serum levels of sICOS and sICOSL correlated with several tumour burden markers, we next assessed the surface expression of these receptors on myeloma cells. Flow cytometry analysis of BM samples from 31 MM patients showed that myeloma cells homogeneously expressed both ICOS (MFI-r 3.6 0.25) and, to a higher extent, ICOSL (MFI-r 7.3 0.66) (Fig 4A).

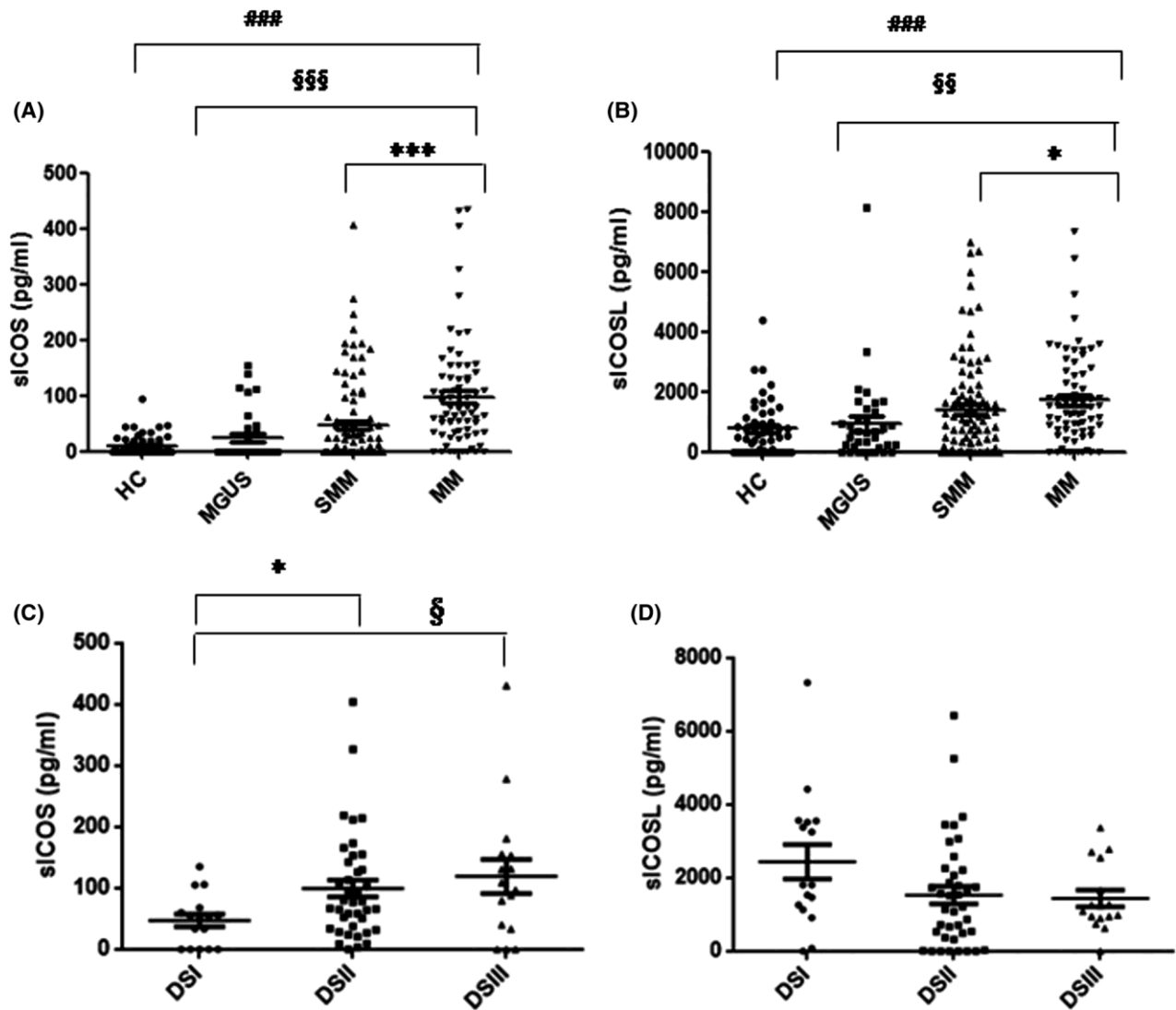


Fig 1. Serum levels of soluble inducible T-cell co-stimulator (sICOS) and sICOS ligand (sICOSL) are increased in multiple-myeloma (MM) patients. (A) sICOS and (B) sICOSL were evaluated in the sera of smouldering MM (SMM) ( $n = 97$ ), MM ( $n = 71$ ) and monoclonal gammopathy of undetermined significance (MGUS) ( $n = 36$ ) patients, and 59 HCs by enzyme-linked immunosorbent assay (ELISA). \*,  $P < 0.05$ , \*\*\*,  $P < 0.0001$  versus SMM; §§,  $P < 0.01$ , §§§,  $P < 0.0001$  versus MGUS, ###,  $P < 0.0001$  versus HC calculated by the Mann–Whitney non-parametric test. (C) sICOS and (D) sICOSL levels in MM patients stratified according to Durie Salmon staging: DS-I ( $n = 16$ ), DS-II ( $n = 39$ ), and DS-III ( $n = 16$ ). \*,  $P < 0.05$  versus DS-II, §,  $P < 0.05$  versus DS-III calculated by the Mann–Whitney non-parametric test. Values are represented as mean  $\pm$  SEM.

To investigate whether ICOS and ICOSL were also expressed on normal plasma cells, we analyzed surface expression of these molecules in BM plasma cells from eight patients affected from immune thrombocytopenia (ITP). We identified two plasma cell subsets, one expressing both ICOS and ICOSL, similar to myeloma cells, and the other expressing ICOSL but not ICOS (Fig 4B). More specifically, the ICOS<sup>+</sup>ICOSL<sup>+</sup> and ICOS<sup>-</sup>ICOSL<sup>+</sup> subsets accounted respectively for 45.8% and 55.8% (mean  $\pm$  SEM) of BM plasma cells.

In MM patients ( $n = 20$ ), a correlation was found between sICOS serum concentration and ICOS cell surface expression on myeloma cells, but not between sICOSL serum concentration and ICOSL cell surface expression (Fig 5A,B).

To assess whether serum sICOS and sICOSL were present as free proteins or associated with the EVs, we analyzed sICOS and sICOSL before and after ultracentrifugation of the serum, which is supposed to precipitate EVs. After centrifugation, sICOS and sICOSL were mainly found in the supernatant, whereas only minimal amounts were found in the EV pellet, suggesting that sICOS and sICOSL are present in the serum as free molecules (Fig 5C,D).

#### Effect of ICOS-Fc on myeloma cells

As we have previously shown that triggering of ICOSL with ICOS-Fc inhibits migration of several types of tumour

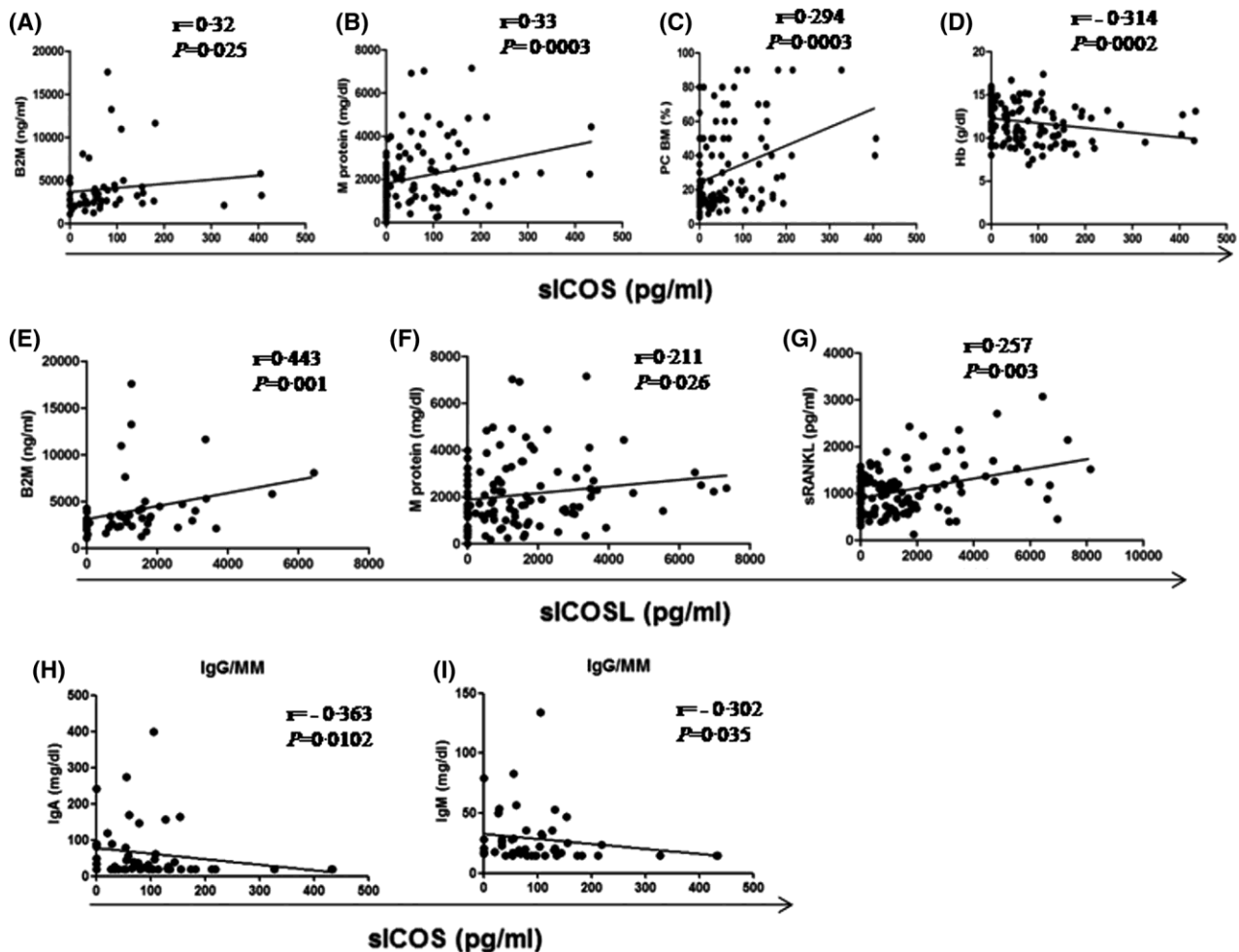


Fig 2. Correlation of serum levels of soluble inducible T-cell co-stimulator (sICOS) and sICOS ligand (sICOSL) with disease markers. Correlations detected in total patients between serum levels of (A–D) sICOS and those of (A)  $\beta$ 2-microglobulin (B2M), (B) M protein, (C) bone marrow (BM) plasma cells (BM PC), (D) haemoglobin (Hb); and between levels of (E–G) sICOSL and those of (E) B2M, (F) M protein, and (G) sRANKL. Panels H–I show the correlation detected in IgG/multiple myeloma (MM) between sICOS and polyclonal (H) IgA and (I) IgM. Spearman's  $\rho$  test.

cells,<sup>25,26</sup> we next asked whether this effect would also be true in myeloma cells. To this end, we performed migration assays using murine myeloma cells expressing either low (MOPC-21) or high levels of ICOSL (MOPC-21<sup>ICOSL</sup>). In addition, we carried out similar experiments using RPMI-8226 human myeloma cells, which spontaneously express high levels of ICOSL (Fig 6A). Cells were seeded in the upper chamber of a transwell plate in the presence or absence of ICOS-Fc—human or mouse, as appropriate—and the extent of migration was assessed in the lower chamber after 18 h, using FCS as chemoattractant. F<sup>119S</sup>ICOS-Fc, a point mutant unable to bind ICOSL, was used as negative control. As shown in Fig 6B, ICOS-Fc inhibited the migration of both RPMI-8226 and MOPC-21<sup>ICOSL</sup> cells but not that of MOPC-21 cells, which migrated to a much lower extent than MOPC-21<sup>ICOSL</sup> cells. As expected, F<sup>119S</sup>ICOS-Fc had no effect on either cell line.

We previously demonstrated that treatment of mice with ICOS-Fc loaded in poly(d,l-lactide-co-glycolide) (PLGA) nanoparticles (ICOS/PLGA) hampered the growth of established tumours arising upon subcutaneous injection of ICOSL<sup>+</sup> melanoma cells.<sup>27</sup> To assess whether this effect would also occur in myeloma cells, we injected subcutaneously MOPC-21<sup>ICOSL</sup> cells in immunodeficient NSG mice and treated them with ICOS/PLGA as soon as the tumour was palpable. NSG mice were chosen to avoid any potential bias due to the effect of ICOS-Fc on the anti-tumour immune response. Control mice were treated with either saline or empty PLGA nanoparticles. Tumour growth monitoring revealed that treatment with ICOS/PLGA significantly decreased tumour growth compared to control mice (Fig 7A).

We next stained tumour sections for CD31 and Ki-67 to assess tumour vessel formation and cancer cell proliferation,

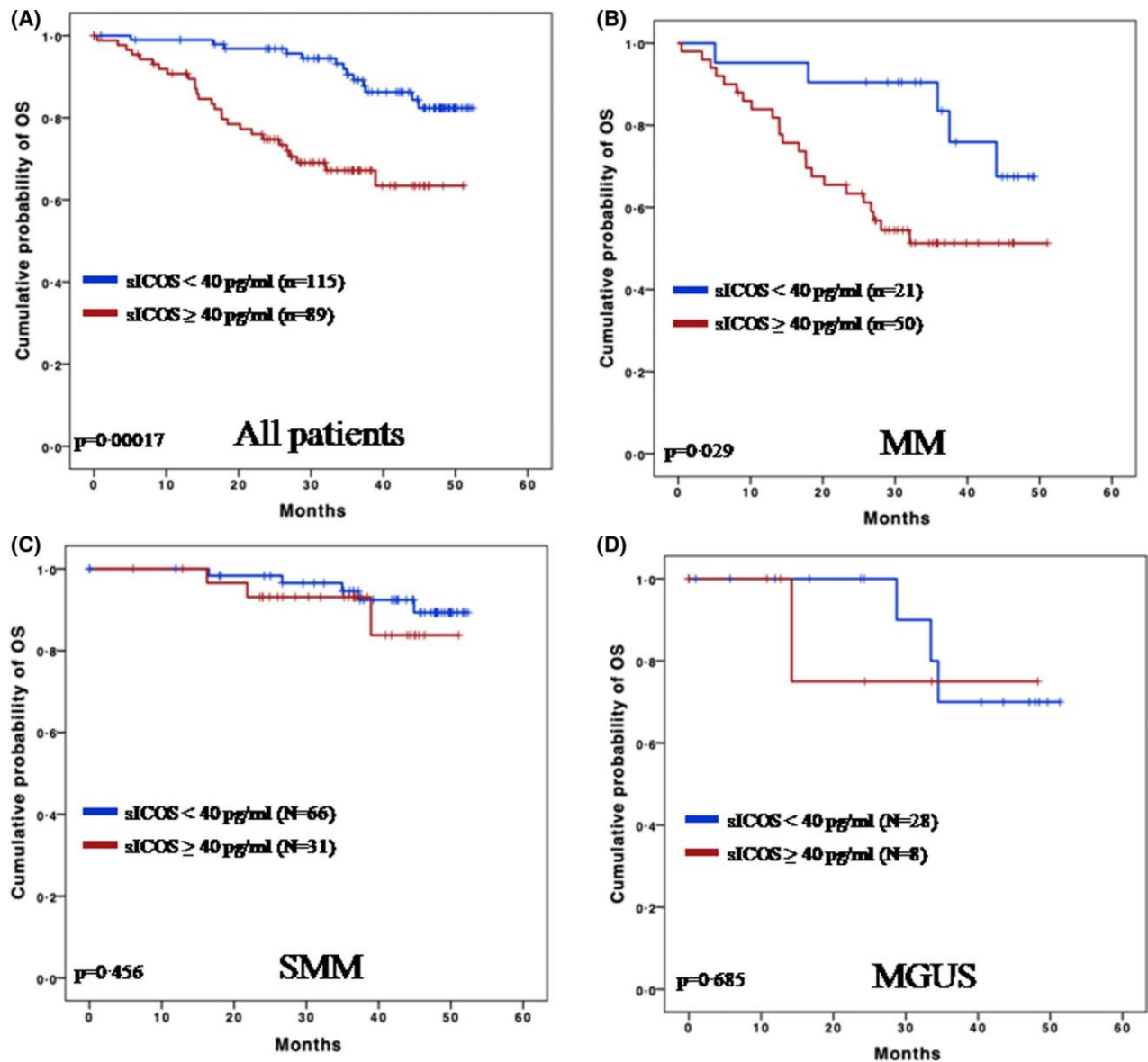


Fig 3. Prognostic impact of soluble inducible T-cell co-stimulator (sICOS) levels on survival. Kaplan–Meier estimates of overall survival (OS) of patients with sICOS above or below the 40 pg/ml cut-off. (A) All patients [multiple myeloma (MM) + smouldering MM (SMM) + monoclonal gammopathy of undetermined significance (MGUS)]. (B) MM patients. (C) SMM patients. (D) MGUS patients. [Colour figure can be viewed at [wileyonlinelibrary.com](http://wileyonlinelibrary.com)]

respectively. Tumours from ICOS-Fc-treated mice displayed decreased tumour vascular density (Fig 7B) and cell proliferation rate compared to mice treated with either empty PLGA or saline (Fig 7C). Real-time polymerase chain reaction (PCR) analysis did not reveal any statistically significant differences in mRNA expression levels of ICOSL, IL-10, IFN- $\gamma$ , IL-6, TNF- $\alpha$ , IL-1 $\beta$ , TGF- $\beta$ , and OPN among the three groups (data not shown).

## Discussion

This study shows that: *i*) sICOSL and sICOS serum levels vary across the spectrum of plasma cell disorders; *ii*) sICOSL

and sICOS serum levels correlate with several markers of tumour burden; *iii*) high serum levels of sICOS but not sICOSL are an independent prognostic factor of shorter survival in patients with plasma cell disorders; *iv*) ICOSL surface expression on neoplastic plasma cells may influence the biological behaviour of MM.

Here, we have applied multiple approaches to investigate the ICOS/ICOSL status in MM, a tumour in which ICOS/ICOSL signalling may exert multiple functions. Our results show that MM patients display higher serum levels of sICOSL and sICOS compared to those observed among MGUS and SMM cases. Moreover, sICOSL and sICOS serum levels positively correlate with the tumour burden markers

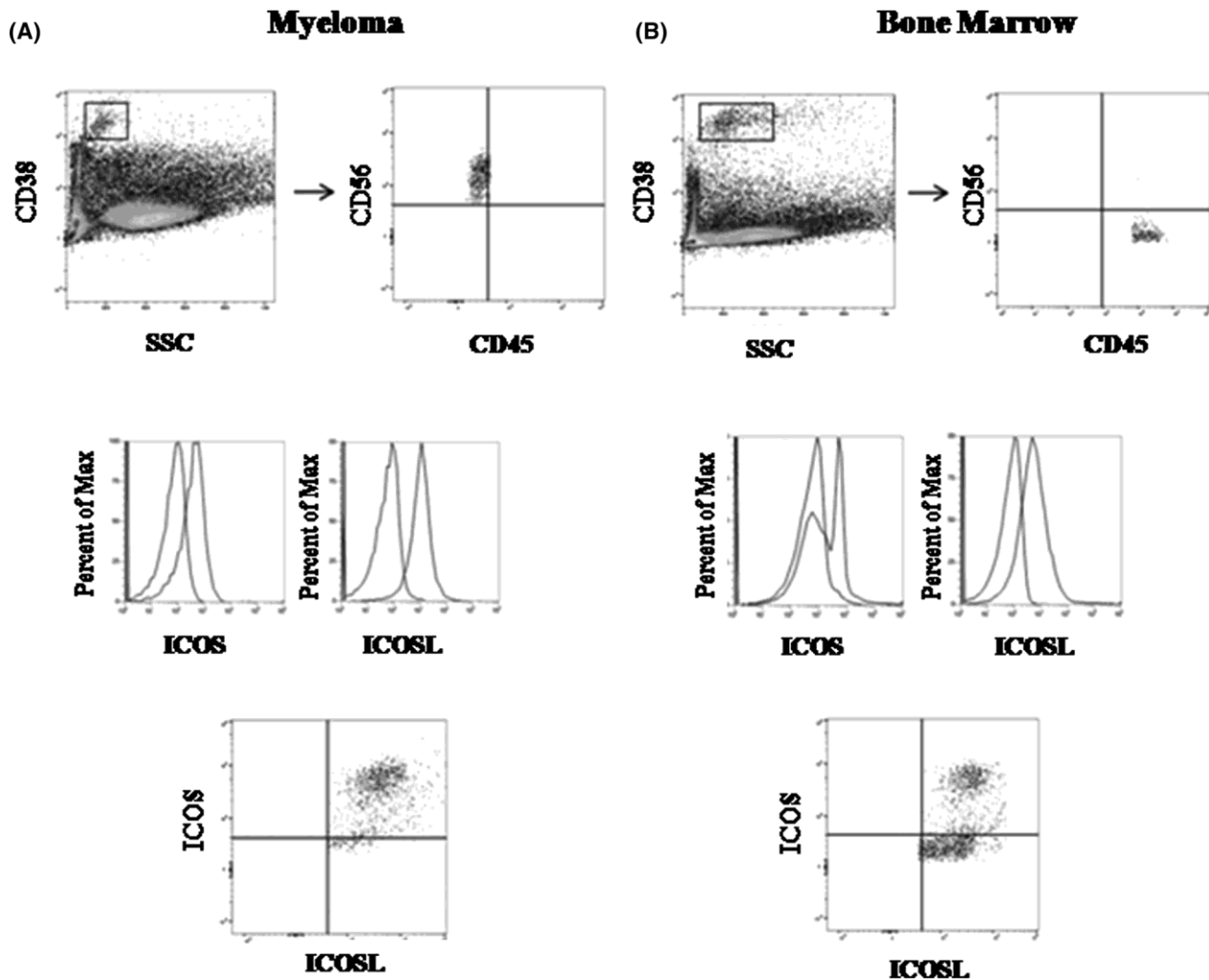


Fig 4. Flow cytometry plots of soluble inducible T-cell co-stimulator (sICOS) and sICOS ligand (sICOSL) expression in bone marrow (BM)-derived myeloma cells and normal plasma cells. Representative dot plots and histograms of (A) myeloma and (B) BM samples. Plasma cells were gated on CD38<sup>bright</sup> (CD38<sup>+++</sup>) cells displaying the expected side scatter profile. Phenotype of the myeloma cells was CD38<sup>+++</sup>/CD45<sup>-</sup>/CD56<sup>+</sup>, that of normal plasma cells was CD38<sup>+++</sup>/CD45<sup>+</sup>/CD56<sup>-</sup>. The histograms show the overlay between control staining and ICOSL or ICOS staining.

B2M, M protein, and BM myeloma plasma cell infiltration, whereas they negatively correlate with Hb levels.

From a clinical standpoint, an optimized threshold of 40 pg/ml sICOS emerged as the best cut-off to split patient survival and retain a prognostic value in multivariate analysis. Although these results point to sICOS and sICOSL as potentially useful prognostic markers of plasma cell dyscrasias, they await further validation in prospective cohorts of MM patients.

Flow cytometry analysis shows that ICOSL and, at lower levels, ICOS are expressed as surface receptors on MM cells, confirming recent findings by mass cytometry.<sup>44</sup> The observation that the serum levels of sICOS correlate with surface expression of ICOS in myeloma cells suggests that at least part of sICOS may derive from the neoplastic cell population. This correlation was not detected for sICOSL, possibly due to the fact that its release from myeloma cells might be

hidden by the basally high serum levels of sICOSL, which are approximately one log-level higher than sICOS levels in HCs. Moreover, increased sICOSL levels in MM may also depend on its release from many types of non-neoplastic ICOSL<sup>+</sup> cells inside and outside of the BM, whereas ICOS expression appears to be restricted to only a few cell types.

The identification of two plasma cell subsets: ICOS<sup>+</sup>ICOSL<sup>-</sup> and ICOS<sup>-</sup>ICOSL<sup>+</sup> in normal BM plasma cells, indicates that ICOS and ICOSL expression may not represent a specific trait of neoplastic plasma cells. The ICOS<sup>+</sup>ICOSL<sup>+</sup> phenotype might comprise long-lived plasma cells, which are the normal counterpart of myeloma cells. Consequently, the ICOS<sup>-</sup>ICOSL<sup>+</sup> subset may comprise plasmablasts, which would be in line with the notion that activated B cells express ICOSL but not ICOS.<sup>45</sup>

The possibility that ICOS/ICOSL signalling plays a role in MM development is supported by our *in vivo* experiments

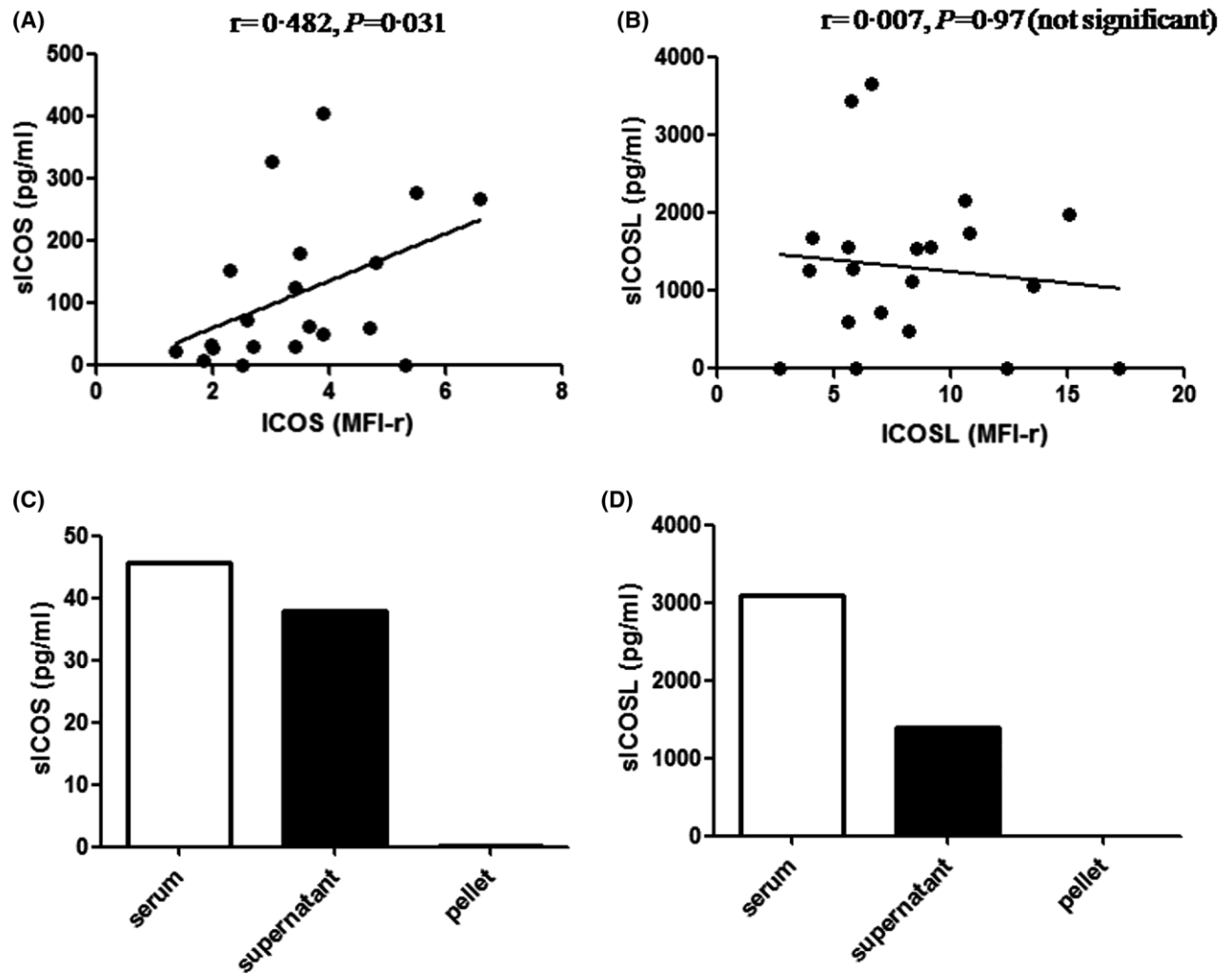


Fig 5. Serum soluble inducible T-cell co-stimulator (sICOS) and sICOS ligand (sICOSL) may be partly released by myeloma cells as free molecules. sICOS serum levels (A) correlate with ICOS surface expression levels on myeloma cells. (B) The correlation between sICOSL and the expression level of ICOSL is not significant in 20 patients with multiple myeloma (MM) (Spearman's  $\rho$  test). ICOS and ICOSL expression levels were evaluated as mean fluorescence intensity ratio (MFI-r). Levels of (C) sICOS and (D) sICOSL evaluated in the serum of a patient before (white bars) and after (black bars) ultracentrifugation, which allowed the separation of EVs in the pellet from the supernatant. The graph represents data from one of two experiments performed with sera from two different patients.

showing that treatment with ICOS-Fc significantly inhibits the growth of MOPC-21<sup>ICOSL</sup> tumours in mice. This effect may be due to inhibition of tumour angiogenesis, as documented by the decreased tumour microvessel density displayed by tumours from mice treated with ICOS-Fc. However, ICOS-Fc might also exert direct effects on myeloma cells by inhibiting their migration, since ICOS-Fc inhibits *in vitro* migration of ICOSL<sup>+</sup> myeloma cells. Moreover, ICOS-Fc might boost the anti-tumour immune response and overcome immune evasion, acting as an immune checkpoint antagonist, as suggested by our previous work on different tumour types<sup>27,46</sup> and several other works showing that inhibition of ICOS function on T cells impairs regulatory T-cell activity.<sup>47</sup> This immunological effect has been underestimated in our experimental model based on subcutaneous tumours in immunodeficient mice, prompting studies in the

immunocompetent BM setting, which might highlight interferences of ICOS-Fc with the complex MM niche, including those with osteoclasts (OC), whose maturation and osteoclast activity is inhibited by ICOS-Fc.<sup>9</sup>

Survival and growth of plasma and myeloma cells depend on their bidirectional crosstalk with the BM microenvironment through a complex network, also including ICOS and ICOSL, which creates a permissive niche.<sup>48–53</sup> Thus, the functional effects of surface and soluble forms of ICOS and ICOSL are likely to depend on the relative amounts of these molecules in the BM niche. In this regard, our data suggest that ICOS and ICOSL expressed on the cell surface of myeloma cells may transduce signals modulating neoplastic cell behaviour, as supported by the observation that increased ICOSL expression not only correlates with enhanced migration of MOPC-21 cells — possibly due to its interaction with

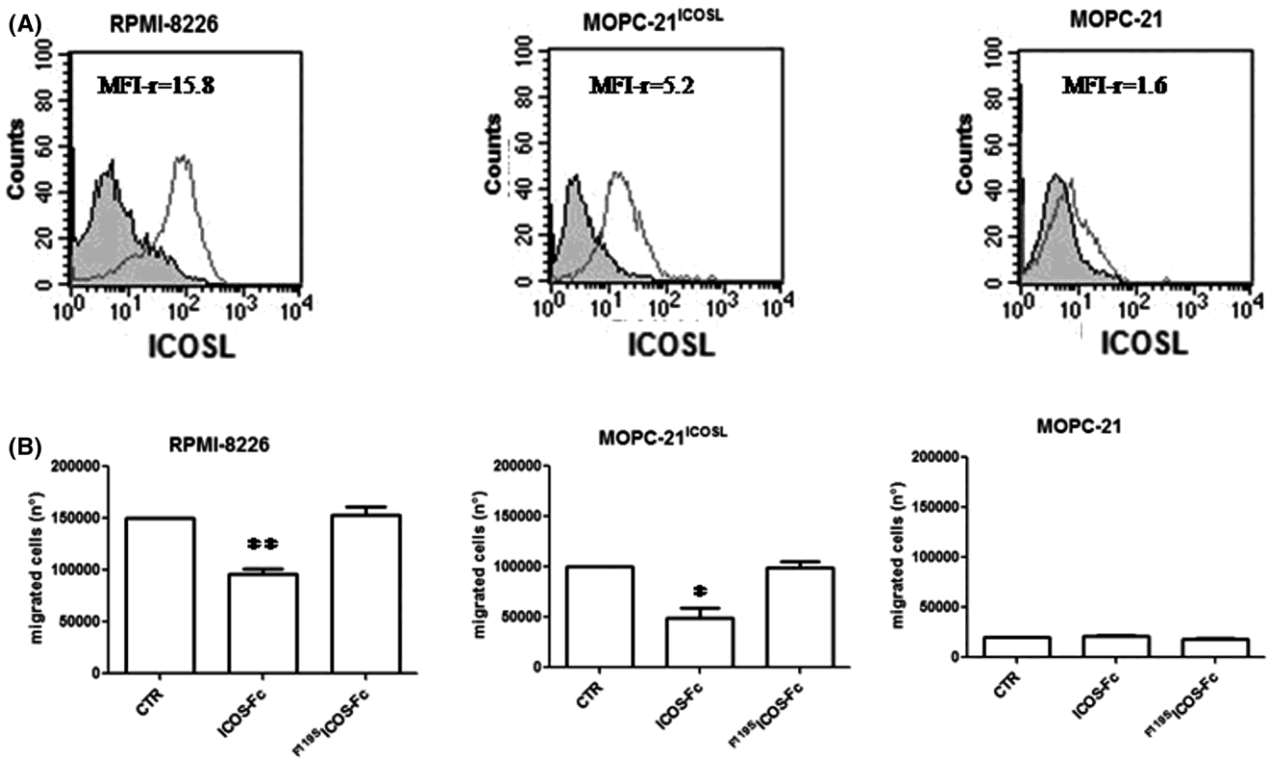


Fig 6. Inducible T-cell co-stimulator (ICOS)-Fc inhibits myeloma cells migration *in vitro*. (A) Representative histograms of ICOS ligand (ICOSL) expression in RPMI-8226, MOPC-21<sup>ICOSL</sup>, and MOPC-21 cells. Each panel shows the overlay between the negative control and the positive staining. Values of mean fluorescence intensity ratio (MFI-r) are indicated. (B) Treatment with ICOS-Fc inhibits migration of RPMI-8226 (human) and MOPC-21<sup>ICOSL</sup> (mouse) myeloma cells expressing ICOSL, but not that of MOPC-21 myeloma cells not expressing ICOSL, compared to both untreated cells and cells treated with the inactive mutant <sup>F1195</sup>ICOS-Fc. \*,  $P < 0.05$ ; \*\*,  $P < 0.01$  calculated by paired *t*-test. Values are represented as mean  $\pm$  SEM ( $n = 3$ ).

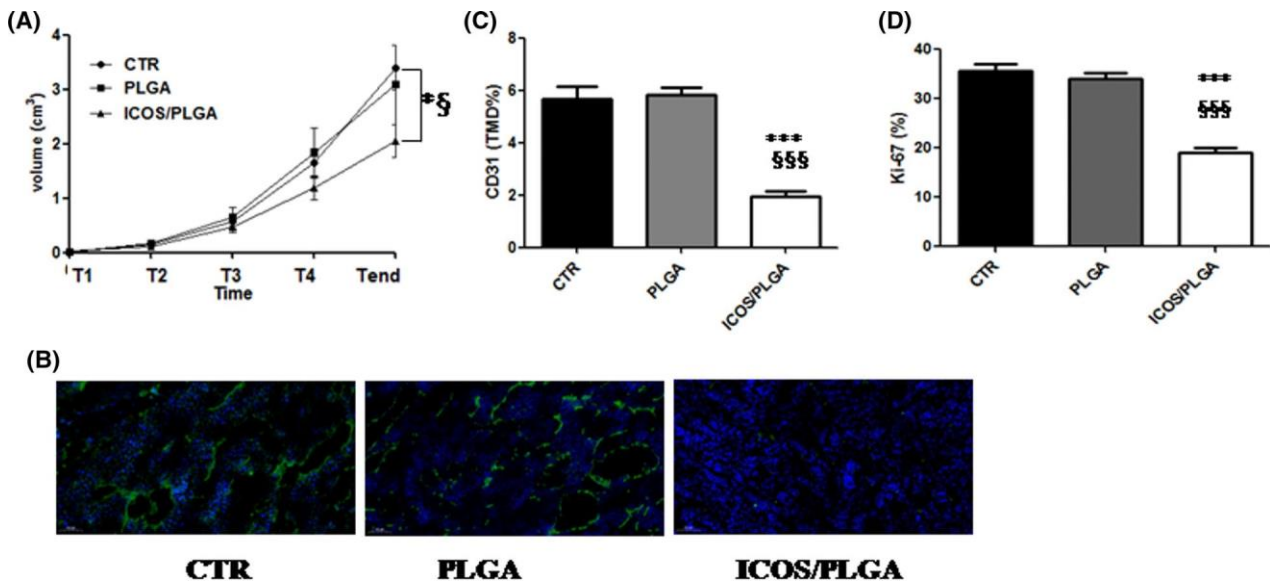


Fig 7. Inducible T-cell co-stimulator (ICOS)-Fc inhibits myeloma cells growth *in vivo*. (A) Treatment with ICOS-Fc loaded in poly(lactic-co-glycolic acid) (PLGA) nanoparticles (ICOS/PLGA,  $n = 15$ ), but not saline [control (CTR),  $n = 17$ ] or empty PLGA nanoparticles ( $n = 14$ ), inhibits subcutaneous growth of MOPC-21<sup>ICOSL+</sup> cells in NSG mice. (B) CD31 staining and (C) tumour microvessel density (TMD) measured on CD31 expression. (D) Proportion of Ki-67 positive tumour cells. Values are represented as mean  $\pm$  SEM; \*,  $P < 0.05$ ; \*\*\*,  $P < 0.0001$  vs CTR; §,  $P < 0.05$ ; §§§,  $P < 0.0001$  vs PLGA, calculated by the Mann-Whitney non-parametric test. [Colour figure can be viewed at [wileyonlinelibrary.com](http://wileyonlinelibrary.com)]

OPN — but also makes these cells susceptible to ICOS-Fc-mediated inhibition of migration. In this context, it is also conceivable that aberrant expression of membrane-bound ICOSL on myeloma cells may antagonize ICOSL expressed on other cell types of the myeloma niche, such as endothelial cells and OC, which would make them resistant to ICOS-mediated inhibition.

It is also unclear what the functional effects of sICOS and sICOSL — present in the serum as free molecules — would be. In general, soluble forms of membrane receptors can act as decoy receptors able to antagonize their membrane-bound counterparts, as shown for several cytokine receptors.<sup>54,55</sup> Alternatively, they may work as agonistic ligands when they are multivalent, as reported for soluble Fas ligand (FasL) trimers, which are capable of inducing cell death upon Fas triggering.<sup>56,57</sup> Both models may apply to sICOSL and sICOS, which can function as either antagonistic monomers or agonistic dimers.<sup>58,59</sup>

Overall, our findings indicate that sICOS and sICOSL may play a role in myeloma cell growth. Furthermore, given their ubiquitous distribution within the tumour microenvironment and neoplastic cell surface, these molecules may also represent attractive therapeutic targets for MM. In this context, the ICOS/ICOSL axis might also be exploited to trigger T-cell immunity to further reinforce the efficacy of novel immunotherapeutic approaches.<sup>47</sup>

## Acknowledgements

We thank Dr. Senora Mendonca from Monash University Clayton Campus, Victoria, Australia for her kind gift of the MOPC-21 cell line; Fondazione Giovanni Gorla, Asti, Italy and Fondazione CRT, Turin, Ital, partially supported CM; Fondazione Umberto Veronesi, Milan, Italy supports EB.

## Conflicts of interest

EB, CLG, and UD are listed as inventors on the patent WO/2016/189428 “Ligands of B7h receptor in the treatment of osteopenia and osteoporosis”, and are founders of an UPO Spinoff (NOVAICOS). AC, UD, CD, EB, NC, and CLG are listed as inventors on the patent PCT/IB2019/050154 “Novel anti-tumour therapeutic agents”.

## Funding information

This work was supported by: Molecular bases of disease dissemination in lymphoid malignancies to optimize curative therapeutic strategies (5 x 1000 No. 21198) and IG 20714 Associazione Italiana per la Ricerca sul Cancro, Milan, Italy; Associazione Italiana contro Leucemie, Linfomi, Mieloma - Novara (AIL, Novara); Progetti di Rilevante Interesse Nazionale (PRIN), (2015ZMRFEA), Rome, Italy; the AGING Project – Department of Excellence – DIMET, Università del Piemonte Orientale, Novara, Italy; Ricerca Finalizzata 2018

(project RF-2018-12365790), MoH, Rome, Italy; Fondazione Cariplo (2017–0535); Fondazione Amici di Jean (Turin).

## Author contributions

EB, CLG, IC, IS, CM, NC, AC and C Dianzani performed the experiments, and analyzed the biological data; RM, AS, PB, LD, C Deambrogi, MV, RR, AC and MG performed clinical analyses, collected the samples and analyzed the clinical data; GG and UD designed the study and wrote the manuscript.

## Supporting Information

Additional supporting information may be found online in the Supporting Information section at the end of the article.

Fig S1. Lack of prognostic impact of sICOS, sICOSL, and sRANKL levels on survival. Kaplan-Meier estimates of overall survival (OS) of patients. (A) MM vs SMM+MGUS. (B–D) All patients (MM+SMM+MGUS) with (B) sICOS, (C) sICOSL, or (D) sRANKL above or below the median level.

## References

1. RoCllig C, Knop S, BornhCauser M. Multiple multiple myeloma. *Lancet*. 2015;385(9983):2197–208. [https://doi.org/10.1016/S0140-6736\(14\)60493-1](https://doi.org/10.1016/S0140-6736(14)60493-1)
2. Michels TC, Petersen KE. Multiple myeloma: diagnosis and treatment. *Am Fam Physician*. 2017;95(6):373–83.
3. Terpos E, Christoulas D, Gavriatopoulou M, Dimopoulos MA. Mechanisms of bone destruction in multiple myeloma. *Eur J Cancer Care (Engl)*. 2017;26(6):e12761. <https://doi.org/10.1111/ecc.12761>
4. Tomasson M, Ali M, De Oliveira V, Xiao Q, Jethava Y, Zhan F, et al. Prevention is the best treatment: the case for understanding the transition from monoclonal gammopathy of undetermined significance to myeloma. *Int J Mol Sci*. 2018;19(11):1–19. <https://doi.org/10.3390/ijms19113621>
5. Fairfield H, Falank C, Avery L, Reagan MR. Multiple myeloma in the marrow: pathogenesis and treatments. *Ann N Y Acad Sci*. 2016;1364(1):32–51. <https://doi.org/10.1111/nyas.13038>
6. Tikhonova AN, Dolgalev I, Hu H, Sivaraj KK, Hoxha E, Cuesta-Domínguez A', et al. The bone marrow microenvironment at single-cell resolution. *Nature*. 2019;569(7755):222–8. <https://doi.org/10.1038/s41586-019-1104-8>
7. Terpos E, Szydlo R, Apperley JF, Hatjiharissi E, Politou M, Meletis J, et al. Soluble receptor activator of nuclear factor kappaB ligand-osteoprotegerin ratio predicts survival in multiple myeloma: proposal for a novel prognostic index. *Blood*. 2003;102(3):1064–9. <https://doi.org/10.1182/blood-2003-02-0380>
8. Buckle CH, de Leenheer E, Lawson MA. Soluble rank ligand produced by myeloma cells causes generalised bone loss in multiple myeloma. *PLoS One*. 2012;7(8):e41127. <https://doi.org/10.1371/journal.pone.0041127>
9. Gigliotti CL, Boggio E, Clemente N, Shivakumar Y, Toth E, Sblattero D, et al. ICOS-ligand triggering impairs osteoclast differentiation and function in vitro and in vivo. *J Immunol*. 2016;197(10):3905–16. <https://doi.org/10.4049/jimmunol.1600424>
10. Hutloff A, Dittrich AM, Beier KC, Eljaschewitsch B, Kraft R, Anagnostopoulos I, et al. ICOS is an inducible T cell co-stimulator structurally and functionally related to CD28. *Nature*. 1999;397(6716):263–6. <https://doi.org/10.1038/16717>
11. Buonfiglio D, Bragardo M, Redoglia V, Vaschetto R, Bottarel F, Bonissoni S, et al. The T cell activation molecule H4 and the CD28-like molecule



- ICOS are identical. *Eur J Immunol.* 2000;30(12):3463–7. [https://doi.org/10.1002/1521-4141\(200012\)30:12<3463::AID-IMMU3463>3.0.CO;2-5](https://doi.org/10.1002/1521-4141(200012)30:12<3463::AID-IMMU3463>3.0.CO;2-5)
12. Redoglia V, Dianzani U, Rojo JM, Portolés P, Bragardo M, Wolff H, et al. Characterization of H4: a mouse T lymphocyte activation molecule functionally associated with the CD3/T cell receptor. *Eur J Immunol.* 1996;26(11):2781–9. <https://doi.org/10.1002/eji.1830261134>
  13. Hedl M, Lahiri A, Ning K, Cho JH, Abraham C. Pattern recognition receptor signaling in human dendritic cells is enhanced by ICOS ligand and modulated by the Crohn's disease ICOSLG risk allele. *Immunity.* 2014;40(5):734–46. <https://doi.org/10.1016/j.immuni.2014.04.011>
  14. Sharpe AH, Freeman GJ. The B7-CD28 superfamily. *Nat Rev Immunol.* 2002;2(2):116–26. <https://doi.org/10.1038/nri727>
  15. Nurieva RI. Regulation of immune and autoimmune responses by ICOS– B7h interaction. *Clin Immunol.* 2005;115(1):19–25. <https://doi.org/10.1016/j.clim.2005.02.010>
  16. Swallow MM, Wallin JJ, Sha WC. B7h, a novel costimulatory homolog of B7.1 and B7.2, is induced by TNF $\alpha$ . *Immunity.* 1999;11(4):423–32. [https://doi.org/10.1016/s1074-7613\(00\)80117-x](https://doi.org/10.1016/s1074-7613(00)80117-x)
  17. Greenwald RJ, Freeman GJ, Sharpe AH. The B7 family revisited. *Annu Rev Immunol.* 2005;23:515–48. <https://doi.org/10.1146/annurev.immunol.23.021704.115611>
  18. Yagi J, Arimura Y, Dianzani U, Uede T, Okamoto T, Uchiyama T. Regulatory roles of IL-2 and IL-4 in H4/inducible costimulator expression on activated CD4+ T cells during Th cell development. *J Immunol.* 2003;171(2):783–94. <https://doi.org/10.4049/jimmunol.171.2.783>
  19. Mesturini R, Nicola S, Chiochetti A, Bernardone IS, Castelli L, Bensi T, et al. ICOS cooperates with CD28, IL-2, and IFN- $\gamma$  and modulates activation of human naive CD4+ T cells. *Eur J Immunol.* 2006;36(10):2601–12. <https://doi.org/10.1002/eji.200535571>
  20. Mesturini R, Gigliotti CL, Orilieri E, Cappellano G, Soluri MF, Boggio E, et al. Differential induction of IL-17, IL-10, and IL-9 in human T helper cells by B7h and B7.1. *Cytokine.* 2013;64(1):322–30. <https://doi.org/10.1016/j.cyto.2013.05.021>
  21. Tafuri A, Shahinian A, Bladt F, Yoshinaga SK, Jordana M, Wakeham A, et al. ICOS is essential for effective T-helper-cell responses. *Nature.* 2001;409(6816):105–9. <https://doi.org/10.1038/35051113>
  22. Mak TW, Shahinian A, Yoshinaga SK, Wakeham A, Boucher L-M, Pintilie M, et al. Costimulation through the inducible costimulator ligand is essential for both T helper and B cell functions in T cell-dependent B cell responses. *Nat Immunol.* 2003;4(8):765–72. <https://doi.org/10.1038/ni947>
  23. Tang G, Qin Q, Zhang P, Wang G, Liu M, Ding Q, et al. Reverse signaling using an inducible costimulator to enhance immunogenic function of dendritic cells. *Cell Mol Life Sci.* 2009;66(18):3067–80. <https://doi.org/10.1007/s00018-009-0090-7>
  24. Occhipinti S, Dianzani C, Chiochetti A, Boggio E, Clemente N, Gigliotti CL, et al. Triggering of B7h by the inducible costimulator modulates maturation and migration of monocyte-derived dendritic cells. *J Immunol.* 2013;190(3):1125–34. <https://doi.org/10.4049/jimmunol.1201816>
  25. Dianzani C, Minelli R, Mesturini R, Chiochetti A, Barrera G, Boscolo S, et al. B7h triggering inhibits umbilical vascular endothelial cell adhesiveness to tumor cell lines and polymorphonuclear cells. *J Immunol.* 2010;185(7):3970–9. <https://doi.org/10.4049/jimmunol.0903269>
  26. Dianzani C, Minelli R, Gigliotti CL, Occhipinti S, Giovarelli M, Conti L, et al. B7h triggering inhibits the migration of tumor cell lines. *J Immunol.* 2014;192(10):4921–31. <https://doi.org/10.4049/jimmunol.1300587>
  27. Clemente N, Boggio E, Gigliotti LC, Raineri D, Ferrara B, Miglio G, et al. Immunotherapy of experimental melanoma with ICOS-Fc loaded in biocompatible and biodegradable nanoparticles. *J Control Release.* 2020;10(320):112–24. <https://doi.org/10.1016/j.jconrel.2020.01.030>
  28. Castello LM, Raineri D, Salmi L, Clemente N, Vaschetto R, Quaglia M, et al. Osteopontin at the crossroads of inflammation and tumor progression. *Mediators Inflamm.* 2017;2017:4049098. <https://doi.org/10.1155/2017/4049098>
  29. Clemente N, Raineri D, Cappellano G, Boggio E, Favero F, Soluri MF, et al. Osteopontin bridging innate and adaptive immunity in autoimmune diseases. *J of Immunol Res.* 2016;2016:7675437. <https://doi.org/10.1155/2016/7675437>
  30. Raineri D, Dianzani C, Cappellano G, Maione F, Baldanzi G, Iacobucci I, et al. Osteopontin binds ICOSL promoting tumor metastatization. *Communicat Biol.* 2020;3(1):615. <https://doi.org/10.1038/s42003-020-01333-1>
  31. Lownik JC, Luker AJ, Damle SR, Cooley LF, El Sayed R, Hutloff A, et al. ADAM10-mediated ICOSL shedding on B cells is necessary for proper T cell ICOS regulation and TFH responses. *J Immunol.* 2017;199(7):2305–15. <https://doi.org/10.4049/jimmunol.1700833>
  32. Lownik JC, Wimberly JL, Conrad DH, Martin RK. B cell ADAM10 controls murine lupus progression through regulation of the ICOS:ICOSL ligand axis. *J Immunol.* 2019;202(3):664–74. <https://doi.org/10.4049/jimmunol.1801207>
  33. Iwai H, Abe M, Hirose S, Tsushima F, Tezuka K, Akiba H, et al. Involvement of inducible costimulator-B7 homologous protein costimulatory pathway in murine lupus nephritis. *J Immunol.* 2003;171(6):2848–54. <https://doi.org/10.4049/jimmunol.171.6.2848>
  34. Her M, Kim D, Oh M, Jeong H, Choi I. Increased expression of soluble inducible costimulator ligand (ICOSL) in patients with systemic lupus erythematosus. *Lupus.* 2009;18(6):501–7. <https://doi.org/10.1177/0961203308099176>
  35. Yu H, Zou X, Peng L, Wang Y, Zhang C, Chen B, et al. Effect of soluble inducible costimulator level and its polymorphisms on age-related macular degeneration. *DNA Cell Biol.* 2013;32(12):717–21. <https://doi.org/10.1089/dna.2013.2127>
  36. Wang D, Zhou D, Du Q, Liang QI, Wang Q, Fang LI, et al. Aberrant production of soluble inducible T-cell co-stimulator (sICOS) and soluble programmed cell death protein 1 (sPD-1) in patients with chronic hepatitis C. *Mol Med Rep.* 2013;7(4):1197–202. <https://doi.org/10.3892/mmr.2013.1326>
  37. Yanaba K, Asano Y, Noda S, Akamata K, Azosa N, Taniguchi T, et al. Increased production of soluble inducible costimulator in patients with diffuse cutaneous systemic sclerosis. *Arch Dermatol Res.* 2013;305(1):17–23. <https://doi.org/10.1007/s00403-012-1292-7>
  38. Moreau P, San Miguel J, Sonneveld P, Mateos MV, Zamagni E, Avet-Loiseau H, et al. Multiple myeloma: ESMO Clinical Practice Guidelines for diagnosis, treatment and follow-up. *Annals Oncol.* 2017;28:iv52–iv61. <https://doi.org/10.1093/annonc/mdx096>
  39. Lin P, Owens R, Tricot G, Wilson CS. Flow cytometric immunophenotypic analysis of 306 cases of multiple myeloma. *Am J Clin Pathol.* 2004;121(4):482–8. <https://doi.org/10.1309/74R4-TB90-BUWH-27JX>
  40. Frigyesi I, Adolfsson J, Ali M, Kronborg Christophersen M, Johnsson E, Turesson I, et al. Robust isolation of malignant plasma cells in multiple myeloma. *Blood.* 2014;123(9):1336–40. <https://doi.org/10.1182/blood-2013-09-529800>
  41. Flores-Montero J, de Tute R, Paiva B, Perez JJ, BoCtcher S, Wind H, et al. Immunophenotype of normal vs. myeloma plasma cells: toward antibody panel specifications for MRD detection in multiple myeloma. *Cytometry B Clin Cytom.* 2016;90(1):61–72. <https://doi.org/10.1002/cyto.b.21265>
  42. Arroz M, Came N, Lin P, Chen W, Yuan C, Lagoo A, et al. Consensus guidelines on plasma cell myeloma minimal residual disease analysis and reporting. *Cytometry B Clin Cytom.* 2016;90(1):31–9. <https://doi.org/10.1002/cyto.b.21228>
  43. Clemente N, Ferrara B, Gigliotti C, Boggio E, Capucchio M, Biasibetti E, et al. Solid lipid nanoparticles carrying temozolomide for melanoma treatment: preliminary in vitro and in vivo studies. *Int J Mol Sci.* 2018;19(2):255. <https://doi.org/10.3390/ijms19020255>
  44. Wang J, Zheng Y, Tu C, Zhang H, Vanderkerken K, Menu E, et al. Identification of the immune checkpoint signature of multiple myeloma using mass cytometry-based single-cell analysis. *Clin Transl Immunol.* 2020;9(5):e01132. <https://doi.org/10.1002/cti2.1132>
  45. Zheng J, Chan P-L, Liu Y, Qin G, Xiang Z, Lam K-T, et al. ICOS regulates the generation and function of human CD4+ Treg in a CTLA-4 dependent manner. *PLoS One.* 2013;8(12):e82203. <https://doi.org/10.1371/journal.pone.0082203>

46. Iwata R, Lee JH, Hayashi M, Dianzani U, Ofune K, Maruyama M, et al. ICOSLG-mediated regulatory T-cell expansion and IL-10 production promote progression of glioblastoma. *Neuro Oncol.* 2020;22(3):333–44. <https://doi.org/10.1093/neuonc/noz204>
47. Amatore F, Laurent Gorvel L, Olive D. Role of inducible co-stimulator (ICOS) in cancer immunotherapy. *Expert Opin Biol Ther.* 2020;20(2):141–50. <https://doi.org/10.1080/14712598.2020.1693540>
48. Lightman SM, Utey A, Lee KP. Survival of long-lived plasma cells (LLPC): piecing together the puzzle. *Front Immunol.* 2019;3(10):965. <https://doi.org/10.3389/fimmu.2019.00965>
49. Winter O, Dame C, Jundt F, Hiepe F. Pathogenic long-lived plasma cells and their survival niches in autoimmunity, malignancy, and allergy. *J Immunol.* 2012;189(11):5105–11. <https://doi.org/10.4049/jimmunol.1202317>
50. Dhodapkar KM, Barbuto S, Matthews P, Kukreja A, Mazumder A, Vesole D, et al. Dendritic cells mediate the induction of polyfunctional human IL17-producing cells (Th17-1 cells) enriched in the bone marrow of patients with myeloma. *Blood.* 2008;112(7):2878–85. <https://doi.org/10.1182/blood-2008-03-143222>
51. Braga WMT, da Silva BR, de Carvalho AC, Maekawa YH, Bortoluzzo AB, Rizzatti EG, et al. FOXP3 and CTLA4 overexpression in multiple myeloma bone marrow as a sign of accumulation of CD4+ T regulatory cells. *Cancer Immunol Immunother.* 2014;63(11):1189–97. <https://doi.org/10.1007/s00262-014-1589-9>
52. Warnatz K, Bossaller L, Salzer U, Skrabl-Baumgartner A, Schwinger W, van der Burg M, et al. Human ICOS deficiency abrogates the germinal center reaction and provides a monogenic model for common variable immunodeficiency. *Blood.* 2006;107(8):3045–52. <https://doi.org/10.1182/blood-2005-07-2955>
53. Dong C, Temann UA, Flavell RA. Cutting edge: critical role of inducible costimulator in germinal center reactions. *J Immunol.* 2001;166(6):3659–62. <https://doi.org/10.4049/jimmunol.166.6.3659>
54. Bonecchi R, Garlanda C, Mantovani A, Riva F. Cytokine decoy and scavenger receptors as key regulators of immunity and inflammation. *Cytokine.* 2016;87:37–45. <https://doi.org/10.1016/j.cyto.2016.06.023>
55. Mantovani A, Locati M, Vecchi A, Sozzani S, Allavena P. Decoy receptors: a strategy to regulate inflammatory cytokines and chemokines. *Trends Immunol.* 2001;22(6):328–36. [https://doi.org/10.1016/s1471-4906\(01\)01941-x](https://doi.org/10.1016/s1471-4906(01)01941-x)
56. Suda T, Hashimoto H, Tanaka M, Ochi T, Nagata S. Membrane Fas ligand kills human peripheral blood T lymphocytes, and soluble Fas ligand blocks the killing. *J Exp Med.* 1997;186(12):2045–50.
57. Schneider P, Holler N, Bodmer JL, Hahne M, Frei K, Fontana A, et al. Conversion of membrane-bound Fas(CD95) ligand to its soluble form is associated with downregulation of its proapoptotic activity and loss of liver toxicity. *J Exp Med.* 1998;187(8):1205–13. <https://doi.org/10.1084/jem.186.12.2045>
58. Levin SD, Evans LS, Bort S, Rickel E, Lewis KE, Wu RP, et al. Novel immunomodulatory proteins generated via directed evolution of variant IgSF domains. *Front Immunol.* 2020;21(10):3086. <https://doi.org/10.3389/fimmu.2019.03086>
59. Chattopadhyay K, Bhatia S, Fiser A, Almo SC, Nathenson SG. Structural basis of inducible costimulator ligand costimulatory function: determination of the cell surface oligomeric state and functional mapping of the receptor binding site of the protein. *J Immunol.* 2006;177(6):3920–9. <https://doi.org/10.4049/jimmunol.177.6.3920>



## Article

# Parenteral Nanoemulsions Loaded with Combined Immuno- and Chemo-Therapy for Melanoma Treatment

Chiara Monge <sup>1,†</sup>, Ian Stoppa <sup>2,†</sup>, Chiara Ferraris <sup>1,3</sup> , Annalisa Bozza <sup>1</sup>, Luigi Battaglia <sup>1,4,\*</sup> , Luigi Cangemi <sup>1</sup>, Gianluca Miglio <sup>1</sup> , Stefania Pizzimenti <sup>5</sup> , Nausicaa Clemente <sup>2</sup> , Casimiro Luca Gigliotti <sup>2</sup> , Elena Boggio <sup>2</sup> , Umberto Dianzani <sup>2,6</sup> and Chiara Dianzani <sup>1</sup>

<sup>1</sup> Dipartimento di Scienza e Tecnologia del Farmaco, Università degli Studi di Torino, via Pietro Giuria 9, 10125 Torino, Italy

<sup>2</sup> Dipartimento di Scienze della Salute, Università del Piemonte Orientale, via Solaroli 17, 28100 Novara, Italy

<sup>3</sup> Dipartimento di Scienze Cliniche e Biologiche, Università degli Studi di Torino, Regione Gonzole 10, 10043 Orbassano, Italy

<sup>4</sup> Nanostructured Interfaces and Surfaces (NIS) Interdepartmental Centre, Università degli Studi di Torino, 10124 Torino, Italy

<sup>5</sup> Dipartimento di Scienze Cliniche e Biologiche, Università degli Studi di Torino, Corso Raffaello 30, 10124 Torino, Italy

<sup>6</sup> Azienda Ospedaliero-Universitaria Maggiore della Carità, Corso Giuseppe Mazzini 18, 28100 Novara, Italy

\* Correspondence: luigi.battaglia@unito.it; Tel.: +39-011-670-7142

† These authors contributed equally to this work.



**Citation:** Monge, C.; Stoppa, I.; Ferraris, C.; Bozza, A.; Battaglia, L.; Cangemi, L.; Miglio, G.; Pizzimenti, S.; Clemente, N.; Gigliotti, C.L.; et al. Parenteral Nanoemulsions Loaded with Combined Immuno- and Chemo-Therapy for Melanoma Treatment. *Nanomaterials* **2022**, *12*, 4233. <https://doi.org/10.3390/nano12234233>

Academic Editor: Jyh-Ping Chen

Received: 20 October 2022

Accepted: 26 November 2022

Published: 28 November 2022

**Publisher's Note:** MDPI stays neutral with regard to jurisdictional claims in published maps and institutional affiliations.



**Copyright:** © 2022 by the authors. Licensee MDPI, Basel, Switzerland. This article is an open access article distributed under the terms and conditions of the Creative Commons Attribution (CC BY) license (<https://creativecommons.org/licenses/by/4.0/>).

**Abstract:** High-grade melanoma remains a major life-threatening illness despite the improvement in therapeutic control that has been achieved by means of targeted therapies and immunotherapies in recent years. This work presents a preclinical-level test of a multi-pronged approach that includes the loading of immunotherapeutic (ICOS-Fc), targeted (sorafenib), and chemotherapeutic (temozolomide) agents within Intralipid<sup>®</sup>, which is a biocompatible nanoemulsion with a long history of safe clinical use for total parenteral nutrition. This drug combination has been shown to inhibit tumor growth and angiogenesis with the involvement of the immune system, and a key role is played by ICOS-Fc. The inhibition of tumor growth in subcutaneous melanoma mouse models has been achieved using sub-therapeutic drug doses, which is most likely the result of the nanoemulsion's targeting properties. If translated to the human setting, this approach should therefore allow therapeutic efficacy to be achieved without increasing the risk of toxic effects.

**Keywords:** Intralipid<sup>®</sup>; ICOS-Fc; combination therapy; melanoma

## 1. Introduction

Therapeutic options for melanoma depend upon disease staging. The surgical removal of a primary tumor is normally practiced in the case of early-stage disease (0–IIA). In stage IIB/C (tumor thickness > 2.0 mm) and stage III, adjuvant chemotherapies are practiced following surgery. Dacarbazine, the standard chemotherapy for stage IV (metastatic) melanoma up to 2011, is simply a palliative care treatment [1]. Temozolomide (TMZ) is an alternative treatment as it can reach the central nervous system (CNS) to treat brain metastases [2]. New pharmacological agents have recently been approved. Since half of the total melanomas show the V-raf murine sarcoma viral oncogene homolog B1 (BRAF) mutation, they may respond to targeted therapies with BRAF (vemurafenib, dabrafenib, encorafenib) and/or mitogen-activated protein kinase (MEK) inhibitors (trametinib, cobimetinib, binimetinib). Moreover, melanomas respond to immunotherapy with monoclonal antibodies that block the immune checkpoint receptors cytotoxic T-lymphocyte antigen 4 (CTLA4), such as ipilimumab, and programmed cell death protein 1 (PD1), such as pembrolizumab and nivolumab [1]. Indeed, melanoma is one of the most immunogenic tumors and its relationship with the host immune system is currently under investigation [3].

Besides immunotherapy with CTLA4 and PD1 inhibitors, we have recently reported the efficacy of targeting the inducible T-cell co-stimulator (ICOS)/ICOS ligand (ICOS-L) dyad in mouse models of melanoma [4]. ICOS [5–7] is an immune checkpoint protein, mainly present on activated T cells, that belongs to the cluster of differentiation 28 (CD28) family, with members such as CTLA4 and PD1. ICOS-L (or B7h) is its natural ligand, and is expressed by several cell types, such as B cells, macrophages, dendritic cells (DC), endothelial cells (EC), epithelial cells, fibroblasts, and several types of tumor cells. However, while CTLA4 and PD1 exert inhibitory functions on T cells, CD28 and ICOS trigger co-stimulatory signals. Indeed, the triggering of ICOS by ICOS-L co-stimulates T cells in inflamed tissues by modulating cytokine secretion from T helper cells, the cytotoxic activity of T cells, and the regulatory development of regulatory T cells [8,9]. On the other hand, the triggering of ICOS-L by ICOS inhibits the migration of vascular EC, DC, and tumor cells, as well as tumor metastatization in vivo [10,11]. In the tumor microenvironment, ICOS-L is expressed by several types of immune cells, by EC, and often by tumor cells, whereas ICOS is expressed by infiltrating T cells. We have recently found that the growth of established mouse melanoma is inhibited by treatment with ICOS-Fc, a recombinant water-soluble ICOS protein, when it is loaded into either biocompatible poly(lactic-co-glycolic acid) (PLGA) or cyclodextrin nanoparticles, which are able to target the drug to the tumor mass [4]. The main effect of ICOS-Fc is the inhibition of tumor angiogenesis, which is accompanied by variable immuno-regulatory activities, depending on the nanoparticle vector, and by direct effects on tumor cells, which are mainly detectable in vitro. Intriguingly, ICOS-L can also bind osteopontin (OPN), which is a well-known pro-neoplastic factor. Triggering of ICOS-L by OPN stimulates angiogenesis and tumor cell migration, whereas ICOS exerts a dominant negative effect on these activities [12]. Moreover, the ICOS/ICOS-L dyad may even play a role in anti-CTLA4 monoclonal antibody (mAb) anti-tumor activity, which results in an expansion of ICOS<sup>+</sup> effector T cells, while its effect is significantly decreased in ICOS<sup>-/-</sup> mice [13].

Nonetheless, despite significant therapeutic advancements, malignant melanoma remains an aggressive and resistant tumor with unpredictable responses to chemotherapy, making it a major health challenge [1]. Targeted therapies are hampered by chemoresistance [14], while the response to immunotherapy strictly correlates to tumor-mutation burden [15–17]. Therefore, a multi-pronged approach that can target melanoma proliferation, angiogenesis, and chemoresistance should be practiced, concurrently to immunotherapy, to improve therapeutic efficacy. We have recently shown that combinations of drugs against melanoma can be loaded into nanoemulsions for total parenteral nutrition, namely Intralipid® 10% (IL), and that the combinations are effective in an in vivo mouse model of melanoma [18]. Specifically, a combination of drugs, including tumor proliferation (TMZ), angiogenesis (bevacizumab), and mTOR inhibitors (rapamycin), was loaded into IL and tested on available cell and animal models. Despite the promising results obtained, a strong dependence on rapamycin dose was observed as the relevant in vivo tumor inhibition was only achieved at a high dose of this drug. This poses a concern for human translation. Indeed, besides synergism between drugs, the rationale for anti-cancer drug combinations focuses on reducing the dose of each component to prevent side effects.

Hence, in the present work, we have optimized an innovative drug combination, which, after loading into IL, may be capable of acting at sub-therapeutic doses of each single component. To this aim, while TMZ was maintained as the main cytotoxic agent, the immune system was involved in the drug combination, unlike in our previous study, by including ICOS-Fc, capable to act on both the immune response and the tumor microenvironment. Since ICOS-Fc would not be compatible with the anti-angiogenic monoclonal antibody, bevacizumab, as they would exceed the maximum protein loading in the IL oil droplets, the new formulation included sorafenib (SOR), loaded into IL instead of rapamycin and bevacizumab, to counteract angiogenesis, which plays a key role in melanoma development. Indeed, SOR is a multi-kinase inhibitor that can exert anti-proliferative activity by inhibiting various intracellular, rapidly accelerated fibrosarcoma (RAF) kinases,

including BRAF. As previously mentioned, targeted therapies for melanoma currently make use of selective BRAF inhibitors (such as vemurafenib), due to the specific melanoma mutational burden, but suffer from the significant limitation of chemoresistance. SOR displays broader anti-angiogenic activity than these compounds as it blocks the vascular endothelial growth factor receptor (VEGFR) with high affinity and at low therapeutic doses, as well as activating the immune response. It has also already been tested for melanoma treatment in combination with TMZ [19–21].

## 2. Experimental

### 2.1. Materials

#### 2.1.1. Chemicals

IL 10% was obtained from Fresenius Kabi (Bad Homburg, Germany). The 3-(4,5-dimethyl thiazol-2-yl)-2,5-diphenyltetrazolium bromide (MTT), 60,000–90,000 MW dextran, acetonitrile, crystal violet, dichloromethane, dimethylformamide (DMF), dimethylsulfoxide (DMSO), polystyrene sulfonate (PS), TMZ, and the TRizol reagent were obtained from Sigma-Aldrich (St. Louis, MO, USA). Ethyl acetate, phosphotungstic acid, silica gel, and sodium docusate (AOT) were obtained from Merck (Darmstadt, Germany). Agarose CL 4B, isopropanol, triethylamine, and trifluoroacetic acid (TFA) were obtained from Alfa-Aesar (Haverhill, MA, USA). Acetic acid, bromododecane, and sodium nitrite were obtained from Carlo Erba (Val De Reuil, France). SOR was obtained from LcLabs (Woburn, MA, USA). Sulfuric acid was obtained from Fluka (Buchs, Switzerland). ICOS-Fc was obtained from Novacos (Novara, Italy). Kolliphor® EL was a kind gift from BASF (Ludwigshafen am Rhein, Germany).

Matrigel was obtained from BD Biosciences (San Jose, CA, USA). Polyclonal rabbit anti-cluster of differentiation 31 (CD31) was obtained from Abcam (Cambridge, UK). Monoclonal mouse anti-human Kiel original clone 67 (Ki-67) antigen was obtained from Thermo Fisher Scientific (Waltham, MA, USA). The QuantiTect Reverse Transcription Kit was obtained from Qiagen (Hilden, Germany). The TaqMan gene expression Assay-on-Demand and TaqMan Universal PCR Master Mix were obtained from Applied Biosystems (Foster City, CA, USA). The CFX96 System was obtained from Bio-Rad Laboratories (Hercules, CA, USA).

#### 2.1.2. Cells

A2058 and M14 human melanoma cells and B16-F10 murine melanoma cells were purchased from the American Type Culture Collection (ATCC; Manassas, VA, USA). D4M cells, a mouse melanoma engineered cell line harboring the BRAF<sup>V600E</sup> mutation, were a gift from D.W. Mullis, Department of Medicine, Norris Cotton Cancer Center, Geisel School of Medicine at Dartmouth, Lebanon, NH, USA. M14 and B16-F10 cells were cultured in Roswell Park Memorial Institute 1640 medium (RPMI 1640; Sigma-Aldrich, St. Louis, MO, USA), while A2058 and D4M were cultured in Dulbecco's Modified Eagle Medium (DMEM; Sigma-Aldrich, St. Louis, MO, USA). All culture media were supplemented with 10% fetal calf serum (FCS; PAA Laboratories, Pasching, Austria), penicillin/streptomycin (100 units/mL), and L-glutamine (2 mmol/L) (both from Sigma-Aldrich, St. Louis, MO, USA). Cell lines were cultured in a 5% CO<sub>2</sub>, 37 °C incubator.

#### 2.1.3. Animals

C57BL/6J mice were obtained from The Jackson Laboratory (Bar Harbor, ME, USA) and were then bred under pathogen-free conditions in the animal facility of the University of Piemonte Orientale, Department of Health Sciences (Authorization No. 61/2005-A – 6 May 2005, issued by the General Directorate of Veterinary and Food Health – Italian Ministry of Health). Experiments were performed using female, 6-to-9-week-old C57BL/6J mice that were treated in accordance with the University Ethical Committee and European guidelines (Experimental protocol authorization No. 241/2022-PR, released on the 15-04-2022 by the Italian Ministry of Health for protocol No. DB064.76).

## 2.2. Preparation of Formulations under Study

### 2.2.1. Prodrug Synthesis

A lipophilic TMZ dodecyl ester (TMZ-C12) was synthesized, in accordance with the literature [18,22,23].

### 2.2.2. Formulation of Drug Combination-Loaded IL

The combination of drugs (IL MIX) was loaded into IL 10% in accordance with the following procedure. pH = 3.0 buffer citrate 0.1 M (40  $\mu$ L) was first added to 1.6 mL of IL. Then, 1.2 mg of TMZ-C12 was dissolved in 80  $\mu$ L of DMF, together with 0.5 mg of SOR, and this solution was added dropwise to IL. Subsequently, 96  $\mu$ L of the AOT stock solution (4.5 mg/mL – 10.1 mM) and variable amounts of the ICOS-Fc stock solutions (either 286  $\mu$ L of 1.75 mg/mL human ICOS-Fc, or 302  $\mu$ L of 1.65 mg/mL mouse ICOS-Fc) were added to IL, forming an ion pair [18,24] at a 1:150 AOT-ICOS-Fc molar ratio. The final drug concentrations in IL were: 0.6 mg/mL (1.65 mM) TMZ-C12, 0.25 mg/mL (0.54 mM) SOR, and 0.25 mg/mL (3.2  $\mu$ M) ICOS-Fc. PS was used as the de-bridging agent exclusively in the case of the formulation of IL MIX with human ICOS-Fc. To this aim, 100  $\mu$ L of a 10 mg/mL PS solution in water was added to avoid droplet aggregation (Figure 1). Human ICOS-Fc was used for in vitro studies on human cell lines (M14, A2058). Mouse ICOS-Fc was used for in vitro studies on mouse cell lines (B16, D4M) and for animal experiments.

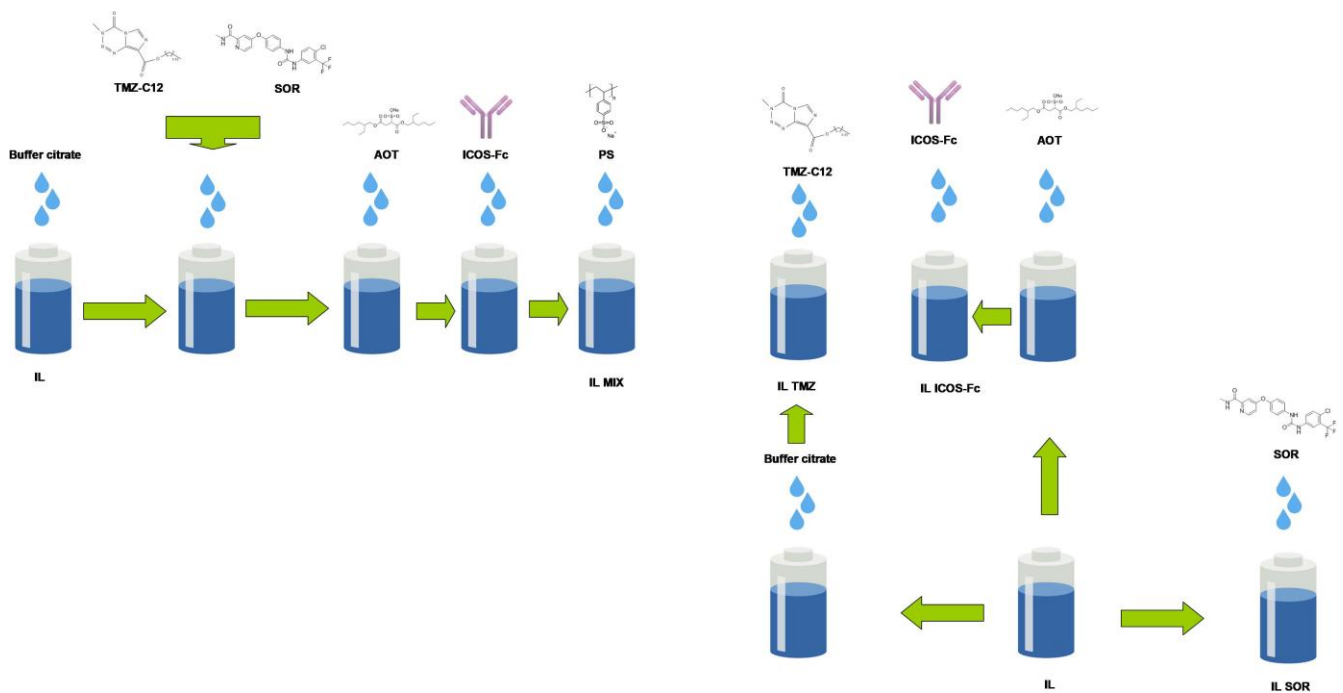


**Figure 1.** Flowchart of the preparation of the drug-loaded nanoemulsions. Abbreviations: AOT: sodium docusate; IL: Intralipid<sup>®</sup> 10%; SOR: sorafenib; TMZ-C12: temozolomide dodecyl ester; MIX: drug combination (temozolomide dodecyl ester, sorafenib, ICOS-Fc); PS: polystyrene sulfonate.

### 2.2.3. Preparation of Control Formulations

The following IL-based controls were used for cell studies: IL TMZ-C12, IL SOR, and IL ICOS-Fc (Figure 1). IL ICOS-Fc was also prepared using a 10-fold lower ICOS-Fc dose (0.025 mg/mL – 0.32  $\mu$ M) for use exclusively in in vitro cell migration experiments. The free-drug solution controls were: free TMZ, dissolved in DMF (6 mg/mL – 31.2 mM), free SOR, dissolved in DMSO (5 mg/mL – 10.8 mM), and free ICOS-Fc mg/mL, dissolved in water (1.75 mg/mL – 22.4  $\mu$ M for human ICOS-Fc; 1.65 mg/mL – 22.1  $\mu$ M for murine ICOS-Fc). A mixture of the free drugs (MIX) was obtained impromptu from the single stock solutions.

The free MIX for the animal experiments was prepared as follows: SOR (0.25 mg/mL – 0.54 mM) was dissolved in Kolliphor® EL/ethanol/normal saline (1:1:6 volume ratio), with mouse ICOS-Fc being added to a final concentration of 0.25 mg/mL (3.2 µM) and TMZ powder being added to the formulation prior to use (0.32 mg/mL – 1.65 µM) in order to avoid pH-dependent degradation.

### 2.3. Characterization of Formulations

#### 2.3.1. Determination of Droplet Size, Morphology, and Zeta Potential

The dynamic light scattering technique (DLS; 90 Plus, Brookhaven, NY, USA) was used to determine the mean droplet size, polydispersity index (PDI), and Zeta potential of the IL-based formulations, at 25 °C and in triplicate. Measurement angles were 90° for particle size and 15° for Zeta potential. Transmission electron microscopy (TEM; High-Resolution JEOL 300 kV) was used via IL-negative staining with 1% phosphotungstic acid [18,25].

#### 2.3.2. Determination of Drug Recovery and Entrapment Efficiency

Drug recovery, defined as the ratio between the actual and theoretical drug concentrations, was determined by high-pressure liquid chromatography (HPLC) [18]. TMZ-C12 and SOR were extracted via the dilution of 50 µL of IL-based formulations in 100 µL of acetonitrile under a vortex, and centrifuging at 14,000 rpm (Allegra 64R centrifuge, Beckman Coulter, Brea, CA, USA). To extract the ICOS-Fc-AOT ion pair, the precipitate obtained in the previous step was dissolved in 100 µL of acetic acid, and lipids were precipitated with 50 µL of water (14,000 rpm centrifugation). Since PS interferes with the HPLC detection of ICOS-Fc, the recovery of IL MIX that was formulated with human ICOS-Fc was determined prior to its addition as the de-bridging agent. Drug entrapment efficiency (EE%), defined as the ratio between the drug amount entrapped in the lipid matrix and the total drug amount in the nanoemulsion, was assessed for each single therapeutic agent either after size exclusion with Agarose CL 4B, or after gradient centrifugation with 30% 60,000–90,000 MW dextran.

#### 2.3.3. HPLC Analysis of MIX

HPLC analyses were performed by modifying a literature method [18,26]. The HPLC system was composed of a YL9110 quaternary pump, a YL9101 vacuum degasser, and a YL9160 photo diode array (PDA) detector, linked to YL-Clarity software for data analysis (Young Lin, Hogyedong, Anyang, Korea). The column was a 300 nm pore size C8 Tracer Excel, 25 × 0.4 cm (Teknokroma, Barcelona, Spain). A gradient was performed at 75 °C and using a 1 mL/min flow rate between eluent A (0.1% TFA) and eluent B (79% isopropanol, 20% acetonitrile, 10% water, 0.1% TFA): 0 min–90% A; 15 min–40% A; 24 min–40% A; 27 min–90% A. The PDA wavelengths were 220 nm (ICOS-Fc), 265 nm (SOR), and 329 nm (TMZ-C12), and the retention times were 11.3 min for ICOS-Fc, 16.2 min for SOR, and 20.6 min for TMZ-C12.

### 2.4. Cytotoxicity: MTT Assay

Cells ( $1 \times 10^3$ /well) were seeded in 96-well plates for 24 h and then treated with the formulations under study. Viability was assessed via an MTT assay at 72 h, according to the manufacturer's instructions. Four replicates were performed in five separate experiments.

### 2.5. Proliferation: Clonogenic Assay

The B16, D4M, M14, and A2058 melanoma cell lines ( $8 \times 10^2$ /well) were seeded into six-well plates. After 24 h, cells were treated with the formulations under study for 3 h. Afterwards, the medium was changed, and cells were cultured in drug-free medium for an additional 7 days. The clonogenic assay was then performed as previously described [18].

### 2.6. Invasion: Boyden Chamber Assay

Preliminary experiments were performed to identify non-toxic drug concentrations. B16, D4M, M14, and A2058 melanoma cells ( $8 \times 10^3$ ) were seeded into 96-well plates and treated for 6 h with the formulations under study. Cell viability was assessed using the Crystal Violet assay, as previously described [18]. Melanoma cells ( $2 \times 10^3$ ) were then plated onto the apical side of a Boyden chamber with filters (0.5  $\mu\text{m}$  pore size and 8.2 mm diameter) that were coated with 50  $\mu\text{g}/\text{mL}$  of Matrigel in serum-free medium. The cells were then either treated with non-toxic concentrations (as previously assessed) of the formulations under study or left untreated. The Boyden chamber-invasion assay was performed as previously described [18].

### 2.7. SOR Release from IL and Internalization into Melanoma Cells

#### 2.7.1. SOR Release from IL

Here, 1 mL of IL SOR was diluted in 4 mL of RPMI under magnetic stirring. At scheduled times, 0.5 mL of the mixture was withdrawn and centrifuged at 25,000 rpm (Allegra 64R centrifuge, Beckman Coulter, Brea, CA, USA), and the obtained supernatant was injected into the HPLC system. The SOR amount that was still present in the lipid matrix at the end of the experiment was assessed via extraction from the centrifuged lipid pellet. Briefly, the pellet was dissolved in 0.5 mL of acetonitrile and the lipid was precipitated with 0.5 mL of water, followed by centrifugation at 25,000 rpm (Allegra 64R centrifuge, Beckman Coulter, Brea, CA, USA).

#### 2.7.2. SOR Internalization in Melanoma Cells

Briefly, 1  $\mu\text{L}$  of free SOR and, separately, 20  $\mu\text{L}$  of IL SOR were diluted in 1 mL of RPMI, with and without FCS, containing  $5 \times 10^3$  melanoma cells. After 3 h of incubation, the cells were isolated by centrifugation and the pellet obtained was extracted using 50  $\mu\text{L}$  of methanol, prior to injection into the HPLC system.

#### 2.7.3. HPLC Analysis of SOR

A Jasco PU 1580 pump and a C18 Beckmann ODS  $25 \times 0.5$  cm column were used. The mobile phase, acetonitrile/water 65:35, was delivered at a flow rate of 1 mL/min. The Jasco UV 1575 UV-visible detector was set at  $\lambda$  264 nm, and the calibration curve ranged between 2.5 and 0.25  $\mu\text{g}/\text{mL}$  ( $R^2 = 0.9994$ , CV = 0.070, LOD = 2.80 ng/mL, LOQ = 9.34 ng/mL).

### 2.8. Animal Experiments

B16-F10 melanoma cells were injected subcutaneously ( $1 \times 10^5$  in 100  $\mu\text{L}/\text{mouse}$ ), and tumor growth was monitored every two days. Ten days after tumor induction, the mice were divided into different groups (five mice each; T0) and either treated, via i.v. injection, with the formulations under study, or with the same volume of phosphate-buffered saline (PBS), used as a control. Mice were treated three times a week for two weeks (six i.v./mouse, T1 to T6) and sacrificed three days after the last injection (Tend), or immediately after they displayed suffering. In each treatment, drug doses were: TMZ 1.5 mg/kg, SOR 1.25 mg/kg, and ICOS-Fc 1.25 mg/kg. Tumor volume was monitored over the treatment period and the final tumor mass and volume were measured at the end of the experiment, after animal sacrifice.

### 2.9. Immunohistochemistry of Tumor Specimens

The immunohistochemical analyses of CD31, an EC marker used to assess tumor micro-vessel density (TMD), and Ki-67, a marker of proliferating cells, were performed in animal-tumor specimens, as previously described [18].

### 2.10. Real-Time Polymerase Chain Reaction (PCR) of Tumors

Ribonucleic acid (RNA) was obtained from snap-frozen tumors, using the TRIzol reagent. Then, 1  $\mu\text{g}$  of RNA was retrotranscribed to cDNA using the QuantiTect Re-



verse Transcription Kit. Interferon- $\gamma$  (IFN- $\gamma$ ), interleukin-1 $\beta$  (IL-1 $\beta$ ), interleukin-6 (IL-6), interleukin-10 (IL-10), and tumor necrosis factor- $\alpha$  (TNF- $\alpha$ ) expression were evaluated using a TaqMan gene expression assay. The complementary deoxyribonucleic acid (cDNA) amounts were normalized using the  $\beta$ -actin gene. Real-time PCR was performed on a CFX96 System and samples were run in duplicate in a 10  $\mu$ L final volume that contained 1  $\mu$ L of diluted cDNA, 5  $\mu$ L of TaqMan Universal PCR Master Mix, and 0.5  $\mu$ L of Assay-on-Demand mix. Relative gene expression was calculated using the  $\Delta\Delta$  threshold cycle method.

### Statistical Analysis

Data are presented as mean  $\pm$  SEM. Statistical analyses were performed using Prism 3.0 software (GraphPad Software, La Jolla, CA, USA) by means of one-way ANOVA and the Dunnett's test.

## 3. Results

### 3.1. Characterization of Formulations

Table 1 shows the characterization of the IL-based formulations. TMZ was loaded into the lipid matrix by means of its ester prodrug, which also increases its stability in biological fluids, preventing premature imidazotetrazine ring-opening at neutral pH [18,27]. ICOS-Fc is a high-molecular-weight and hydrophilic protein that was associated with the lipid matrix via ion pairing with AOT [18,24]. However, in some cases, the high density of positively charged amino groups on the ICOS-Fc molecule can cause the negatively charged IL droplets to aggregate, especially when the combination of drugs is loaded together with ICOS-Fc in the lipid matrix, meaning that PS was added, as a de-bridging agent, to the IL MIX formulation with human ICOS-Fc.

**Table 1.** Characterization of Intralipid<sup>®</sup> (IL)-based formulations. Abbreviations: EE%: % entrapment efficiency; MIX: drug combination (temozolomide dodecyl ester, sorafenib, ICOS-Fc); N.D.: not determined; PS: polystyrene sulfonate; SOR: sorafenib; TMZ-C12: temozolomide dodecyl ester.

	Mean Size (nm)	Polydispersity	Z Potential (mV)	Recovery %	EE %	
					Size Exclusion	Dextran Gradient
IL MIX (human ICOS-Fc)	279.9 $\pm$ 3.0	0.146	-28.50 $\pm$ 3.35	TMZ-C12: 94.0 $\pm$ 8.0 SOR: 96.1 $\pm$ 6.0 ICOS-Fc: 106.3 $\pm$ 11.7	TMZ-C12: 95.9 SOR: 84.6	TMZ-C12: 94 SOR: 74
IL MIX (human ICOS-Fc low dose)	269.3 $\pm$ 10.1	0.025	-29.41 $\pm$ 3.06	TMZ-C12: 100 $\pm$ 5.1 $\pm$ SOR: 91 6.7 ICOS-Fc: N.D.	N.D.	N.D.
IL MIX (mouse ICOS-Fc)	270.2 $\pm$ 2.1	0.099	-39.08 $\pm$ 3.69	TMZ-C12: 99 $\pm$ 11.1 SOR: 119 $\pm$ 11.8 ICOS-Fc: 107 $\pm$ 21.4	N.D.	N.D.
IL MIX without ICOS-Fc	257.6 $\pm$ 5.0	0.129	-33.58 $\pm$ 3.03	SOR: 105 $\pm$ 6.0 TMZ-C12: 91 $\pm$ 6.5	N.D.	N.D.
IL TMZ-C12	275.0 $\pm$ 0.7	0.003	-39.52 $\pm$ 7.22	68 $\pm$ 5.0	N.D.	N.D.
IL SOR	262.6 $\pm$ 1.2	0.071	-20.72 $\pm$ 1.91	102.7 $\pm$ 11.7	N.D.	N.D.
IL mouse ICOS-Fc	348.3 $\pm$ 6.1	0.142	-33.17 $\pm$ 4.5	116 $\pm$ 10.2	47	97
IL human ICOS-Fc	265.6 $\pm$ 1.6	0.028	-26.79 $\pm$ 3.40	78 $\pm$ 9.8	55.4	97
IL human ICOS-Fc (+PS)	262.0 $\pm$ 3.7	0.050	-48.08 $\pm$ 8.47	88.7 $\pm$ 9.3	N.D.	N.D.
IL human ICOS-Fc low concentration	244.6 $\pm$ 18.0	0.051	-15.72 $\pm$ 1.83	N.D.	N.D.	N.D.
Blank IL	290.0 $\pm$ 1.9	0.005	-39.53 $\pm$ 2.07	N.D.	N.D.	N.D.

Overall, the drug combination was efficiently loaded into the lipid matrix without relevant changes in mean IL droplet size. The EE% of ICOS-Fc was determined exclusively on IL ICOS-Fc in the absence of PS, which would prevent the HPLC detection of the protein, as previously reported. The loading of SOR, whether alone or used in combination, led to a reduction in the Zeta potential absolute value, and this is probably due to the amino group

present in the compound. The same occurred with ICOS-Fc, and this is probably caused by the excess amino groups of the protein that are exposed on the IL surface. However, the original Zeta potential was restored when the negatively charged PS was added as a de-bridging agent.

The loading of ICOS-Fc was further investigated by TEM (Figure 2). The presence of condensed material on the surface of the IL droplets may be attributed to the ion-paired protein that is loaded into IL, as shown in a previous work by our research group [18].

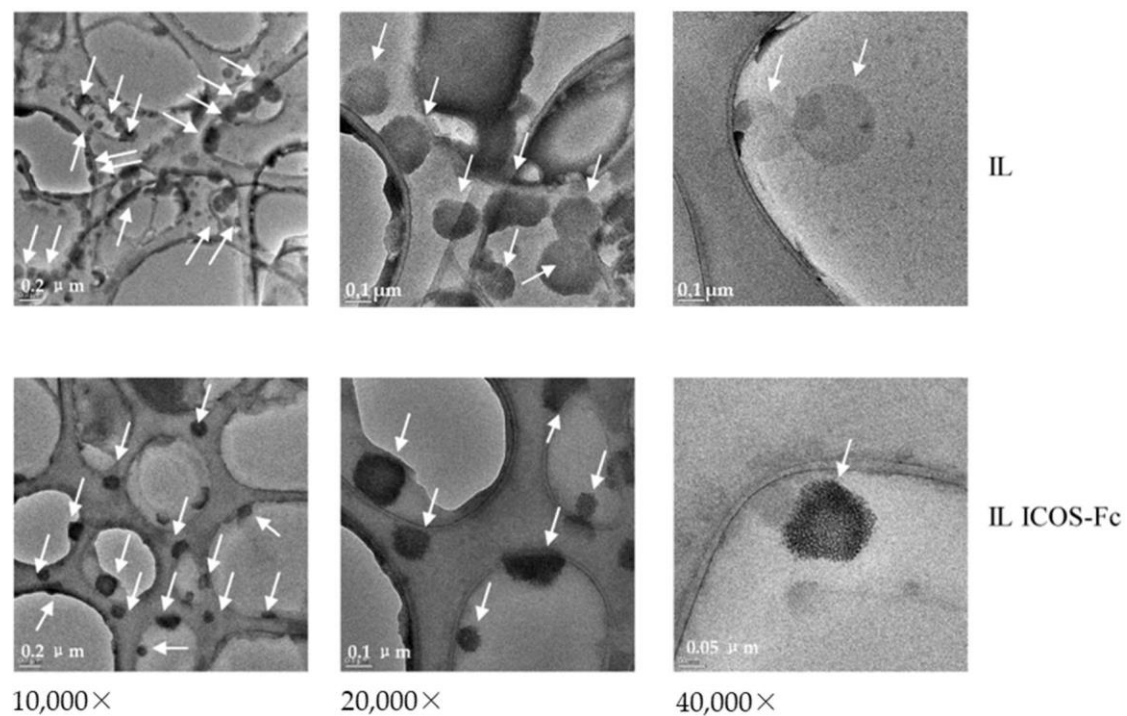


**Figure 2.** Transmission electron microscopy (TEM) images of Intralipid® (IL) and ICOS-Fc-loaded IL.

### 3.2. In Vitro Studies

To preliminarily assess the biological effects of the IL formulations, we evaluated the effect on cell viability assessed by the MTT (Figure 3) and clonogenic (Figure 4) assays using the B16, D4M, M14, and A2058 cell lines, and on cell invasion (Figure 5) using B16 and D4M cells. The ICOS-Fc control (low concentration) was only included in the invasion experiments (Figure 5) since it is known not to affect cell viability (MTT—Figure 3, clonogenic assay—Figure 4).

The comparison between the activity of free drugs and that of the corresponding IL-loaded ones showed that IL loading always increased the inhibitory effect on cell invasion. In contrast, the effect on cell toxicity (i.e., inhibition of cell viability) was variable using the different drugs, cell lines, and assays. Compared to free drug, IL SOR decreased the cell toxicity detected by MTT in all the cell lines, whereas in B16 and D4M (mouse cell lines), it increased that detected by the clonogenic assay. IL loading increased TMZ cell toxicity in all the cell lines, even if in D4M and A2058 a less pronounced effect was detected by the MTT compared to the clonogenic assay. IL loading of MIX increased the cell toxicity detected by the clonogenic assay in all the cell lines, except in M14, where it showed no effect; while, with MTT, it increased cell toxicity only in M14, displaying the opposite effect in the other cells. In the MTT assay, an additive effect between IL SOR and IL TMZ could be hypothesized for IL MIX on M14 cells, since this is the only cell line where IL SOR exerts a relevant cytotoxic effect.

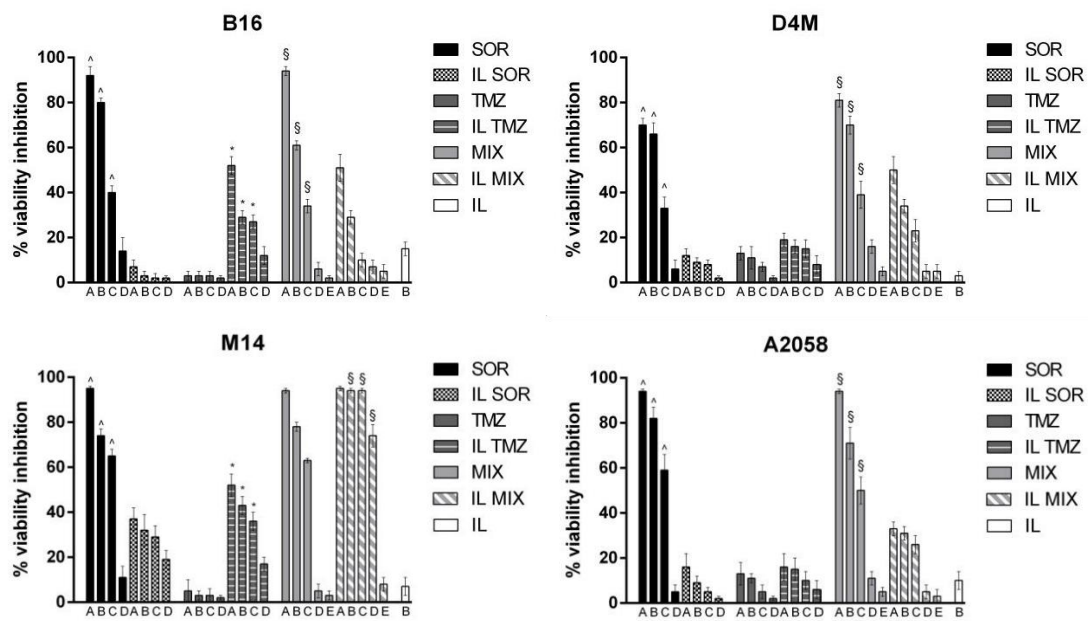


**Figure 3.** MTT assay performed after 72 h of incubation with the formulations under study. B16 cells: upper left panel; D4M cells: upper right panel; M14 cells: lower left panel; A2058 cells: lower right panel. Abbreviations: IL: Intralipid® 10%; SOR: sorafenib; TMZ: temozolomide; MIX: drug combination (temozolomide dodecyl ester, sorafenib, ICOS-Fc). Concentrations employed: SOR A = 16 µM; B = 10 µM; C = 8 µM; D = 4.5 µM; E = 0.8 µM. TMZ A = 48 µM; B = 32 µM; C = 24 µM; D = 16 µM; E = 2.4 µM. Statistical analysis: ^  $p < 0.05$  SOR vs. IL SOR; \*  $p < 0.05$  TMZ vs. IL TMZ; §  $p < 0.05$  MIX vs. IL MIX.

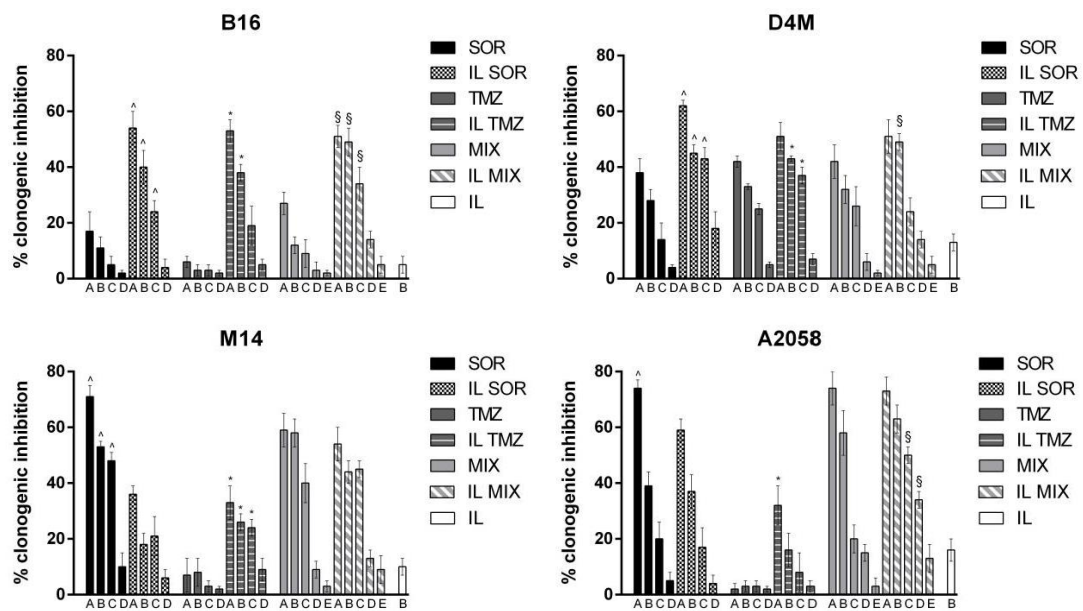


**Figure 4.** Clonogenic assay with B16 (upper left panel), D4M (upper right panel), M14 (lower left panel), and A2058 (lower right panel) melanoma cells. Abbreviations: IL: Intralipid® 10%; SOR: sorafenib; TMZ: temozolomide; MIX: drug combination (temozolomide dodecyl ester, sorafenib, ICOS-Fc). Cells were treated with the formulations under study for 3 h. Afterwards, the medium was changed, and cells were cultured in drug-free medium for an additional 7 days. Concentrations employed: SOR A = 16 µM; B = 10 µM; C = 8 µM; D = 4.5 µM; E = 0.8 µM. TMZ A = 48 µM; B = 32 µM; C = 24 µM; D = 16 µM; E = 2.4 µM. Statistical analysis: ^  $p < 0.05$  SOR vs. IL SOR; \*  $p < 0.05$  TMZ vs. IL TMZ; §  $p < 0.05$  MIX vs. IL MIX.

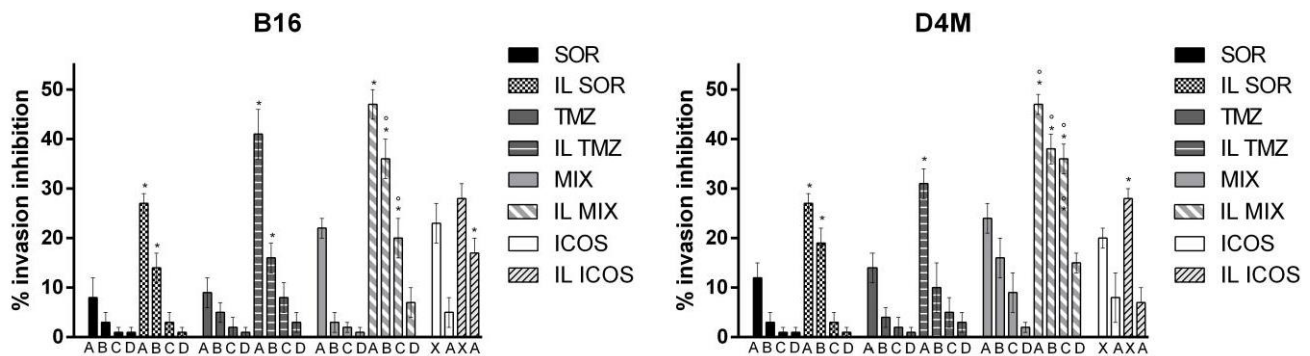


**Figure 5.** Migration assay with B16 (left panel) and D4M (right panel) melanoma cells. Abbreviations: IL: Intralipid® 10%; SOR: sorafenib; TMZ: temozolomide; MIX: drug combination (temozolomide dodecyl ester, sorafenib, ICOS-Fc). Concentrations employed: SOR A = 16  $\mu$ M; B = 10  $\mu$ M; C = 8  $\mu$ M; D = 4.5  $\mu$ M. TMZ A = 48  $\mu$ M; B = 32  $\mu$ M; C = 24  $\mu$ M; D = 16  $\mu$ M. ICOS X = 2  $\mu$ g/mL; A = 0.5  $\mu$ g/mL. Statistical analysis: \*  $p < 0.05$  IL-loaded vs. free; °  $p < 0.05$  additive effect between drugs.

Considering that interpreting the effect of IL MIX is complex, because it is influenced by the single drugs and the carrier, besides the cell phenotype, the most controversial results came from SOR-based formulations. This evidence further drove our investigations into the SOR mechanism of action. Release experiments in cell culture medium showed the unexpected profile that is depicted in Figure 6a. After an initial burst release, drug concentration decreased over time in the release medium. This cannot be ascribed to drug degradation, as the compound that was missing from the release medium was recovered in the lipid pellet obtained after centrifugation. Indeed, it appears that competition occurs between the release medium and the lipid matrix of IL. The internalization studies in melanoma cell lines (Figure 6b) showed that FCS strongly inhibited the internalization of free SOR, while it was ineffective on IL SOR. Moreover, IL SOR internalization was lower than that of free SOR, and this is probably because IL has an entry mechanism that is subject to saturation.

The mechanism depicted in Figure 6c may therefore be hypothesized. IL SOR internalization might be limited by a saturation-like effect, thus reducing the total SOR internalized within the cell, leading to reduced cytotoxic action (MTT assay), that is mediated exclusively by the inhibition of intracellular RAF kinases. On the other hand, extracellular SOR acts on receptor tyrosine kinases (RTK), which are located on the cell membrane and are responsible for angiogenesis and migration processes [28]. In the case of cell membrane-associated RTK, the availability of extracellular SOR in the culture medium is lowered by interactions with proteins, such as those of FCS [29,30]. When SOR is loaded into IL, competition is established between the lipid matrix and the culture medium, preventing SOR from protein sequestration and inactivation effects, thus resulting in more pronounced migration inhibition. The clonogenic assay, instead, entails the proliferation process, which is regulated, to various extents, by both RAF kinases and RTK, and this probably accounts for the variable results obtained among cell lines. In this case, the most striking differences were found between mouse (B16 and D4M) and human (M14 and A2058) cell lines, whose cellular targets (that is RAF kinases and RTK) could probably show different sensitivities to SOR.

These considerations suggest that the variable results obtained in the cell experiments with IL SOR may be ascribable to the experimental setting, rather than to the formulation itself.

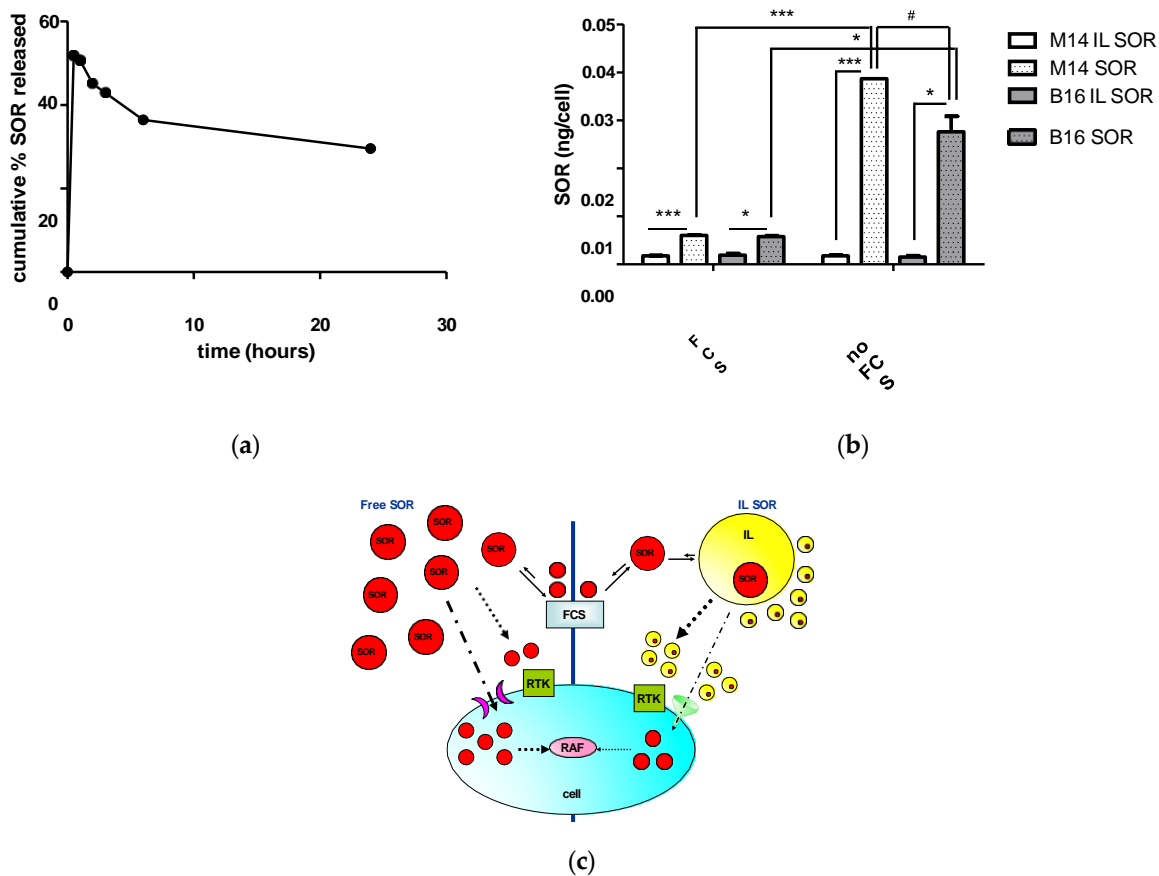


**Figure 6.** Hypothesized sorafenib (SOR) mechanism of action: (a) SOR release profile in culture medium, and (b) SOR internalization migration assay (B16, M14 melanoma cells): \*\*\*  $p < 0.005$ , \*  $p < 0.05$ , #  $p < 0.01$ . (c) Hypothesized cellular pathways. Abbreviations: FCS: fetal calf serum; IL: Intralipid® 10%; RAF: rapidly accelerated fibrosarcoma kinases; RTK: receptor tyrosine kinases.

### 3.3. In Vivo Studies

Animal experiments were performed by comparing the growth inhibition of IL MIX and free MIX on the established subcutaneous B16-F10 melanoma mouse model. Moreover, an animal group treated with IL ICOS-Fc was also included to clarify the contribution of immunotherapy to the total therapeutic effect.

The results (Figure 7) show that only IL MIX was able to significantly reduce tumor volume and the mitotic index (Ki67), compared to the control animals. In contrast, tumor angiogenesis (CD31) was also decreased in animals treated with IL ICOS-Fc. Moreover, only treatment with IL MIX altered the cytokine expression pattern, inducing significant increases in IFN- $\gamma$ , IL-1 $\beta$ , IL-6, and IL-10, while no effect on TNF- $\alpha$  was measured. No substantial toxicity was detected in analyses of the target organs, except for a slight increase in spleen weights for all the treated groups (Table 2).

**Table 2.** Animal experiments (I): organ weights (grams). Abbreviations: CTR: control; IL: Intralipid®; MIX: drug combination (temozolomide dodecyl ester, sorafenib, ICOS-Fc).

	Liver	Spleen	Kidneys	Lungs	Heart
CTR	1.07 ± 0.06	0.13 ± 0.01	0.25 ± 0.02	0.18 ± 0.03	0.14 ± 0.02
MIX	1.05 ± 0.08	0.25 ± 0.04	0.24 ± 0.00	0.15 ± 0.01	0.15 ± 0.03
IL MIX	0.91 ± 0.07	0.17 ± 0.05	0.22 ± 0.01	0.16 ± 0.01	0.12 ± 0.01
IL ICOS-Fc	1.00 ± 0.06	0.27 ± 0.04	0.22 ± 0.00	0.17 ± 0.01	0.15 ± 0.01

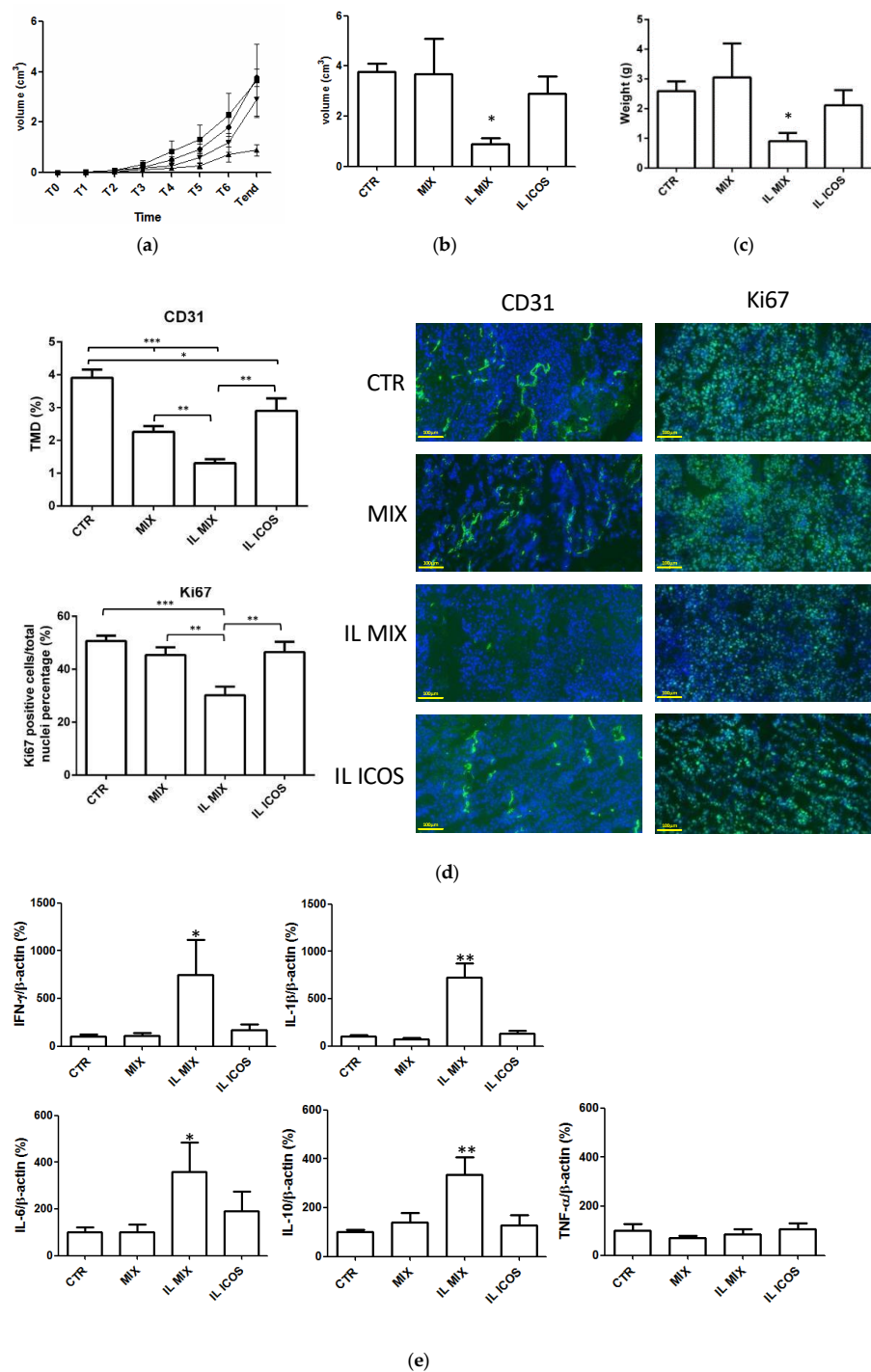


**Figure 7.** Animal experiments (I): (a) time course tumor volume, (b) endpoint tumor volume, (c) endpoint tumor weight, (d) tumor immunohistochemistry, and (e) tumor cytokines. Abbreviations: CD31: cluster of differentiation 31; CTR: control; IFN- $\gamma$ : Interferon- $\gamma$ ; IL: Intralipid<sup>®</sup> 10%; IL-10: Interleukin-10; IL-1 $\beta$ : Interleukin-1 $\beta$ ; IL-6: Interleukin-6; IL ICOS: Intralipid<sup>®</sup> 10% loaded with ICOS-Fc; IL MIX: Intralipid<sup>®</sup> 10% loaded with temozolomide dodecyl ester, sorafenib, and ICOS-Fc; Ki-67: Kiel original clone 67; MIX: free drug combination (temozolomide dodecyl ester, sorafenib, ICOS-Fc); TMD: tumor micro-vessel density; TNF- $\alpha$ : tumor necrosis factor- $\alpha$ . Days after B16-F10 cell subcutaneous injection ( $1 \times 10^5$  in 100  $\mu$ L/mouse): T0 = 10 days; T1 = 14 days; T2 = 16 days; T3 = 19 days; T4 = 21 days; T5 = 23 days; T6 = 25 days; Tend = 28 days. T0: assignment to groups; T1 to T6: treatments; Tend: sacrifice. For this experiment, 20 mice were used ( $n = 5$  each group). Statistical analysis \*\*\* =  $p < 0.0001$ ; \*\*  $p < 0.005$ ; \*  $p < 0.05$ .

Further in vivo experiments were performed to investigate the therapeutic contribution of ICOS-Fc in the IL MIX, and to this aim, the effect of IL MIX was compared to that of IL MIX formulated without ICOS-Fc (Figure 8, Table 3). The removal of ICOS-Fc from IL MIX resulted in it having a lesser effect on tumor growth (mass, volume), cell proliferation (Ki67), and immune modulation, in terms of IL-1 $\beta$ , IL-6, and IL-10 expression. In contrast, no significant differences were detected in terms of angiogenesis (CD31) and IFN- $\gamma$  expression.

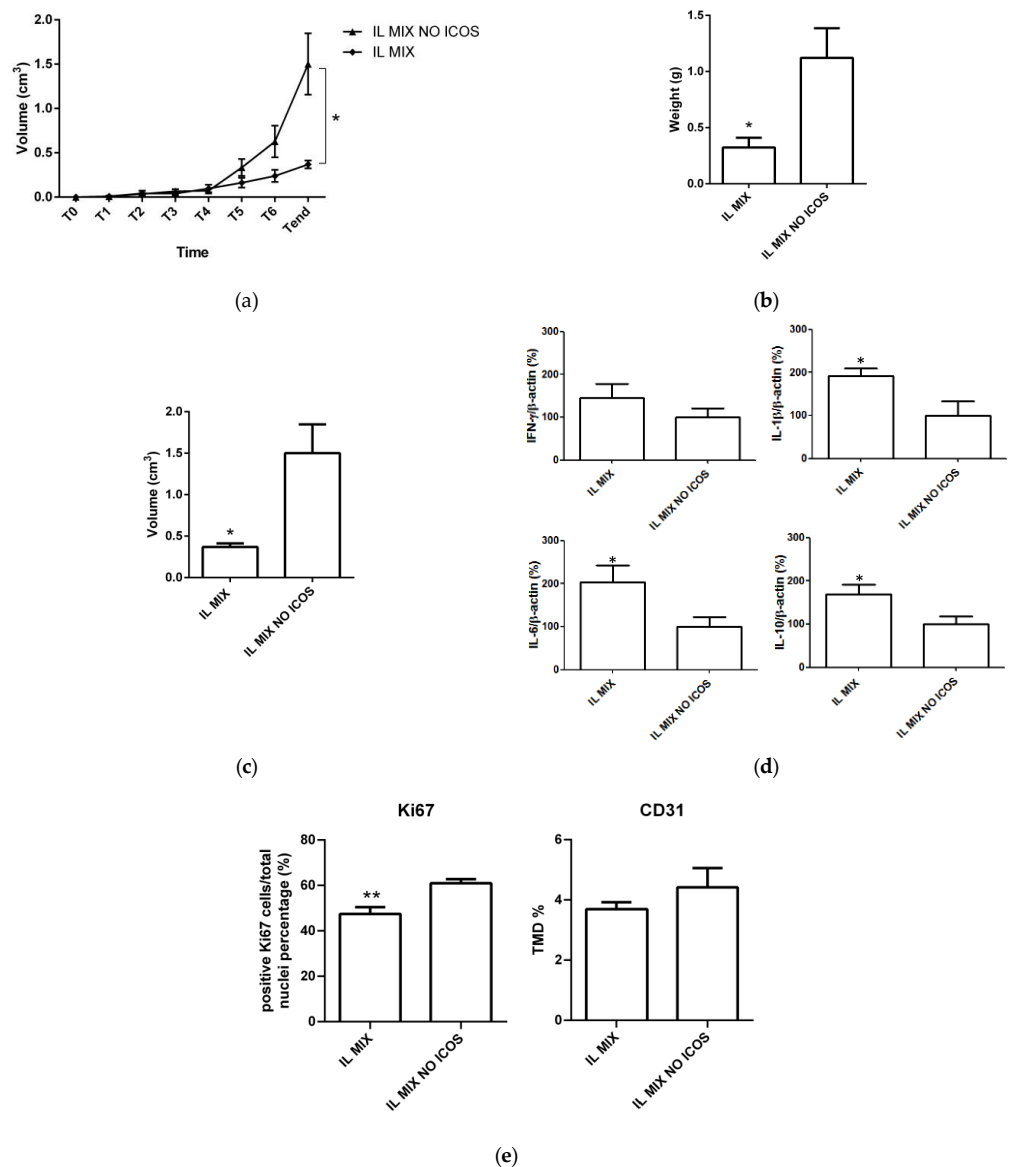


**Figure 8.** Animal experiments (II): (a) time-course tumor volume, (b) endpoint tumor volume, (c) endpoint tumor weight, (d) tumor cytokines, and (e) tumor immunohistochemistry. Abbreviations: IL: Intralipid® 10%; CD31: cluster of differentiation 31; IFN- $\gamma$ : Interferon- $\gamma$ ; IL-10: Interleukin-10; IL-1 $\beta$ : Interleukin-1 $\beta$ ; IL-6: Interleukin-6; IL MIX: Intralipid® 10% loaded with temozolomide dodecyl ester, sorafenib, and ICOS-Fc; IL MIX NO ICOS: Intralipid® 10% loaded with temozolomide dodecyl ester and sorafenib; Ki-67: Kiel original clone 67; TMD: tumor micro-vessel density. Days after B16-F10 cell subcutaneous injection ( $1 \times 10^5$  in 100  $\mu$ L/mouse): T0 = 10 days; T1 = 14 days; T2 = 16 days; T3 = 19 days; T4 = 21 days; T5 = 23 days; T6 = 25 days; Tend = 28 days. T0: assignment to groups; T1 to T6: treatment; Tend: sacrifice. For this experiment, 10 mice were used ( $n = 5$  each group). Statistical analysis \*\*  $p < 0.005$ ; \*  $p < 0.05$ .

**Table 3.** Animal experiments (II): organ weights (grams). Abbreviations: IL: Intralipid®; MIX: drug combination (temozolomide dodecyl ester, sorafenib, ICOS-Fc).

	Liver	Spleen	Kidneys	Lungs	Heart
IL MIX	0.86 ± 0.05	0.16 ± 0.04	0.20 ± 0.03	0.28 ± 0.14	0.13 ± 0.00
IL MIX NO ICOS-Fc	0.87 ± 0.06	0.18 ± 0.03	0.23 ± 0.01	0.16 ± 0.01	0.23 ± 0.08

## 4. Discussion

### 4.1. Challenges of Current Melanoma Chemotherapy

Targeted therapies and immunotherapies have allowed the improved therapeutic control of malignant melanoma to be achieved. However, several drawbacks (e.g., chemoresistance for targeted therapies, need for high mutational burden in immunotherapies) still limit the effectiveness of these approaches. It is worth noting that combinations of the two are currently under study and have provided promising results, despite the higher incidence of side effects [1]. This experimental study therefore proposes a multi-target approach that merges immunotherapy (ICOS-Fc), targeted therapy (SOR), and chemotherapy (TMZ) and evaluates it at a preclinical level. This approach targets three of the major factors driving melanoma growth, i.e., proliferation, angiogenesis, and the immune response. Using previous encouraging results that have been achieved by our research group [18], this combination was loaded into a biocompatible colloidal vehicle, namely the nanoemulsion for total parenteral nutrition. This formulation is already employed in marketed drug-delivery systems and is under evaluation for anti-cancer drug delivery because of its range of potential targeting mechanisms [31]. Indeed, passive targeting mechanisms are favored by both its nanometric size range and its high lipid content, which acts by saturating the reticuloendothelial system (RES) [32]. Moreover, recent findings showed that it can reduce blood viscosity, by interrupting the binding between fibrinogen and red blood cells, and thus increase the tumor blood flow, which plays a key role in passive targeting. Indeed, upregulation of fibrinogen has been reported in cancer, whereas fibrinogen-mediated clot formation is responsible for the reduced tumor blood flow, a major barrier to drug delivery to tumors [33].

### 4.2. Advantages of Merging Different Approaches into One Biocompatible Lipid Vehicle

The variability of the data obtained, especially on cell toxicity in the case of SOR, is mainly a result of the experimental *in vitro* setting, which does not account for the *in vivo* fate of drug-loaded IL. Indeed, the *in vivo* results indicate that IL MIX has promising therapeutic efficacy, while no relevant signs of toxicity were detected due to the sub-therapeutic doses employed for each compound: in our experiments, TMZ 1.5 mg/kg, SOR 1.25 mg/kg, and ICOS-Fc 1.25 mg/kg were co-administered, while in the literature TMZ 40.0 mg/kg, SOR 9.0 mg/kg, and ICOS-Fc 5.0 mg/kg were employed [4,18,34,35]. It is worth noting that the *in vivo* experiments demonstrated the efficacy of the proposed approach as such (IL MIX), since the administration of free MIX, IL ICOS-Fc, and IL MIX without ICOS-Fc failed to provide substantial therapeutic effects in terms of tumor growth, angiogenesis inhibition, and immunomodulation. The inefficacy of IL ICOS-Fc is in apparent conflict with the previously documented efficacy of ICOS-Fc-loaded PLGA and cyclodextrin nanoparticles in the same tumor model [4]. This discrepancy can be ascribed to the ICOS-Fc dose, which, in IL, was only 25% of that used in the other nanoparticles. However, the effect of ICOS-Fc in the IL MIX is highlighted by the significant loss of the anti-tumor effects displayed in the IL MIX that lacked ICOS-Fc. The main effect of IL MIX appears to be its action against angiogenesis, which may take advantage of the ability of SOR and ICOS-Fc to inhibit VEGF and OPN induction, respectively.

### 4.3. The Role of Immune Modulation

It is noteworthy that multi-functional nanomedicines able to act as both immunomodulators and drug carriers have been suggested, including autologous microparticles [36].



Within this context, IL MIX also displayed substantial effects in terms of immune modulation, as detected by the increased expression of IFN $\gamma$ , IL-1, IL-6, and IL-10. Intriguingly, the increase of IL-1, IL-6, and IL-10 was mostly dependent on the whole IL MIX drug combination, since these cytokines were not increased in mice treated with free MIX or IL ICOS and were significantly lower in mice treated with IL MIX without ICOS than in those treated with the whole IL MIX. In contrast, the increase of IFN- $\gamma$  was independent from the presence of ICOS-Fc, since it was increased at similar levels in mice treated either with IL MIX or IL MIX without ICOS, while it was not increased in mice treated with free MIX or IL ICOS. The increased expression of IL-10 was unexpected since IL-10 usually works as an anti-inflammatory and pro-oncogenic agent because it is associated with regulatory T lymphocytes and the M2 polarization of tumor-associated macrophages. Conversely, IFN- $\gamma$  is produced by lymphocytes with anti-tumor and pro-inflammatory activity, such as T helper type 1 lymphocytes, cytotoxic T lymphocytes, and natural killer (NK) cells [37]. Moreover, it is well-known that IL promotes the polarization of macrophages to the anti-cancer M1-like phenotype after i.v. administration [33]. However, the effect of IL-10 may vary depending on the tissue context as it can even trigger IFN- $\gamma$  secretion and increase cytotoxic anti-tumor lymphocytes and tumor rejection [38]. Previous evidence that we have accrued [18,27] suggests that the increase in IL-10 may be mediated by the activation of P38 mitogen-activated protein kinase (MAPK) in B lymphocytes, as induced by cytostatic agents such as TMZ [39,40] (Figure 9). In contrast, the involvement of ICOS-Fc in this mechanism is unlikely, since our previous work has shown that ICOS-Fc decreases IL-10 expression in the tumor mass when loaded into cyclodextrin nanospheres, but not in PLGA nanoparticles. In this scenario, it is also noteworthy that, of the cytokines involved in acute inflammation, the expression of IL-6 and IL-1 was increased, but that of TNF- $\alpha$  was not.

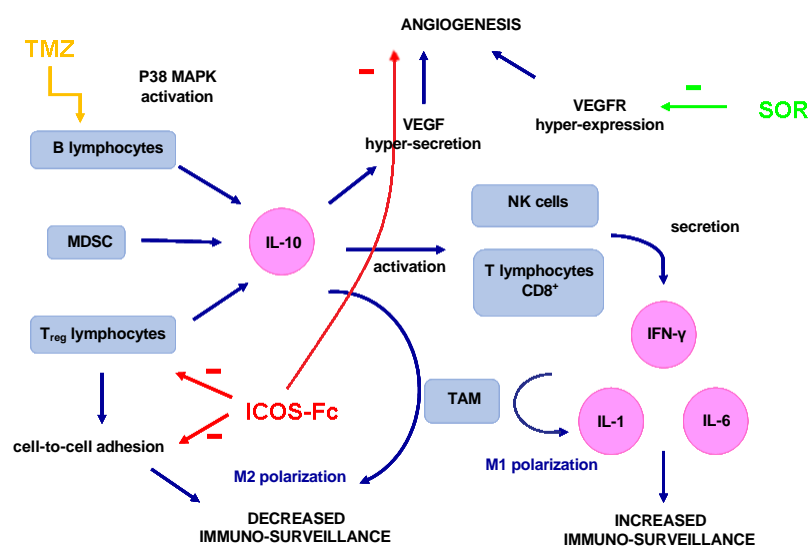


**Figure 9.** Scheme of immunologic pathways involved in polychemotherapy (MIX). Abbreviations: CD8: cluster of differentiation 8; IFN- $\gamma$ : interferon- $\gamma$ ; IL-1: interleukin 1; IL-6: interleukin 6; IL-10: interleukin 10; MAPK: mitogen-activated protein kinase; MDSC: myeloid-derived suppressor cells; NK: natural killer; SOR: sorafenib; TAM: tumor-associated macrophages; TMZ: temozolomide; T<sub>reg</sub>: lymphocytes T regulators; VEGF: vascular endothelial growth factor; VEGFR: VEGF receptor.

However, the immunological context can vary with the mouse model employed. Indeed, the immunocompetent B16-F10 model in this experimental work was selected because it expresses a large amount of ICOS-L (data not shown). Nonetheless, it is not a BRAF-mutated model. Therefore, we will also assess our approach in BRAF-mutated models in future studies to take advantage of the promising in vitro results obtained in genetically modified BRAF-mutated D4M cells. In this case, selective BRAF inhibitors

(such as vemurafenib) could be included in the drug combination to provide the necessary advantages.

## 5. Conclusions

Despite the relevant advances in the pharmacological therapy of high-grade melanoma obtained in recent years, this disease still represents a serious threat. This research work therefore presented a combination therapy that has been engineered to include ICOS-Fc as the immuno-stimulating agent, a cytostatic agent (TMZ), and a kinase inhibitor (SOR) for loading into a nanoemulsion used for total parenteral nutrition. Results showed that this therapy was effective in inhibiting the growth of mouse melanoma *in vivo* by exerting a potent anti-angiogenic effect and complex immuno-regulatory activity. This is the first attempt to introduce an immunotherapeutic drug working in the ICOS/ICOS-L axis in a polychemotherapy approach, and the results showed that this approach allows to substantially decrease the drug dose needed to obtain a therapeutic effect. Use of ICOS-Fc is innovative since it works as both an immunostimulatory and antiangiogenic agent, and therefore would be optimally synergistic with the other drugs loaded in the nanoparticles. Tumor growth inhibition was obtained without any sign of systemic toxicity. Indeed, sub-therapeutic drug doses were most probably effective because of the hypothesized targeting properties of IL. This approach might represent a potential future tool that can merge immunotherapy, targeted therapy, and chemotherapy into one safe delivery vehicle to improve therapeutic efficacy, without increasing the incidence of the adverse side effects that are typical of combination therapies.

## 6. Patents

PCT IB/2019/050154.

**Author Contributions:** C.D., L.B. and U.D. conceived and designed the experiments; I.S., C.M., C.D., L.C., C.F., N.C. and E.B. performed the experiments; C.L.G. performed data analysis; A.B., G.M. and S.P. provided technical support and corrections to the manuscript; L.B. wrote the manuscript. All authors have read and agreed to the published version of the manuscript.

**Funding:** This work was supported by the University of Turin (Ricerca Locale 2019–2021), Fondazione CRT (2019.2252), Associazione Italiana Ricerca sul Cancro (IG20714), Fondazione Amici di Jean (Torino), Fondazione Veronesi and Fondazione Cariplo (2017–0535).

**Data Availability Statement:** Not applicable.

**Acknowledgments:** We thank D.W. Mullis (Department of Medicine, Norris Cotton Cancer Center, Geisel School of Medicine at Dartmouth, Lebanon, NH, USA) for the D4M cells. We thank Dale Lawson for English editing of the manuscript.

**Conflicts of Interest:** A patent application has been submitted for the use of ICOS-L ligands loaded into nanoparticles in tumor treatment (PCT IB/2019/050154).

## References

1. Battaglia, L.; Scomparin, A.; Dianzani, C.; Milla, P.; Muntoni, E.; Arpicco, S.; Cavalli, R. Nanotechnology Addressing Cutaneous Melanoma: The Italian Landscape. *Pharmaceutics* **2021**, *13*, 1617. [[CrossRef](#)] [[PubMed](#)]
2. Velho, T.R. Metastatic Melanoma – A Review of Current and Future Drugs. *Drugs Context* **2012**, *2012*, 212242. [[CrossRef](#)]
3. Passarelli, A.; Tucci, M.; Mannavola, F.; Felici, C.; Silvestris, F. The metabolic milieu in melanoma: Role of immune suppression by CD73/adenosine. *Tumour Biol.* **2019**, *41*, 1010428319837138. [[CrossRef](#)]
4. Clemente, N.; Boggio, E.; Gigliotti, L.C.; Raineri, D.; Ferrara, B.; Miglio, G.; Argenziano, M.; Chiocchetti, A.; Cappellano, G.; Trotta, F.; et al. Immunotherapy of experimental melanoma with ICOS-Fc loaded in biocompatible and biodegradable nanoparticles. *J. Control. Release* **2020**, *320*, 112–124. [[CrossRef](#)] [[PubMed](#)]
5. Redoglia, V.; Dianzani, U.; Rojo, J.M.; Portolés, P.; Bragardo, M.; Wolff, H.; Buonfiglio, D.; Bonissoni, S.; Janeway, C.A. Characterization of H4: A Mouse T Lymphocyte Activation Molecule Functionally Associated with the CD3/T Cell Receptor. *Eur. J. Immunol.* **1996**, *26*, 2781–2789. [[CrossRef](#)] [[PubMed](#)]

6. Buonfiglio, D.; Bragardo, M.; Bonissoni, S.; Redoglia, V.; Cauda, R.; Zupo, S.; Burgio, V.L.; Wolff, H.; Franssila, K.; Gaidano, G.; et al. Characterization of a Novel Human Surface Molecule Selectively Expressed by Mature Thymocytes, Activated T Cells and Subsets of T Cell Lymphomas. *Eur. J. Immunol.* **1999**, *29*, 2863–2874. [[CrossRef](#)]
7. Hutloff, A.; Dittrich, A.M.; Beier, K.C.; Eljaschewitsch, B.; Kraft, R.; Anagnostopoulos, I.; Kroczeck, R.A. ICOS Is an Inducible T-Cell Co-Stimulator Structurally and Functionally Related to CD28. *Nature* **1999**, *397*, 263–266. [[CrossRef](#)]
8. Mesturini, R.; Nicola, S.; Chiocchetti, A.; Bernardone, I.S.; Castelli, L.; Bensi, T.; Ferretti, M.; Comi, C.; Dong, C.; Rojo, J.M.; et al. ICOS Cooperates with CD28, IL-2, and IFN- $\gamma$  and Modulates Activation of Human Naïve CD4+ T Cells. *Eur. J. Immunol.* **2006**, *36*, 2601–2612. [[CrossRef](#)]
9. Yong, P.F.K.; Salzer, U.; Grimbacher, B. The Role of Costimulation in Antibody Deficiencies: ICOS and Common Variable Immunodeficiency. *Immunol. Rev.* **2009**, *229*, 101–113. [[CrossRef](#)]
10. Occhipinti, S.; Dianzani, C.; Chiocchetti, A.; Boggio, E.; Clemente, N.; Gigliotti, C.L.; Soluri, M.F.; Minelli, R.; Fantozzi, R.; Yagi, J.; et al. Triggering of B7h by the ICOS Modulates Maturation and Migration of Monocyte-Derived Dendritic Cells. *J. Immunol.* **2013**, *190*, 1125–1134. [[CrossRef](#)]
11. Hedl, M.; Lahiri, A.; Ning, K.; Cho, J.H.; Abraham, C. Pattern Recognition Receptor Signaling in Human Dendritic Cells Is Enhanced by ICOS Ligand and Modulated by the Crohn's Disease ICOSLG Risk Allele. *Immunity* **2014**, *40*, 734–746. [[CrossRef](#)]
12. Raineri, D.; Dianzani, C.; Cappellano, G.; Maione, F.; Baldanzi, G.; Iacobucci, I.; Clemente, N.; Baldone, G.; Boggio, E.; Gigliotti, C.L.; et al. Osteopontin Binds ICOSL Promoting Tumour Metastasis. *Commun. Biol.* **2020**, *3*, 615. [[CrossRef](#)]
13. Fu, T.; He, Q.; Sharma, P. The ICOS/ICOSL Pathway Is Required for Optimal Antitumour Responses Mediated by Anti-CTLA-4 Therapy. *Cancer Res.* **2011**, *71*, 5445–5454. [[CrossRef](#)]
14. Sun, J.; Carr, M.J.; Khushalani, N.I. Principles of Targeted Therapy for Melanoma. *Surg. Clin. N. Am.* **2020**, *100*, 175–188. [[CrossRef](#)]
15. Snyder, A.; Makarov, V.; Merghoub, T.; Yuan, J.; Zaretsky, J.M.; Desrichard, A.; Walsh, L.A.; Postow, M.A.; Wong, P.; Ho, T.S.; et al. Genetic Basis for Clinical Response to CTLA-4 Blockade in Melanoma. *N. Engl. J. Med.* **2014**, *371*, 2189–2199. [[CrossRef](#)]
16. Hugo, W.; Zaretsky, J.M.; Sun, L.; Song, C.; Moreno, B.H.; Hu-Lieskovan, S.; Berent-Maoz, B.; Pang, J.; Chmielowski, B.; Cherry, G.; et al. Genomic and Transcriptomic Features of Response to Anti-PD-1 Therapy in Metastatic Melanoma. *Cell* **2016**, *165*, 35–44. [[CrossRef](#)]
17. Riaz, N.; Havel, J.J.; Makarov, V.; Desrichard, A.; Urba, W.J.; Sims, J.S.; Hodi, F.S.; Martín-Algarra, S.; Mandal, R.; Sharfman, W.H.; et al. Tumour and Microenvironment Evolution during Immunotherapy with Nivolumab. *Cell* **2017**, *171*, 934–949. [[CrossRef](#)] [[PubMed](#)]
18. Dianzani, C.; Monge, C.; Miglio, G.; Serpe, L.; Martina, K.; Cangemi, L.; Ferraris, C.; Mioletti, S.; Osella, S.; Gigliotti, C.L.; et al. Nanoemulsions as Delivery Systems for Poly-Chemotherapy Aiming at Melanoma Treatment. *Cancers* **2020**, *12*, 1198. [[CrossRef](#)] [[PubMed](#)]
19. Amaravadi, R.K.; Schuchter, L.M.; McDermott, D.F.; Kramer, A.; Giles, L.; Gramlich, K.; Carberry, M.; Troxel, A.B.; Letrero, R.; Nathanson, K.L.; et al. Phase II Trial of Temozolomide and Sorafenib in Advanced Melanoma Patients with or without Brain Metastases. *Clin. Cancer Res.* **2009**, *15*, 7711–7718. [[CrossRef](#)] [[PubMed](#)]
20. Xiong, Y.-Q.; Sun, H.-C.; Zhang, W.; Zhu, X.-D.; Zhuang, P.-Y.; Zhang, J.-B.; Wang, L.; Wu, W.; Qin, L.-X.; Tang, Z.-Y. Human Hepatocellular Carcinoma Tumour-Derived Endothelial Cells Manifest Increased Angiogenesis Capability and Drug Resistance Compared with Normal Endothelial Cells. *Clin. Cancer Res.* **2009**, *15*, 4838–4846. [[CrossRef](#)] [[PubMed](#)]
21. Cao, M.; Xu, Y.; Youn, J.; Cabrera, R.; Zhang, X.; Gabrilovich, D.; Nelson, D.R.; Liu, C. Kinase Inhibitor Sorafenib Modulates Immunosuppressive Cell Populations in a Murine Liver Cancer Model. *Lab. Investig.* **2011**, *91*, 598–608. [[CrossRef](#)]
22. Suppasansatorn, P.; Wang, G.; Conway, B.R.; Wang, W.; Wang, Y. Skin Delivery Potency and Antitumour Activities of Temozolomide Ester Prodrugs. *Cancer Lett.* **2006**, *244*, 42–52. [[CrossRef](#)] [[PubMed](#)]
23. Annovazzi, L.; Schiffer, D.; Mellai, M.; Gallarate, M.; Battaglia, L.; Chirio, D.; Peira, E.; Muntoni, E.; Chegaev, K.; Barge, A.; et al. Solid Lipid Nanoparticles Loaded with Antitumour Lipophilic Prodrugs Aimed to Glioblastoma Treatment: Preliminary Studies on Cultured Cells. *J. Nanosci. Nanotechnol.* **2017**, *17*, 3606–3614. [[CrossRef](#)]
24. Battaglia, L.; Gallarate, M.; Peira, E.; Chirio, D.; Solazzi, I.; Giordano, S.M.A.; Gigliotti, C.L.; Riganti, C. Dianzani Bevacizumab loaded solid lipid nanoparticles prepared by the coacervation technique: Preliminary in vitro studies. *Nanotechnology* **2015**, *26*, 255102. [[CrossRef](#)]
25. Ganta, S.; Paxton, J.W.; Baguley, B.C.; Garg, S. Pharmacokinetics and pharmacodynamics of chlorambucil delivered in parenteral emulsion. *Int. J. Pharm.* **2008**, *360*, 115–121. [[CrossRef](#)]
26. Navas, N.; Herrera, A.; Martínez-Ortega, A.; Salmerón-García, A.; Cabeza, J.; Cuadros-Rodríguez, L. Quantification of an Intact Monoclonal Antibody, Rituximab, by (RP)HPLC/DAD in Compliance with ICH Guidelines. *Anal. Bioanal. Chem.* **2013**, *405*, 9351–9363. [[CrossRef](#)] [[PubMed](#)]
27. Clemente, N.; Ferrara, B.; Gigliotti, C.; Boggio, E.; Capucchio, M.; Biasibetti, E.; Schiffer, D.; Mellai, M.; Annovazzi, L.; Cangemi, L.; et al. Solid Lipid Nanoparticles Carrying Temozolomide for Melanoma Treatment. Preliminary In Vitro and In Vivo Studies. *Int. J. Mol. Sci.* **2018**, *19*, 255. [[CrossRef](#)] [[PubMed](#)]

28. Wilhelm, S.M.; Adnane, L.; Newell, P.; Villanueva, A.; Llovet, J.M.; Lynch, M. Preclinical Overview of Sorafenib, a Multikinase Inhibitor That Targets Both Raf and VEGF and PDGF Receptor Tyrosine Kinase Signaling. *Mol. Cancer Ther.* **2008**, *7*, 3129–3140. [[CrossRef](#)]
29. Villarroel, M.C.; Pratz, K.W.; Xu, L.; Wright, J.J.; Smith, B.D.; Rudek, M.A. Plasma Protein Binding of Sorafenib, a Multi Kinase Inhibitor: In Vitro and in Cancer Patients. *Investig. New Drugs* **2012**, *30*, 2096–2102. [[CrossRef](#)]
30. Kanno, S.-I.; Itoh, K.; Suzuki, N.; Tomizawa, A.; Yomogida, S.; Ishikawa, M. Exogenous Albumin Inhibits Sorafenib-Induced Cytotoxicity in Human Cancer Cell Lines. *Mol. Clin. Oncol.* **2013**, *1*, 29–34. [[CrossRef](#)]
31. Hippalgaonkar, K.; Majumdar, S.; Kansara, V. Injectable Lipid Emulsions – Advancements, Opportunities and Challenges. *AAPS PharmSciTech* **2010**, *11*, 1526–1540. [[CrossRef](#)] [[PubMed](#)]
32. Islam, R.; Gao, S.; Islam, W.; Šubr, V.; Zhou, J.-R.; Yokomizo, K.; Etrych, T.; Maeda, H.; Fang, J. Unraveling the Role of Intralipid in Suppressing Off-Target Delivery and Augmenting the Therapeutic Effects of Anticancer Nanomedicines. *Acta Biomater.* **2021**, *126*, 372–383. [[CrossRef](#)] [[PubMed](#)]
33. Liu, L.; Ho, C. Using Intralipid to Improve Delivery of Anti-Cancer Nanodrugs: Effects on RES Clearance and Toxicity, EPR, and Immune Modulation. *J. Nanotechnol. Nanomater.* **2021**, *2*, 76–82.
34. Zhang, N.; Zhang, B.; Gong, X.; Wang, T.; Liu, Y.; Yang, S. In Vivo Biodistribution, Biocompatibility, and Efficacy of Sorafenib-Loaded Lipid-Based Nanosuspensions Evaluated Experimentally in Cancer. *Int. J. Nanomed.* **2016**, *11*, 2329. [[CrossRef](#)]
35. Mathieu, V.; Le Mercier, M.; De Neve, N.; Sauvage, S.; Gras, T.; Roland, I.; Lefranc, F.; Kiss, R. Galectin-1 Knockdown Increases Sensitivity to Temozolomide in a B16F10 Mouse Metastatic Melanoma Model. *J. Investig. Dermatol.* **2007**, *127*, 2399–2410. [[CrossRef](#)]
36. Yin, B.; Ni, J.; Witherel, C.E.; Yang, M.; Burdick, J.A.; Wen, C.; Wong, S.H.D. Harnessing Tissue-derived Extracellular Vesicles for Osteoarthritis Theranostics. *Theranostics* **2022**, *12*, 207–231. [[CrossRef](#)]
37. Conciatori, F.; Bazzichetto, C.; Falcone, I.; Pilotto, S.; Bria, E.; Cognetti, F.; Milella, M.; Ciuffreda, L. Molecular Sciences Role of MTOR Signaling in Tumour Microenvironment: An Overview. *Int. J. Mol. Sci.* **2018**, *19*, 2453. [[CrossRef](#)]
38. Oft, M. IL-10: Master Switch from Tumour-Promoting Inflammation to Antitumour Immunity. *Cancer Immunol. Res.* **2014**, *2*, 194–199. [[CrossRef](#)]
39. Lu, L.; Yoshimoto, K.; Morita, A.; Kameda, H.; Takeuchi, T. AB0074 Alkylating Agents Enhance Interleukin-10 Secretion from B Cells via P38 MAP Kinase Activation. *Ann. Rheum. Dis.* **2014**, *73*, 828. [[CrossRef](#)]
40. Lu, L.; Yoshimoto, K.; Morita, A.; Kameda, H.; Takeuchi, T. Bendamustine Increases Interleukin-10 Secretion from B Cells via P38 MAP Kinase Activation. *Int. Immunopharmacol.* **2016**, *39*, 273–279. [[CrossRef](#)]



Article

# ICOSL Stimulation by ICOS-Fc Accelerates Cutaneous Wound Healing In Vivo

Ian Stoppa <sup>1,2,†</sup>, Casimiro Luca Gigliotti <sup>1,2,†</sup> , Nausicaa Clemente <sup>1</sup> , Deepika Pantham <sup>1,2</sup>, Chiara Dianzani <sup>3</sup> , Chiara Monge <sup>3</sup>, Chiara Puricelli <sup>1,4</sup> , Roberta Rolla <sup>1,4</sup> , Salvatore Sutti <sup>1</sup> , Filippo Renò <sup>1</sup> , Renzo Boldorini <sup>1,4</sup>, Elena Boggio <sup>1,2,\*,‡</sup> and Umberto Dianzani <sup>1,4,‡</sup>

- <sup>1</sup> Department of Health Sciences and Interdisciplinary Research Center of Autoimmune Diseases (IRCAD), Università del Piemonte Orientale, 28100 Novara, Italy; ian.stoppa@uniupo.it (I.S.); luca.gigliotti@med.uniupo.it (C.L.G.); nausicaa.clemente@med.uniupo.it (N.C.); deepika.pantham@uniupo.it (D.P.); 20032501@studenti.uniupo.it (C.P.); roberta.rolla@med.uniupo.it (R.R.); salvatore.sutti@med.uniupo.it (S.S.); filippo.reno@med.uniupo.it (F.R.); renzo.boldorini@med.uniupo.it (R.B.); umberto.dianzani@med.uniupo.it (U.D.)
- <sup>2</sup> NOVAICOS srls, 28100 Novara, Italy
- <sup>3</sup> Department of Scienza e Tecnologia del Farmaco, University of Turin, 10124 Turin, Italy; chiara.dianzani@unito.it (C.D.); chiara.monge@unito.it (C.M.)
- <sup>4</sup> Maggiore della Carità University Hospital, 28100 Novara, Italy
- \* Correspondence: elena.boggio@med.uniupo.it; Tel.: +39-0321660658
- † These authors contributed equally to this work.
- ‡ These authors contributed equally to this work.



**Citation:** Stoppa, I.; Gigliotti, C.L.; Clemente, N.; Pantham, D.; Dianzani, C.; Monge, C.; Puricelli, C.; Rolla, R.; Sutti, S.; Renò, F.; et al. ICOSL Stimulation by ICOS-Fc Accelerates Cutaneous Wound Healing In Vivo. *Int. J. Mol. Sci.* **2022**, *23*, 7363. <https://doi.org/10.3390/ijms23137363>

Academic Editor: Bum-Ho Bin

Received: 1 June 2022

Accepted: 30 June 2022

Published: 1 July 2022

**Publisher's Note:** MDPI stays neutral with regard to jurisdictional claims in published maps and institutional affiliations.



**Copyright:** © 2022 by the authors. Licensee MDPI, Basel, Switzerland. This article is an open access article distributed under the terms and conditions of the Creative Commons Attribution (CC BY) license (<https://creativecommons.org/licenses/by/4.0/>).

**Abstract:** Background: ICOS and its ligand ICOSL are immune receptors whose interaction triggers bidirectional signals that modulate the immune response and tissue repair. Aim: The aim of this study was to assess the in vivo effects of ICOSL triggering by ICOS-Fc, a recombinant soluble form of ICOS, on skin wound healing. Methods: The effect of human ICOS-Fc on wound healing was assessed, in vitro, and, in vivo, by skin wound healing assay using ICOS<sup>-/-</sup> and ICOSL<sup>-/-</sup> knockout (KO) mice and NOD-SCID-IL2R null (NSG) mice. Results: We show that, in wild type mice, treatment with ICOS-Fc improves wound healing, promotes angiogenesis, preceded by upregulation of IL-6 and VEGF expression; increases the number of fibroblasts and T cells, whereas it reduces that of neutrophils; and increases the number of M2 vs. M1 macrophages. Fittingly, ICOS-Fc enhanced M2 macrophage migration, while it hampered that of M1 macrophages. ICOS<sup>-/-</sup> and ICOSL<sup>-/-</sup> KO, and NSG mice showed delayed wound healing, and treatment with ICOS-Fc improved wound closure in ICOS<sup>-/-</sup> and NSG mice. Conclusion: These data show that the ICOS/ICOSL network cooperates in tissue repair, and that triggering of ICOSL by ICOS-Fc improves cutaneous wound healing by increasing angiogenesis and recruitment of reparative macrophages.

**Keywords:** ICOS:ICOSL system; wound healing; reparative macrophages

## 1. Introduction

Skin wound healing starts immediately after injury and evolves in three phases. The first one is an inflammatory phase during which platelets tend to aggregate, while inflammatory cells are recruited to the wound site. The second proliferative phase is characterized by the formation of granulation tissue and re-epithelialization due to the migration and proliferation of keratinocytes, fibroblasts, and ECs, and by ECM deposition. The last one is the so-called remodeling phase during which the regenerative process comes to an end and the wound becomes avascular and acellular, thereby allowing the reorganization of the connective tissue to promote scar formation [1,2].

ICOS (CD278) is a T cell co-stimulatory receptor, member of the CD28 family [3], mainly expressed on activated T-cells. ICOS binds ICOSL (CD275, also called B7h, GL50, B7H2), a member of the B7 family. ICOS triggering in T cells promotes not only the

activation of effector T cells in peripheral tissues but also the development of regulatory T cells [4]. ICOSL is expressed on multiple cell types, including antigen presenting cells (APCs), activated ECs, epithelial cells, fibroblasts, and keratinocytes [5,6]. ICOSL triggering mediated by ICOS drives a “reverse signal” that inhibits the migration of endothelial, dendritic, and tumor cells, modulates cytokine secretion while promoting antigen cross-presentation in dendritic cells, and inhibits osteoclast differentiation and functions [7–11].

We have recently shown that ICOSL also binds osteopontin (OPN) at a different site from that used to bind ICOS [12], which suggests that the ICOSL/OPN axis may play a role in wound healing besides tumorigenesis. This hypothesis is also supported by the observation that OPN can act as both an ECM component and a soluble cytokine involved in inflammation and angiogenesis [13,14]. Indeed, ICOSL triggering by OPN induces tumor cell migration and promotes tumor angiogenesis, both of which are counteracted by ICOS-mediated activation of ICOSL [12].

The formal demonstration of a functional role of the ICOS/ICOSL pathway in wound healing comes from the observation that ICOS<sup>-/-</sup>, ICOSL<sup>-/-</sup>, and ICOS/ICOSL<sup>-/-</sup> mice show delayed wound healing [15] likely due to decreased production of IL-6 [16]. In good agreement with a role of the ICOS/ICOSL dyad in normal tissue repair, we have recently shown that CCl<sub>4</sub>-induced liver damage, which is dependent on massive recruitment of blood-derived monocytes/macrophages, is dramatically worsened in both ICOS<sup>-/-</sup> and ICOSL<sup>-/-</sup> mice [17]. Interestingly, we were able to rescue this impairment by treating mice with ICOS-Fc, a recombinant soluble protein composed of the ICOS extracellular portion fused to the IgG1 Fc portion, which has been previously shown to trigger ICOSL, thereby inhibiting the development of experimental tumor metastases in vitro and tumor angiogenesis in vivo [9,11,17,18].

As the aforementioned findings support a functional role of ICOS/ICOSL in tissue repair, in the present study, we sought to determine the effect of ICOS-Fc in both in vitro and in vivo models of skin wound healing. Our in vivo results show that ICOS-Fc improves wound healing likely by increasing angiogenesis and recruitment of reparative macrophages.

## 2. Results

### 2.1. ICOSL Activation by ICOS-Fc Increases Keratinocyte Migration In Vitro

To begin to explore the role of ICOSL in tissue repair, we assessed the effect of human ICOS-Fc on keratinocyte wound healing in vitro by scratch assay on HaCat human keratinocytes, which are known to express ICOSL but not ICOS (Figure 1a). For this purpose, we performed a linear scratch on a confluent monolayer of HaCat cells, which were then cultured in serum-free medium to minimize cell proliferation in the presence or absence of human ICOS-Fc or human <sup>119</sup>S-ICOS-Fc (2 µg/mL), an ICOS-Fc mutant unable to bind ICOSL. After 24 h, microscopic evaluation revealed that treatment with ICOS-Fc but not <sup>119</sup>S-ICOS-Fc led to a substantial increase in the percentage of migrating cells compared to that of the untreated control (Figure 1b,c). This result came as a surprise given that we had previously shown that ICOS-Fc inhibited migration of several cell types and wound closure in scratch assays performed on ECs and several tumor cell lines [8–10].

### 2.2. ICOS-Fc Treatment Accelerates Skin Wound Healing In Vivo

To assess the effect of ICOS-Fc on skin wound healing in vivo, skin wounds were created on the back of wild-type C57BL/6 mice, which were then daily instilled with 1x PBS with or without mouse ICOS-Fc. Wound healing was then followed up for 10 days. Consistent with our in vitro data, we found that treatment with ICOS-Fc significantly improved wound closure at days 1–6, while the healing curve gradually aligned with control levels at later time points (Figure 2a). Histological staining of fibroblasts and collagen performed at day 3 and 4 by H&E and picrosirius red staining, respectively, revealed that treatment with ICOS-Fc increased fibroblast migration into the wound compared to control at day 3 and, to a higher extent, day 4. In contrast, collagen deposition in ICOS-Fc-treated mice was similar to that of their control counterparts, indicating that treatment with ICOS-Fc

favors repair but not scar formation (Figure 2b–d). Consistently, we observed a dramatic increase in  $\alpha$ SMA gene expression, a marker of reparative myofibroblasts [19], at day 2 following treatment with ICOS-Fc, which decreased to control levels in the following days (Figure 2e).

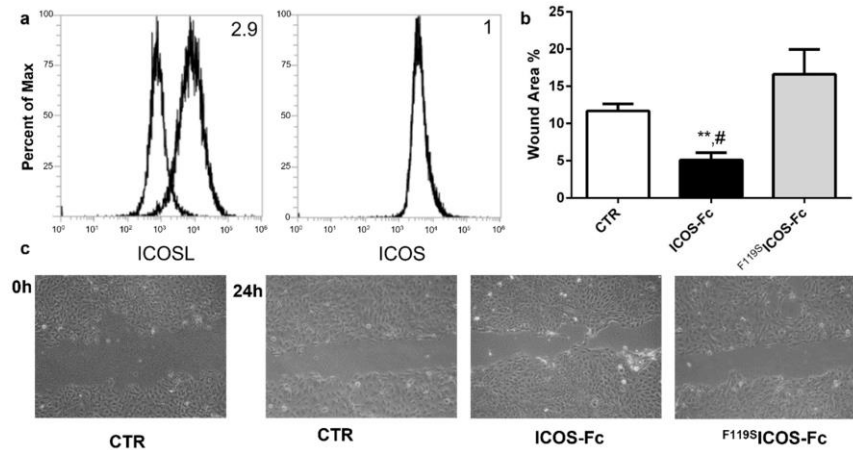


**Figure 1.** Effect of ICOS-Fc stimulation on the motility of HaCat cells by scratch assay. HaCat cells were cultured to confluence on 6-well plates. A scratch was made through the cell layer using a pipette tip and cells were then cultured in the presence or absence of 2  $\mu$ g/mL ICOS-Fc or  $F^{1195S}$ ICOS-Fc for 24 h. (a) ICOS and ICOSL expression in HaCat cells. (b) Wound area % after 24 h of treatment as above, calculated as:  $1 - (\text{scratch width of the treated group} / \text{scratch width of the control group}) \times 100$ ; results are the means from three independent experiments; \*\*  $p < 0.01$  vs. CTR; #  $p < 0.05$  vs.  $F^{1195S}$ ICOS-Fc, calculated by paired  $t$ -test. (c) Representative microphotographs of the wounded area taken immediately after the scratch was made 0 h and 24 h later to monitor cell migration into the wounded area (original magnification 10 $\times$ ).

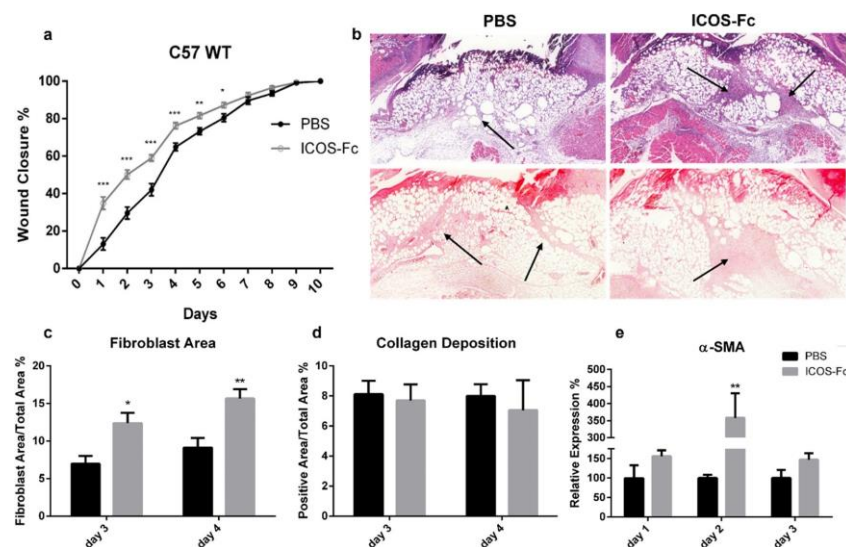


**Figure 2.** Effect of treatment with ICOS-Fc on wound healing in wild-type C57BL/6 mice. (a) Wound healing % in mice treated with PBS (n = 21) or ICOS-Fc (n = 22) calculated as  $(\text{wound area}^{T0} - \text{wound area}^{TX}) / \text{wound area}^{T0} \times 100\%$ ; mean  $\pm$  SE; (b) representative microphotographs of the staining (magnification 200 $\times$ ) at day 4; upper panels: Hematoxylin/eosin (H&E) for fibroblast area quantification (black arrows); lower panels: picrosirius red for collagen deposition quantification (black arrows). (c,d) Wound area % occupied by fibroblasts and collagen as detected by H&E and picrosirius red staining, respectively, at day 3 and day 4. (e)  $\alpha$ SMA mRNA expression analysis by real time PCR at day 1, day 2, and day 3. Results are expressed as mean  $\pm$  SE from 4 independent experiments; \*  $p < 0.05$ ; \*\*  $p < 0.005$ ; \*\*\*  $p < 0.001$ , calculated by Mann–Whitney test.

Next, immunohistochemical staining of vessels with an anti-CD31 antibody revealed a significant increase in CD31<sup>+</sup> vessels in mice treated with ICOS-Fc at day 3 and 4 compared to their control counterparts (Figure 3a), indicating enhanced wound angiogenesis. This was further supported by augmented CD31 and VEGF mRNA levels at day 1, both of which decreased to control levels in the subsequent days (Figure 3b).

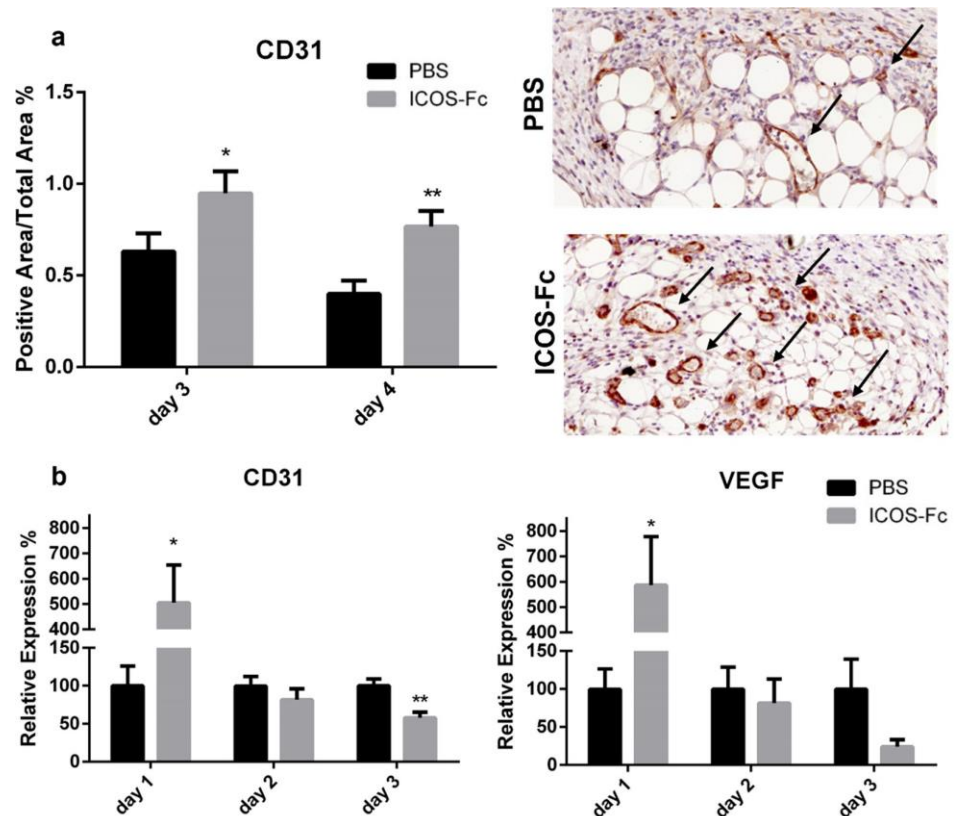


**Figure 3.** Treatment with ICOS-Fc stimulates angiogenesis during wound healing. (a) Wound area occupied by CD31<sup>+</sup> vessels as detected by immunohistochemistry. Left panel: results at day 3 and day 4 expressed as mean  $\pm$  SE from four independent experiments. Right panels: Representative microphotographs of CD31 staining (magnification 200 $\times$ ) at day 4. (b) Expression of the CD31 (left) and VEGF (right) mRNA levels as assessed by real time PCR at day 3 and day 4 and expressed as mean  $\pm$  SE from four independent experiments. Results are expressed as % of the mRNA amount detected in PBS-treated mice at each time point; \*  $p < 0.05$ ; \*\*  $p < 0.005$ ; calculated by unpaired Student's *t*-test.

To further characterize the healing process in wounded mice, we next sought to determine the infiltration extent of inflammatory cells by immunohistochemistry using antibodies specific for MPO, CD3, and F4/80. Results showed that treatment with ICOS-Fc decreased MPO<sup>+</sup> neutrophils at day 3, whereas it increased CD3<sup>+</sup> T cells at day 3 and 4, and F4/80<sup>+</sup> monocyte/macrophages at day 3 (Figure 4a–c).

To better characterize the inflammatory microenvironment of the healing wound, we next assessed mRNA expression levels of IL-6, TNF- $\alpha$ , TGF- $\beta$ , IL-33, IL-10, IL4, IFN- $\gamma$ , OPN, TREM1, TREM2, ICOS, and ICOSL at day 1 to 3 by real time PCR. We found that treatment with ICOS-Fc strikingly increased expression of IL-6 at day 2, which decreased in the following days (Figure 5a). In contrast, expression of TNF- $\alpha$  was homogeneously decreased at all time points, while expression of TGF- $\beta$  was moderately decreased at day 3 (Figure 5b,c). Expression of TREM1 and TREM2, respective markers of M1 and M2 macrophages, displayed opposite patterns since treatment with ICOS-Fc downregulated TREM1 and upregulated TREM2 at day 1, so that the TREM2/TREM1 ratio was increased about 5-fold (Figure 5d,e,g). ICOSL gene expression was decreased at day 3 upon ICOS-Fc



treatment (Figure 5f), whereas no differences were detected for IL-10, IL-33, IL-4, IFN- $\gamma$ , OPN, and ICOS (data not shown).

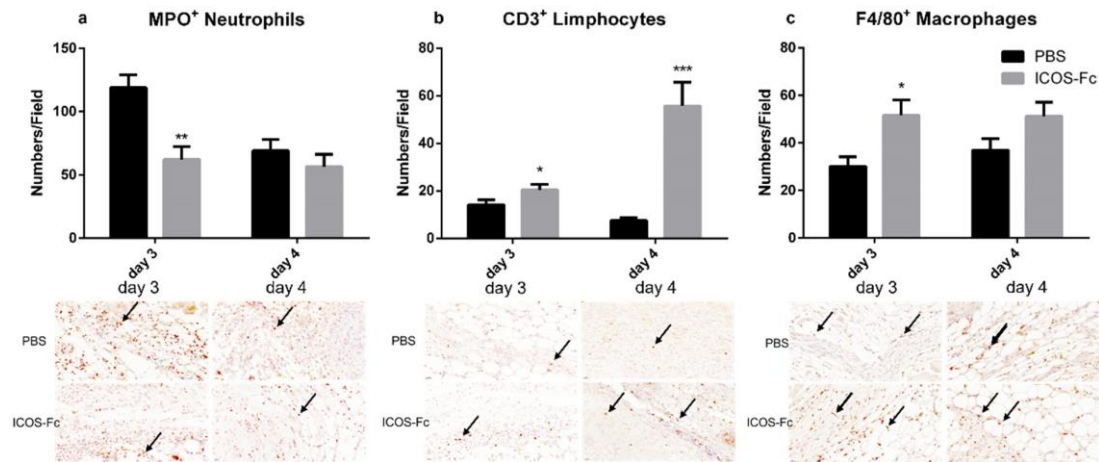


**Figure 4.** Effect of treatment with ICOS-Fc on the infiltration of inflammatory cells in the wound bed. Infiltration by neutrophils, T cells, and macrophages was assessed by immunohistochemistry using antibodies against MPO (a), CD3 (b), and F4/80 (c), respectively. Upper panels: number of positive cells per field counting 9 fields in each experiment at day 3 and day 4; results are expressed as mean  $\pm$  SE. Lower panels: representative immunohistochemical staining (magnification 400 $\times$ ) at day 3. Statistical analysis was performed with Mann-Whitney test: \*  $p < 0.05$ ; \*\*  $p < 0.01$ ; \*\*\*  $p < 0.0005$ .

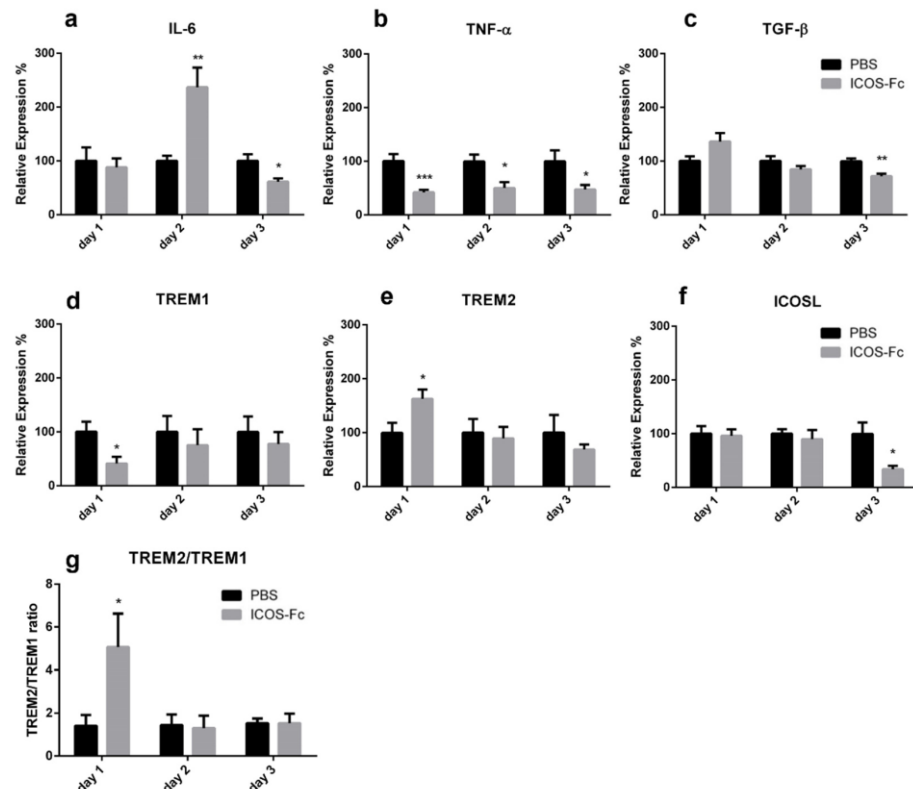


**Figure 5.** Effect of treatment with ICOS-Fc on the expression of inflammatory molecules in the wound. Expression of IL-6 (a), TNF- $\alpha$  (b), TGF- $\beta$  (c), TREM1 (d), TREM2 (e), and ICOSL (f) mRNA as assessed by real time PCR at day 1, day 2, and day 3, and expressed as mean  $\pm$  SE from 3 independent experiments. (g) TREM2/TREM1 ratio. Results are expressed as % of the mRNA amount detected in PBS-treated mice at each time point; \*  $p < 0.05$ ; \*\*  $p < 0.005$ ; \*\*\*  $p < 0.001$ , calculated by unpaired Student's *t*-test.

### 2.3. Effects of ICOSL Triggering on Macrophages

As our results demonstrated that treatment with ICOS-Fc increases the recruitment of macrophages to the healing wound, with apparent predominance of TREM2<sup>+</sup> M2 macrophages, we sought to determine the effect of ICOS-Fc treatment on the migration of mouse M1 and M2 macrophages differentiated in vitro. To this end, spleen adherent cells were differentiated into macrophages by culturing them for 14 days in the presence of M-CSF. Cells were then cultured for an additional 2 days in the presence of IFN- $\gamma$  to obtain M1 cells, or with IL-4 to obtain M2 cells; both culture conditions were performed in the presence or absence of LPS. At the end of the culture, differentiation was assessed by evaluating expression of NOS2 and ARG1 mRNA levels, marking M1 and M2 cells, respectively. As expected, M1 cells expressed higher levels of NOS2 and lower levels of ARG1 than M2 cells (Figure 6a). Analysis of ICOS and ICOSL mRNA showed that both M1 and M2 macrophages expressed ICOSL but not ICOS (data not shown), whereas M1 cells expressed higher ICOSL levels than M2 cells (Figure 6b).

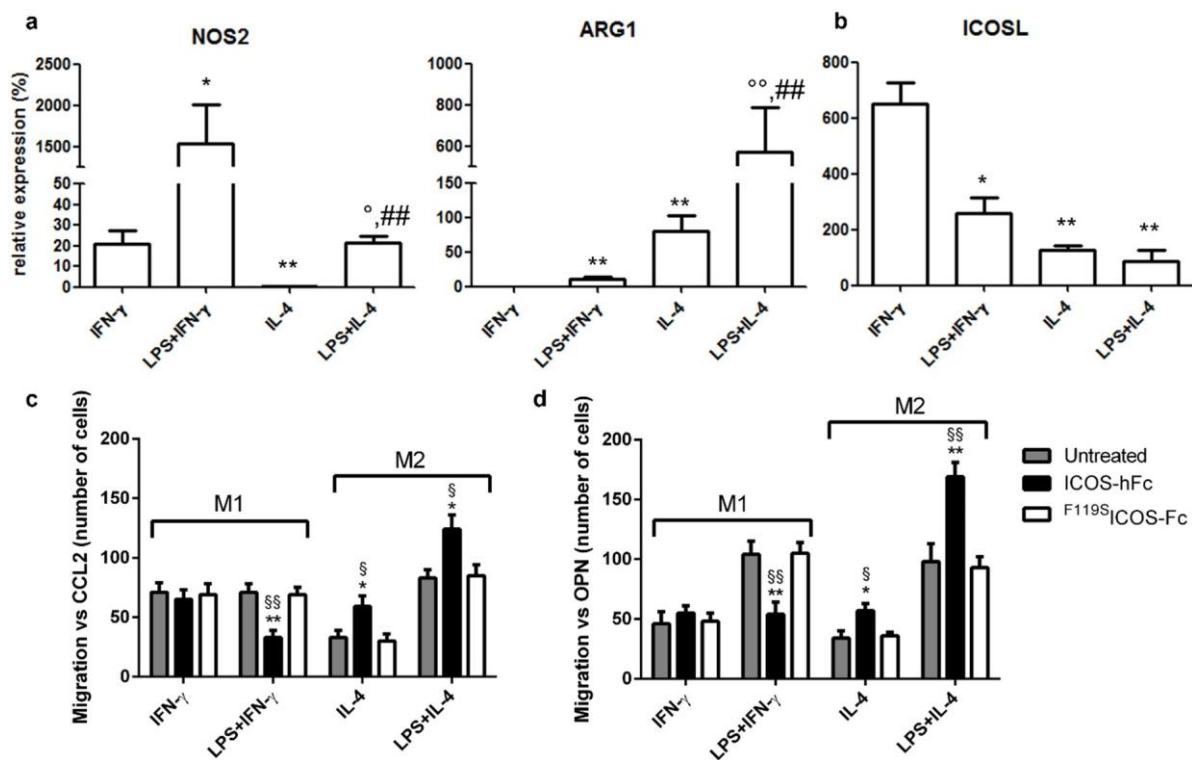


**Figure 6.** Effect of ICOS-Fc on the migration of murine M1 and M2 macrophages. Macrophages obtained by culturing adherent spleen cells with M-CSF for 14 days (M0) were polarized to M1 or M2 macrophages by culturing them with IFN- $\gamma$  or LPS + IFN- $\gamma$  (M1) or with IL-4 or LPS + IL-4 (M2) for 48 h. (a) NOS2, ARG1, and (b) ICOSL gene expression analysis by real-time PCR. Values are expressed as % of the mRNA detected in M0 macrophages stimulated with LPS for 48 h (\*  $p < 0.05$ , \*\*  $p < 0.01$  vs. IFN- $\gamma$ , <sup>°</sup>  $p < 0.05$ , <sup>°°</sup>  $p < 0.01$  vs. IL-4, ###  $p < 0.01$  vs. LPS + IFN- $\gamma$ , Mann-Whitney test). (c,d) Cell migration assay. Murine M1 and M2 macrophages were cultured in the presence and absence of ICOS-hFc or <sup>F119S</sup>ICOS-Fc using either CCL2 (30 nM) (c) or OPN (10  $\mu$ g/mL) (d) as chemotactic factors. Values are expressed as number of migrating cells, stimulated with either CCL2 or OPN. The results are expressed as mean  $\pm$  SE from  $n = 3$ –8 experiments; differences versus either <sup>F119S</sup>ICOS-Fc (\*  $p < 0.05$ ; \*\*  $p < 0.01$ ) or the untreated control (<sup>§</sup>  $p < 0.05$ ; <sup>§§</sup>  $p < 0.01$ ) for each condition are calculated by Dunnett test.

These cells were then used to assess the effect of ICOS-Fc on cell migration induced by either CCL2 or OPN through Boyden chamber assay. To minimize the possible confounding effects due to interactions with Fc $\gamma$  receptors (Fc $\gamma$ R<sub>s</sub>), we used the recombinant ICOS-hFc,

which consists of the extracellular portion of murine ICOS fused to the Fc of human IgG1. In addition, human  $^{F119S}$ ICOS-Fc, which does not bind to either ICOSL or mouse Fc $\gamma$ Rs, was used as negative control [8–11]. Consistent with our previous results *in vivo*, stimulation with ICOS-hFc increased the migration of M2 macrophages—regardless of the presence of LPS in the culture medium—compared to that of  $^{F119S}$ ICOS-Fc-treated cells. In contrast, ICOS-hFc treatment inhibited the migration of M1 macrophages stimulated with LPS, whereas it had no effect on those cultured in the absence of LPS. Similar results were observed by using either CCL2 (Figure 6c) or OPN as chemoattractant stimuli (Figure 6d). On the other hand, treatment with  $^{F119S}$ ICOS-Fc did not show any effect under any experimental conditions when compared to control migration assays performed in the absence of any form of ICOS-Fc.

#### 2.4. Wound Healing in KO Mice

To determine the functional role of ICOS and ICOSL in wound healing *in vivo*, we investigated the effect of ICOS-Fc treatment in wounded mice deficient for ICOS or ICOSL, and NSG mice, lacking T, B, and NK cells.

Analysis of wound healing in the absence of ICOS-Fc treatment showed that ICOS $^{-/-}$ , ICOSL $^{-/-}$ , and NSG mice displayed a substantial healing delay, compared to wild type mice, starting from day 4 (Figure 7a). Treatment with ICOS-Fc significantly improved wound closure in ICOS $^{-/-}$  and NSG mice, while it was ineffective in ICOSL $^{-/-}$  mice (Figure 7b–d). Thus, the fact that ICOS-Fc treatment promotes wound healing in all strains expressing ICOSL but fails to do so in ICOSL $^{-/-}$  mice suggests that ICOSL triggering drives tissue repair. Consistent with the data obtained in wild type mice, also in ICOS $^{-/-}$  and NSG mice, ICOS-Fc significantly improved wound closure mainly in the initial part of healing (day 1–6), while the healing curve gradually aligned with control levels at later time points.

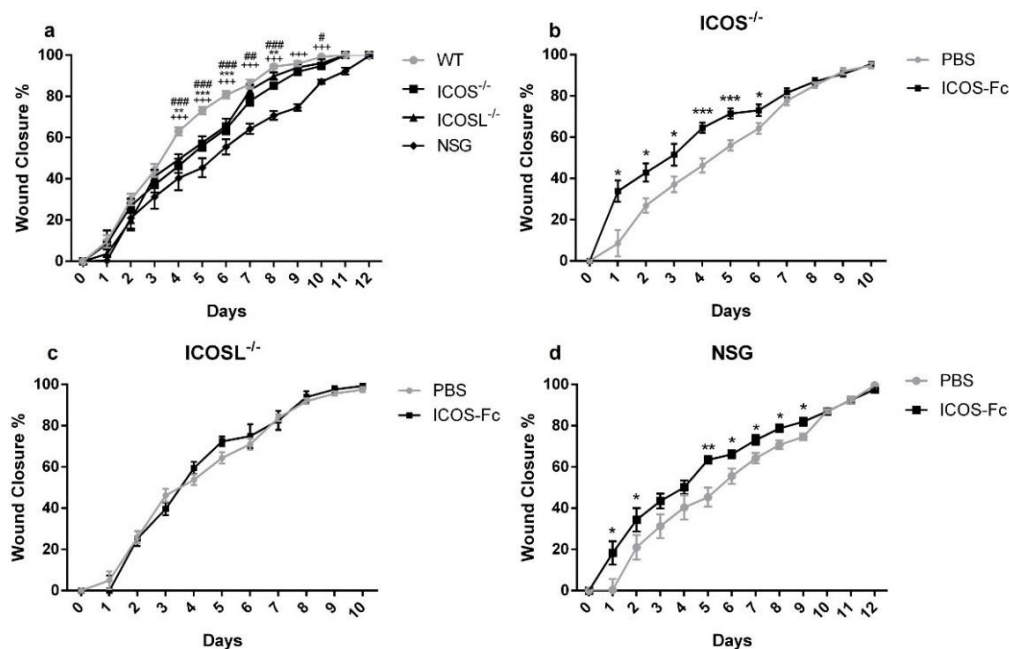


**Figure 7.** Effect of treatment with ICOS-Fc on wound healing in various KO mice. Wound healing % was calculated as described in the legend to Figure 2. (a) Comparison of wound healing in wild-type mice (n = 21), ICOS $^{-/-}$  (n = 16), ICOSL $^{-/-}$  (n = 18), and NSG (n = 15) mice. (b–d) Effect of treatment with ICOS-Fc on wound healing in ICOS $^{-/-}$  (PBS: n = 16; ICOS-Fc: n = 11), ICOSL $^{-/-}$  (PBS: n = 9; ICOS-Fc: n = 9), and NSG (PBS: n = 15; ICOS-Fc: n = 16) mice. \*  $p < 0.05$ ; \*\*  $p < 0.005$ ; \*\*\*  $p < 0.001$ ; #  $p < 0.05$ ; ##  $p < 0.005$ ; ###  $p < 0.001$ ; +  $p < 0.001$ ; ++  $p < 0.001$ ; +++  $p < 0.001$ ; calculated by Mann–Whitney test.

### 3. Discussion

The present study shows that ICOS and ICOSL cooperate in skin wound healing and that triggering of ICOSL by instillation of ICOS-Fc into the wound bed favors tissue repair *in vivo*. These results extend those obtained by Maeda et al. [15] showing that wound healing is delayed in ICOS<sup>-/-</sup>, ICOSL<sup>-/-</sup>, or ICOS/ICOSL<sup>-/-</sup> mice, possibly due to defective production of IL-4, IL-10, and, especially, IL-6 at the wound site. Since this defective repair was overcome by adoptive transfer of wild-type T cells (expressing ICOS) in ICOS<sup>-/-</sup> but not ICOSL<sup>-/-</sup> mice, the authors concluded that the healing defect in KO mice could be ascribed to the impaired development of T helper type 2 cells due to the lack of ICOS-mediated co-stimulation of T cells.

Even though our findings confirm that wound healing is defective in mice lacking ICOS or ICOSL, the observation that ICOSL stimulation by ICOS-Fc is sufficient to accelerate the early phases of the healing process underscores the importance of ICOSL in ICOS/ICOSL-mediated tissue repair. Indeed, enhanced wound healing in response to ICOS-Fc treatment is readily apparent in both wild-type and ICOS<sup>-/-</sup> mice, but not in mice lacking ICOSL, which indicates that this effect is not due to the inhibition of ICOS activity in T cells, but it is instead caused by ICOSL-mediated “reverse signaling” in other cell types. The fact that ICOS-Fc treatment is effective also in immunodeficient NSG mice confirms that T cells are not involved in ICOS-Fc-induced wound healing. Moreover, the lack of effect in ICOSL<sup>-/-</sup> mice rules out possible confounding effects due to the potential interaction of ICOS-Fc with Fcγ receptors.

A key effect of ICOS-Fc is represented by increased angiogenesis and recruitment of fibroblasts at day 3 and 4, as judged by histologic analysis, both of which are preceded by upregulation of CD31 and VEGF-α – two markers of angiogenesis – and αSMA – a marker of reparative myofibroblasts – mRNA expression at day 1 and 2, respectively. Enhanced angiogenesis in response to ICOSL triggering was unexpected since previous works had shown that *in vivo* treatment with ICOS-Fc curbed neoplastic angiogenesis in several mouse tumor types, and *in vitro* experiments showed that ICOS-Fc had no effect on angiogenesis induced by VEGF whereas it inhibited that induced by OPN [8,18].

Another interesting observation from our histological analysis is that ICOS-Fc treatment can also modulate the infiltration of inflammatory cells by decreasing neutrophils and increasing T cells and macrophages. The decrease in neutrophils is in line with previous data showing that ICOS-Fc inhibits neutrophil adhesion to ECs, which may affect their recruitment into inflamed tissues [8]. The increase in T cells might be ascribable to the enhanced vascularization of the wound or to the functional antagonism between ICOS-Fc and ICOS expressed on T cells given that, at least in tumors, ICOS-Fc treatment is known to increase effector T cells and decrease regulatory T cells [18,20]. The increase in macrophages is quite intriguing as it is accompanied by a five-fold increase in TREM2/TREM1 expression ratio, which suggests that ICOS-Fc favors recruitment of TREM2<sup>+</sup> M2-like reparative macrophages, as compared to TREM1<sup>+</sup> M1-like inflammatory macrophages. This possibility is also supported by our cell migration experiments *in vitro*, showing that ICOS-Fc enhances the migration of M2 macrophages, whereas it inhibits that of M1 macrophages. The increased migration of M2 macrophages was unexpected, since ICOS-Fc had always inhibited the migration response of all cell types analyzed until then [8–10,12,20,21]. The different response of mouse M1 and M2 macrophages may be due to differences in their migration and adhesive properties likely caused by higher expression levels of β2 integrins in M1 vs. M2 cells [22]. Intriguingly, ICOS-Fc treatment also led to increased migration of keratinocytes, as judged by our scratch assay analysis, which could be the result of changes in size, shape, adhesiveness, and organization of keratin intermediate filaments of these cells as shown previously [23].

Overall, the effects of ICOS-Fc on wound healing are in line with our previous work showing that CCl<sub>4</sub>-treated ICOS<sup>-/-</sup> or ICOSL<sup>-/-</sup> mice develop a more severely acute inflammatory liver damage, along with a reduction of reparative macrophages, compared to their wild-type counterparts. Moreover, treatment with ICOS-Fc protected ICOS-deficient

mice from this increased damage, simultaneously restoring the number of reparative macrophages, whereas it had no effects in ICOSL<sup>-/-</sup> mice [17]. These findings are also in line with the aforementioned study by Maeda et al. [15], showing that mice lacking ICOS and/or ICOSL display decreased angiogenesis and a reduction of T cells and macrophages at the wound site. Intriguingly, the authors observed decreased IL-6 in the wounds of these mice, and local application of exogenous IL-6 in the initial phase of healing (day 1) led to a substantial improvement of tissue repair. A potential role of ICOSL-induced IL-6 production in wound healing is also supported by our observation that treatment with ICOS-Fc of wounded wild-type mice increases the expression of IL-6 at day 2 [15].

#### 4. Materials and Methods

##### 4.1. Scratch Assay

HaCat cells (human keratinocytes) were purchased from ATCC (Manassas, VA, USA) and grown in DMEM (Life Technologies, Carlsbad, CA, USA) medium plus 10% fetal bovine serum (FBS; Life Technologies). HaCat cells were plated in six-well plates at a concentration of 10<sup>6</sup> cells/well and grown to confluence. To prevent cell proliferation, cells were incubated for 12 h in FBS-free medium. Cell monolayers were wounded by scratching with a sterile plastic pipette tip along the diameter of the well. Cells were then incubated in culture medium in the absence or presence of 2 µg/mL human ICOS-Fc or <sup>125</sup>I-ICOS-Fc, an ICOS-Fc mutant unable to bind ICOSL. To monitor cell migration in the wound, five fields of each wound were analyzed and photographed immediately after scratching (0 h) and 24 h later. The wound closure was calculated with the following formula: (1 (scratch width of the treated group/scratch width of the control group)) × 100%.

ICOS and ICOSL expression was assessed by immunofluorescence and flow cytometry (Attune NxT, Thermo-Fisher, Waltham, MA, USA) using PE-conjugated mAb to ICOS or ICOSL (R&D System, Minneapolis, MN, USA). The mean fluorescence intensity ratio (MFI-R) was calculated according to the following formula: MFI of the stained sample histogram (arbitrary units)/MFI of the control histogram (arbitrary units).

##### 4.2. Mice

C57BL6/J (WT), NOD-SCID-IL2R γ-null mice (NSG) and knockout B6.129P2-Icos<sup>tm1Mak</sup>/J (ICOS<sup>-/-</sup>) and B6.129P2-Icosl<sup>tm1Mak</sup>/J (ICOSL<sup>-/-</sup>) mice (The Jackson Laboratory, Bar Harbor, ME, USA) were bred under pathogen-free conditions in the animal facility at Università del Piemonte Orientale, Department of Health Sciences (Authorization No. 217/2020-PR) and treated in accordance with the Ethical Committee and European guidelines.

##### 4.3. In Vivo Wounds

The day before wound induction (day-1), WT, NSG, ICOS<sup>-/-</sup>, and ICOSL<sup>-/-</sup> mice were anesthetized with 2% isoflurane and their back was shaved. At day 0, mice were anesthetized as above, and wounds were made on their back using a 4 mm puncher (Kai Medical, Solingen, Germany). The wound area was photographed and measured using the following formula: (a/2) × (b/2) × 3.14, where “a” and “b” are the two perpendicular diameters. In the following days, wound closure was calculated using the following formula: (wound area<sup>T0</sup>-wound area<sup>TX</sup>)/wound area<sup>T0</sup> × 100%. Mice were treated daily with 10 µg/mouse ICOS-Fc in PBS instilled directly into the wound site; controls were treated with an equal volume of PBS. Mice were monitored daily for 12 days, at which point in time the wound was closed. In some experiments, mice were sacrificed at day 1, 2, 3, and 4 to harvest and analyze the healing tissue. Each experiment involved 4–7 mice for each condition tested; each condition was tested in 2–3 independent experiments. Sample size was calculated using G\*Power (RRID:SCR\_013726) software (Power: 80%; Significance: 95%).

#### 4.4. Real-Time PCR Analysis

Total RNA was isolated from skin samples collected at day 1, 2, and 3 post-injury, or from in vitro-differentiated macrophages using TRIzol reagent (Sigma-Aldrich, St. Louis, MO, USA). RNA (1 µg) was retro-transcribed using QuantiTect Reverse Transcription Kit (Qiagen, Hilden, Germany). Expression of the IL-6, TNF- $\alpha$ , TGF- $\beta$ , IL-33, IL-10, IL-4, IFN- $\gamma$ , OPN, TREM1, TREM2, VEGF- $\alpha$ ,  $\alpha$ -SMA, ICOS, NOS2, ARG1, and ICOSL mRNA were evaluated by real-time PCR (Assay-on Demand; Applied Biosystems, Foster City, CA, USA). The  $\beta$ -actin gene was used to normalize the cDNA amounts. Real-time PCR was performed using the CFX96 System (Bio-Rad Laboratories, Hercules, CA, USA) in duplicate for each sample in a 10 µL final volume containing 1 µL of diluted cDNA, 5 µL of TaqMan Universal PCR Master Mix (Applied Biosystems, Foster City, CA, USA), and 0.5 µL of Assay-on-Demand mix. The results were analyzed with a  $\Delta\Delta$  threshold cycle method.

#### 4.5. Histological Analysis

Skin samples were collected at day 3 and 4 post-injury and processed for paraffin embedding. Samples were cut at 4-µm thickness and stained with hematoxylin and eosin (H&E) (Sigma-Aldrich) for tissue morphology and fibroblast evaluation, or with picrosirius red (Abcam, Cambridge, UK) to evaluate the extent of fibrosis.

Immunohistochemical staining of CD31, MPO, CD3, and F4/80 was performed to detect neo vessel formation and infiltration of immune cells (i.e., neutrophils, T cells, and macrophages). Samples were treated with citrate buffer (Vector Laboratories, Burlingame, CA, USA) for antigen retrieval, and endogenous peroxidases were blocked with 3% H<sub>2</sub>O<sub>2</sub> (Sigma-Aldrich). To avoid secondary antibody unspecific binding, samples were pre-incubated with 5% normal goat serum (NGS) (Sigma-Aldrich) for 1 h at room temperature (RT). Samples were stained with rabbit antibodies against CD31 (Abcam, 1:50), MPO (Invitrogen, 1:100), CD3 (Invitrogen, 1:150), or F4/80 (Invitrogen, 1:100) overnight at 4 °C and, then, with a goat anti-rabbit horseradish peroxidase (HRP)-conjugated secondary antibody (Sigma-Aldrich), followed by 3,3'-diaminobenzidine (DAB) (Agilent Dako, Santa Clara, CA, USA). Successively, samples were counterstained with hematoxylin (Sigma-Aldrich), dehydrated, and mounted on cover slips. Slides were acquired using Panoramic MIDI (3D Histech, Budapest, Hungary) at 200 $\times$  magnification. The positive areas for CD31, fibroblasts, and collagen were calculated using the following formula: (positive area/total area)  $\times$  100%. MPO, CD3, and F4/80 positive cells were expressed as cell number/field counted in 15 fields for each sample.

#### 4.6. Macrophage Migration Assay

Spleen cells were separated by density gradient centrifugation using the Ficoll-Hypaque reagent (Lympholyte-M, Cedarlane Laboratories, Burlington, ON, Canada) and incubated in tissue culture dishes for 2 h with DMEM supplemented with 10% FBS. Subsequently, supernatants and non-adherent cells were discarded, and the adherent cells were rinsed three times and cultured in DMEM (Life Technologies) medium supplemented with 10% FBS, 1% glutamine, and 1% penicillin/streptomycin plus 20 ng/mL M-CSF (Immunotools, Friesoythe, Germany) for 14 days (normal DMEM medium). At day 14, adherent cells were cultured for additional 48 h with interferon- $\gamma$  (IFN- $\gamma$ ; 100 U/mL Immunotools) to obtain M1 macrophages, and with interleukin-4 (IL-4; 20 ng/mL Immunotools) to obtain M2 macrophages; each culture condition was performed in the presence or absence of LPS (LPS; 100 ng/mL Sigma).

Macrophage migration was assessed by the Boyden chamber migration assay (BD Biosciences, San Jose, CA, USA). Cells were plated (10<sup>4</sup> cell/well) onto the apical side of 50 µg/mL Matrigel-coated filters in serum-free medium in the presence or absence of msICOS-huFc (2 µg/mL), composed by the extracellular portion of murine ICOS fused to the Fc of human IgG1, or human <sup>F119S</sup>ICOS-Fc (2 µg/mL). Mouse CCL2 (30 nM, Immunotools) or OPN (10 µg/mL) were used as chemoattractants in the bottom chamber. After 6 h, the cells on the apical side were wiped off with Q-tips. Cells on the bottom of the filter

were stained with crystal violet and all counted (quadruplicate filter) with an inverted microscope. Data are shown as number of migrating cells [12].

#### 4.7. Statistical Analyses

Statistical analyses were performed using Mann–Whitney U test, Wilcoxon test, Dunnett’s test, or Student’s *t*-test using GraphPad InStat Software (GraphPad Software, San Diego, CA, USA), as indicated. Data are expressed as mean and standard error of the mean (SEM) and statistical significance was set at  $p < 0.05$ .

### 5. Conclusions

In conclusion, this work shows that ICOSL plays a key role in wound healing and that triggering of ICOSL by ICOS-Fc favors healing by increasing angiogenesis and the recruitment of fibroblasts and reparative macrophages. Therefore, ICOS-Fc and other molecules capable of triggering ICOSL might be exploited to improve wound closure in patients with impaired tissue repair.

**Author Contributions:** Conceptualization, U.D., F.R., R.B. and E.B.; methodology, I.S., C.L.G., N.C., D.P., C.D., C.M. and C.P. validation, E.B., C.D. and U.D.; formal analysis, I.S., R.R., C.L.G. and E.B.; investigation, I.S., C.L.G., C.M., C.P., D.P. and C.D.; resources, U.D. and C.D.; data curation, R.B., F.R. and U.D.; writing—original draft preparation, I.S., C.L.G. and E.B.; writing—review and editing, I.S., C.L.G., S.S., C.D., F.R. and U.D.; visualization, I.S. and E.B.; supervision, U.D.; project administration, U.D.; funding acquisition, U.D. and C.D. All authors have read and agreed to the published version of the manuscript.

**Funding:** IG 20714 Associazione Italiana per la Ricerca sul Cancro, Milan, Italy; Fondazione Cariplo (2017–0535); University of Turin fund (DIAC\_RILO\_21).

**Institutional Review Board Statement:** The study was approved by the Italian Ministry of Health (Authorization No. 217/2020-PR), in accordance with the local Ethical Committee and European guidelines.

**Informed Consent Statement:** Not applicable.

**Data Availability Statement:** Raw data are available on request from the corresponding author.

**Acknowledgments:** The authors thank Michela Salvo who performed the H&E staining.

**Conflicts of Interest:** E.B., C.L.G. and U.D. are listed as inventors on the patent WO/2016/189428 “Ligands of B7h receptor in the treatment of osteopenia and osteoporosis” and are founders of an UPO Spinoff (NOVAICOS). U.D., C.D., E.B., N.C. and C.L.G. are listed as inventors on the patent PCT/IB2019/050154 “Novel anti-tumor therapeutic agents”.

### References

1. Singer, A.J.; Clark, R.A. Cutaneous wound healing. *N. Engl. J. Med.* **1999**, *341*, 738–746. [[CrossRef](#)] [[PubMed](#)]
2. Singampalli, K.L.; Balaji, S.; Wang, X.; Parikh, U.M.; Kaul, A.; Gilley, J.; Birla, R.K.; Bollyky, P.L.; Keswani, S.G. The Role of an IL-10/Hyaluronan Axis in Dermal Wound Healing. *Front. Cell Dev. Biol.* **2020**, *8*, 636. [[CrossRef](#)] [[PubMed](#)]
3. Aicher, A.; Hayden-Ledbetter, M.; Brady, W.A.; Pezzutto, A.; Richter, G.; Magaletti, D.; Buckwalter, S.; Ledbetter, J.A.; Clark, E.A. Characterization of human inducible costimulator ligand expression and function. *J. Immunol.* **2000**, *164*, 4689–4696. [[CrossRef](#)] [[PubMed](#)]
4. Li, D.; Xiong, X. ICOS<sup>+</sup> Tregs: A Functional Subset of Tregs in Immune Diseases. *Front. Immunol.* **2020**, *11*, 2104, Correction in *Front. Immunol.* **2021**, *12*, 701515. [[CrossRef](#)]
5. Yoshinaga, S.K.; Whoriskey, J.S.; Khare, S.D.; Sarmiento, U.; Guo, J.; Horan, T.; Shih, G.; Zhang, M.; Coccia, M.A.; Kohno, T.; et al. T-cell co-stimulation through B7RP-1 and ICOS. *Nature* **1999**, *402*, 827–832. [[CrossRef](#)] [[PubMed](#)]
6. Sharpe, A.H.; Freeman, G.J. The B7-CD28 superfamily. *Nat. Rev. Immunol.* **2002**, *2*, 116–126. [[CrossRef](#)]
7. Tang, G.; Qin, Q.; Zhang, P.; Wang, G.; Liu, M.; Ding, Q.; Qin, Y.; Shen, Q. Reverse signaling using an inducible costimulator to enhance immunogenic function of dendritic cells. *Cell. Mol. Life Sci.* **2009**, *66*, 3067–3080. [[CrossRef](#)]
8. Dianzani, C.; Minelli, R.; Mesturini, R.; Chiocchetti, A.; Barrera, G.; Boscolo, S.; Sarasso, C.; Gigliotti, C.L.; Sblattero, D.; Yagi, J.; et al. B7h triggering inhibits umbilical vascular endothelial cell adhesiveness to tumor cell lines and polymorphonuclear cells. *J. Immunol.* **2010**, *185*, 3970–3979. [[CrossRef](#)]
9. Dianzani, C.; Minelli, R.; Gigliotti, C.L.; Occhipinti, S.; Giovarelli, M.; Conti, L.; Boggio, E.; Shivakumar, Y.; Baldanzi, G.; Malacarne, V.; et al. B7h triggering inhibits the migration of tumor cell lines. *J. Immunol.* **2014**, *192*, 4921–4931. [[CrossRef](#)]

10. Occhipinti, S.; Dianzani, C.; Chiocchetti, A.; Boggio, E.; Clemente, N.; Gigliotti, C.L.; Soluri, M.F.; Minelli, R.; Fantozzi, R.; Yagi, J.; et al. Triggering of B7h by the ICOS modulates maturation and migration of monocyte-derived dendritic cells. *J. Immunol.* **2013**, *190*, 1125–1134. [[CrossRef](#)]
11. Gigliotti, C.L.; Boggio, E.; Clemente, N.; Shivakumar, Y.; Toth, E.; Sblattero, D.; D'Amelio, P.; Isaia, G.C.; Dianzani, C.; Yagi, J.; et al. ICOS-Ligand Triggering Impairs Osteoclast Differentiation and Function In Vitro and In Vivo. *J. Immunol.* **2016**, *197*, 3905–3916. [[CrossRef](#)] [[PubMed](#)]
12. Raineri, D.; Dianzani, C.; Cappellano, G.; Maione, F.; Baldanzi, G.; Iacobucci, I.; Clemente, N.; Baldone, G.; Boggio, E.; Gigliotti, C.L.; et al. Osteopontin binds ICOSL promoting tumor metastasis. *Commun. Biol.* **2020**, *3*, 615. [[CrossRef](#)] [[PubMed](#)]
13. Weber, C.E.; Li, N.Y.; Wai, P.Y.; Kuo, P.C. Epithelial-mesenchymal transition, TGF- $\beta$ , and osteopontin in wound healing and tissue remodeling after injury. *J. Burn Care Res.* **2012**, *33*, 311–318. [[CrossRef](#)] [[PubMed](#)]
14. Mori, R.; Shaw, T.J.; Martin, P. Molecular mechanisms linking wound inflammation and fibrosis: Knockdown of osteopontin leads to rapid repair and reduced scarring. *J. Exp. Med.* **2008**, *205*, 43–51. [[CrossRef](#)]
15. Maeda, S.; Fujimoto, M.; Matsushita, T.; Hamaguchi, Y.; Takehara, K.; Hasegawa, M. Inducible costimulator (ICOS) and ICOS ligand signaling has pivotal roles in skin wound healing via cytokine production. *Am. J. Pathol.* **2011**, *179*, 2360–2369. [[CrossRef](#)]
16. Johnson, B.Z.; Stevenson, A.W.; Prêle, C.M.; Fear, M.W.; Wood, F.M. The Role of IL-6 in Skin Fibrosis and Cutaneous Wound Healing. *Biomedicines* **2020**, *8*, 101. [[CrossRef](#)]
17. Ramavath, N.N.; Gadipudi, L.L.; Provera, A.; Gigliotti, L.C.; Boggio, E.; Bozzola, C.; Albano, E.; Dianzani, U.; Sutti, S. Inducible T-Cell Costimulator Mediates Lymphocyte/Macrophage Interactions During Liver Repair. *Front. Immunol.* **2021**, *12*, 786680. [[CrossRef](#)]
18. Clemente, N.; Boggio, E.; Gigliotti, L.C.; Raineri, D.; Ferrara, B.; Miglio, G.; Argenziano, M.; Chiocchetti, A.; Cappellano, G.; Trotta, F.; et al. Immunotherapy of experimental melanoma with ICOS-Fc loaded in biocompatible and biodegradable nanoparticles. *J. Control. Release* **2020**, *320*, 112–124. [[CrossRef](#)]
19. Darby, I.A.; Laverdet, B.; Bonté, F.; Desmoulière, A. Fibroblasts and myofibroblasts in wound healing. *Clin. Cosmet. Investig. Dermatol.* **2014**, *7*, 301–311.
20. Raineri, D.; Cappellano, G.; Vilardo, B.; Maione, F.; Clemente, N.; Canciani, E.; Boggio, E.; Gigliotti, C.L.; Monge, C.; Dianzani, C.; et al. Inducible T-Cell Costimulator Ligand Plays a Dual Role in Melanoma Metastasis upon Binding to Osteopontin or Inducible T-Cell Costimulator. *Biomedicines* **2021**, *10*, 51. [[CrossRef](#)]
21. Boggio, E.; Gigliotti, C.L.; Moia, R.; Scotta, A.; Crespi, I.; Boggione, P.; De Paoli, L.; Deambrogi, C.; Garzaro, M.; Vidali, M.; et al. Inducible T-cell co-stimulator (ICOS) and ICOS ligand are novel players in the multiple-myeloma microenvironment. *Br. J. Haematol.* **2022**, *196*, 1369–1380. [[CrossRef](#)] [[PubMed](#)]
22. Cui, K.; Ardell, C.L.; Podolnikova, N.P.; Yakubenko, V.P. Distinct Migratory Properties of M1, M2, and Resident Macrophages Are Regulated by  $\alpha$ D $\beta$ 2 and  $\alpha$ M $\beta$ 2 Integrin-Mediated Adhesion. *Front. Immunol.* **2018**, *9*, 2650. [[CrossRef](#)] [[PubMed](#)]
23. Wang, F.; Chen, S.; Liu, H.B.; Parent, C.A.; Coulombe, P.A. Keratin 6 regulates collective keratinocyte migration by altering cell-cell and cell-matrix adhesion. *J. Cell Biol.* **2018**, *217*, 4314–4330. [[CrossRef](#)] [[PubMed](#)]





## OPEN ACCESS

## EDITED BY

Laura Dugo,  
Campus Bio-Medico University, Italy

## REVIEWED BY

Rosanna Di Paola,  
University of Messina, Italy  
Valerio Chirchiù,  
National Research Council, CNR, Italy

## \*CORRESPONDENCE

Massimo Collino  
massimo.collino@unito.it

†These authors have contributed  
equally to this work

## SPECIALTY SECTION

This article was submitted to  
Inflammation,  
a section of the journal  
Frontiers in Immunology

RECEIVED 12 July 2022

ACCEPTED 08 August 2022

PUBLISHED 02 September 2022

## CITATION

Alves GF, Stoppa I, Aimaretti E,  
Monge C, Mastrocola R, Porchietto E,  
Einaudi G, Collotta D, Bertocchi I,  
Boggio E, Gigliotti CL, Clemente N,  
Aragno M, Fernandes D, Cifani C,  
Thiemermann C, Dianzani C,  
Dianzani U and Collino M (2022)  
ICOS-Fc as innovative  
immunomodulatory approach to  
counteract inflammation and organ  
injury in sepsis.  
*Front. Immunol.* 13:992614.  
doi: 10.3389/fimmu.2022.992614

## COPYRIGHT

© 2022 Alves, Stoppa, Aimaretti, Monge,  
Mastrocola, Porchietto, Einaudi, Collotta,  
Bertocchi, Boggio, Gigliotti, Clemente,  
Aragno, Fernandes, Cifani,  
Thiemermann, Dianzani, Dianzani and  
Collino. This is an open-access article  
distributed under the terms of the  
[Creative Commons Attribution License  
\(CC BY\)](https://creativecommons.org/licenses/by/4.0/). The use, distribution or  
reproduction in other forums is  
permitted, provided the original  
author(s) and the copyright owner(s)  
are credited and that the original  
publication in this journal is cited, in  
accordance with accepted academic  
practice. No use, distribution or  
reproduction is permitted which does  
not comply with these terms.

# ICOS-Fc as innovative immunomodulatory approach to counteract inflammation and organ injury in sepsis

Gustavo Ferreira Alves<sup>1</sup>, Ian Stoppa<sup>2</sup>, Eleonora Aimaretti<sup>3</sup>, Chiara Monge<sup>4</sup>, Raffaella Mastrocola<sup>3</sup>, Elisa Porchietto<sup>5</sup>, Giacomo Einaudi<sup>5</sup>, Debora Collotta<sup>1</sup>, Ilaria Bertocchi<sup>1</sup>, Elena Boggio<sup>2</sup>, Casimiro Luca Gigliotti<sup>2</sup>, Nausicaa Clemente<sup>2</sup>, Manuela Aragno<sup>3</sup>, Daniel Fernandes<sup>6</sup>, Carlo Cifani<sup>5</sup>, Christoph Thiemermann<sup>7</sup>, Chiara Dianzani<sup>4</sup>, Umberto Dianzani<sup>2†</sup> and Massimo Collino<sup>1\*†</sup>

<sup>1</sup>Department of Neurosciences (Rita Levi Montalcini), University of Turin, Turin, Italy, <sup>2</sup>Department of Health Sciences, Università del Piemonte Orientale, Novara, Italy, <sup>3</sup>Department of Clinical and Biological Sciences, University of Turin, Turin, Italy, <sup>4</sup>Department of Drug Science and Technology, University of Turin, Turin, Italy, <sup>5</sup>Pharmacology Unit, School of Pharmacy, University of Camerino, Camerino, Italy, <sup>6</sup>Department of Pharmacology, Federal University of Santa Catarina, Florianópolis, Brazil, <sup>7</sup>William Harvey Research Institute, Bart's and The London School of Medicine and Dentistry, Queen Mary University of London, London, United Kingdom

Inducible T cell co-stimulator (ICOS), an immune checkpoint protein expressed on activated T cells and its unique ligand, ICOSL, which is expressed on antigen-presenting cells and non-hematopoietic cells, have been extensively investigated in the immune response. Recent findings showed that a soluble recombinant form of ICOS (ICOS-Fc) can act as an innovative immunomodulatory drug as both antagonist of ICOS and agonist of ICOSL, modulating cytokine release and cell migration to inflamed tissues. Although the ICOS-ICOSL pathway has been poorly investigated in the septic context, a few studies have reported that septic patients have reduced ICOS expression in whole blood and increased serum levels of osteopontin (OPN), that is another ligand of ICOSL. Thus, we investigated the pathological role of the ICOS-ICOSL axis in the context of sepsis and the potential protective effects of its immunomodulation by administering ICOS-Fc in a murine model of sepsis. Polymicrobial sepsis was induced by cecal ligation and puncture (CLP) in five-month-old male wild-type (WT) C57BL/6, ICOS<sup>-/-</sup>, ICOSL<sup>-/-</sup> and OPN<sup>-/-</sup> mice. One hour after the surgical procedure, either CLP or Sham (control) mice were randomly assigned to receive once ICOS-Fc, F<sup>119S</sup>ICOS-Fc, a mutated form incapable to bind ICOSL, or vehicle intravenously. Organs and plasma were collected 24 h after surgery for analyses. When compared to Sham mice, WT mice that underwent CLP developed within 24 h a higher clinical severity score, a reduced body temperature, an increase in plasma cytokines (TNF- $\alpha$ , IL-1 $\beta$ , IL-6, IFN- $\gamma$  and IL-10), liver injury (AST and ALT) and kidney (creatinine and urea) dysfunction. Administration of ICOS-Fc to WT CLP mice reduced all of these abnormalities caused by sepsis. Similar beneficial effects were not seen in CLP-mice

treated with <sup>F119S</sup>ICOS-Fc. Treatment of CLP-mice with ICOS-Fc also attenuated the sepsis-induced local activation of FAK, P38 MAPK and NLRP3 inflammasome. ICOS-Fc seemed to act at both sides of the ICOS-ICOSL interaction, as the protective effect was lost in septic knockout mice for the ICOS or ICOSL genes, whereas it was maintained in OPN knockout mice. Collectively, our data show the beneficial effects of pharmacological modulation of the ICOS-ICOSL pathway in counteracting the sepsis-induced inflammation and organ dysfunction.

#### KEYWORDS

sepsis, inflammation, ICOS (inducible co-stimulatory molecule), cecal ligation and puncture, osteopontin (OPN)

## Introduction

Sepsis is a life-threatening medical emergency characterized by a complex interplay of pro- and anti-inflammatory host responses, resulting in multiple organ dysfunction that can ultimately lead to death (1). Currently, deaths from sepsis correspond to nearly 20% of all deaths worldwide, and there is still no specific treatment available (2). The inducible T cell co-stimulator (ICOS, also known as CD278) belongs to the CD28 family of co-stimulatory immunoreceptors. It is a type I transmembrane glycoprotein whose expression is rapidly upregulated upon T cells activation (3). ICOS binds to its unique ligand (ICOSL, also known as CD275 or B7h), a member of the B7 family highly expressed on antigen-presenting cells (APCs) and non-hematopoietic cells under inflammatory stimuli (4–5). Thus far, the role of ICOS-ICOSL interaction has been poorly investigated in sepsis, although recent findings report that ICOS expression is reduced in whole blood of septic patients (6), and that reduced ICOS levels are strongly associated with organ dysfunction (7). To date, it is very well documented that the ICOS-ICOSL axis may display bidirectional effects. On the one hand, ICOS triggering modulates cytokine production in activated T cells and contributes to T regulatory (Treg) cells differentiation and survival (8–9). Given the fact that both animals and septic patients have an increased percentage of circulating Treg cells (10–12), it is suggestive that ICOS triggering may play a role in the septic immunosuppressive status. On the other hand, ICOSL triggering by ICOS may exert anti-inflammatory effects *via* responses, such as modulating the maturation and migration of macrophage and dendritic cells and the endothelial cell adhesiveness (13).

Recently, another ligand for ICOSL has been identified, osteopontin (OPN), an inflammatory mediator that binds to ICOSL in an alternative binding domain to that used by ICOS. Intriguingly, ICOS and OPN exert different and often opposite

effects upon ICOSL triggering since OPN stimulates, whereas ICOS inhibits, migration of several cell types and tumor angiogenesis (14–16). Conventionally, a soluble recombinant form of ICOS (ICOS-Fc) has been designed by fusing a cloned extracellular portion of human or mouse ICOS with an Fc IgG1 portion and this molecule has been shown to trigger ICOSL thus promoting down-stream responses (17).

*In vitro*, ICOS-Fc inhibits adhesiveness of endothelial cells toward polymorphonuclear cells and tumor cells and migration of endothelial cells and tumor cells (15). These ICOS-Fc effects can also be recorded in dendritic cells (DC), along with modulated cytokine release and antigen cross-presentation in class I major histocompatibility complex molecules (13), while in osteoclasts, ICOS-Fc inhibits differentiation and function (18). *In vivo*, ICOS-Fc inhibits tumor growth and metastasis, development of osteoporosis, liver damage induced by acute inflammation following treatment with CCl<sub>4</sub>, and it favors skin wound healing (18–21). Nevertheless, little is known about the molecular mechanism(s) involved in ICOSL-mediated inflammatory response. The p38 MAPK, a well-known mediator that drives inflammation through upregulation of several pro-inflammatory cytokines such as TNF- $\alpha$  and IL-6 (22), and the NOD-like receptor protein 3 (NLRP3) inflammasome, able to induce the release of IL-1 $\beta$  and IL-18 and promote cell death by pyroptosis (23), are two of the most well characterized signaling pathways involved in the activation of the cytokine storm that contributes to organ dysfunction during sepsis. Furthermore, their pharmacological or genetic inhibition has been shown to reduce sepsis-related mortality (22–24). Finally, a non-receptor protein kinase namely Focal adhesion kinase (FAK) has been recently reported to signal inflammation downstream of the Toll-like receptor 4 upon lipopolysaccharide (LPS) challenge in macrophages and lung tissues (25). Therefore, here we investigated, for the first time, the pathological role of ICOS-ICOSL axis in the context of sepsis, its impact on selective inflammatory pathways and the potential protective effects of its

immunomodulation by administering ICOS-Fc in an experimental model of sepsis.

## Material and methods

### Animals and ethical statement

Inbred wild-type (WT, C57BL/6) mice, ICOSL knockout mice (ICOSL<sup>-/-</sup>, B6.129P2-*Icosl*<sup>tm1Mak/J</sup>), ICOS knockout mice (ICOS<sup>-/-</sup>, B6.129P2-*Icos*<sup>tm1Mak/J</sup>) and OPN knockout mice (OPN<sup>-/-</sup>, B6.129S6(Cg)-*Spp1*<sup>tm1Blh/J</sup>) were purchased from Envigo laboratories, (IT) and The Jackson Laboratory (Bar Harbor, ME, USA). Mice were housed under standard laboratory conditions, such as room temperature (25 ± 2°C) and light-controlled with free access to water and rodent chow for four weeks prior starting the experimental procedures. All animal protocols reported in this study followed the ARRIVE guidelines (26) and the recommendations for preclinical studies of sepsis provided by the MQTiPSS (27) The procedures were approved by the University's Institutional Ethics Committee as well as the National Authorities (Protocol number: 855/2021).

### Cecal ligation and puncture (CLP)-induced sepsis model

Polymicrobial sepsis was carried out by CLP surgery in male, five-month-old mice. Mice were initially placed in an anaesthesia chamber (3% isoflurane -IsoFlo, Abbott Laboratories – delivered in oxygen 0.4 L/min), then kept under anaesthesia throughout surgery with 2% isoflurane delivered in oxygen 0.4 L/min *via* a nosecone. The body temperature was maintained at 37 °C through a homoeothermic blanket and constantly monitored by a rectal thermometer. Briefly, a mid-line laparotomy (~1.0 cm) was performed in the abdomen, exposing the cecum. The cecum was then totally ligated just below the ileocecal valve and a G-21 needle was used to puncture the ligated cecum in a single through-and-through manner. A small amount (droplet, ~3mm) of fecal content was released from the cecum which was carefully relocated into the peritoneum. Sham mice underwent the same surgical procedure, but without CLP. All animals received Carprofen (5 mg/kg, s.c.) as an analgesic agent and resuscitation fluid (0.9% NaCl, 50 mL/kg, s.c.) at 37°C. Mice were constantly monitored post-surgical and then placed back into fresh clean cages.

At 24 h, body temperature and a clinical score to assess symptoms consistent with murine sepsis were recorded blindly. The following 6 criteria were used for the clinical score: lethargy, piloerection, tremors, periorbital exudates, respiratory distress and diarrhea. An observed clinical score >3 was considered as

severe sepsis, while a score between 3 and 1 was considered as moderate sepsis (28).

### Study design

Seventy-two mice were randomized into eight groups (9 mice per group): Sham + Vehicle, CLP + Vehicle, CLP + ICOS-Fc, CLP + F119S-ICOS-Fc, CLP ICOSL<sup>-/-</sup> + Vehicle, CLP ICOS<sup>-/-</sup> + Vehicle, CLP ICOS<sup>-/-</sup> + ICOS-Fc and OPN<sup>-/-</sup> + Vehicle. Treatment was given once one hour after surgery, where mice received either ICOS-Fc (100 µg each), F119S-ICOS-Fc (100 µg each) or Vehicle (PBS, pH 7.4, 100 µl each) by intravenous injection (Figure 1).

### Blood collection and organ harvesting

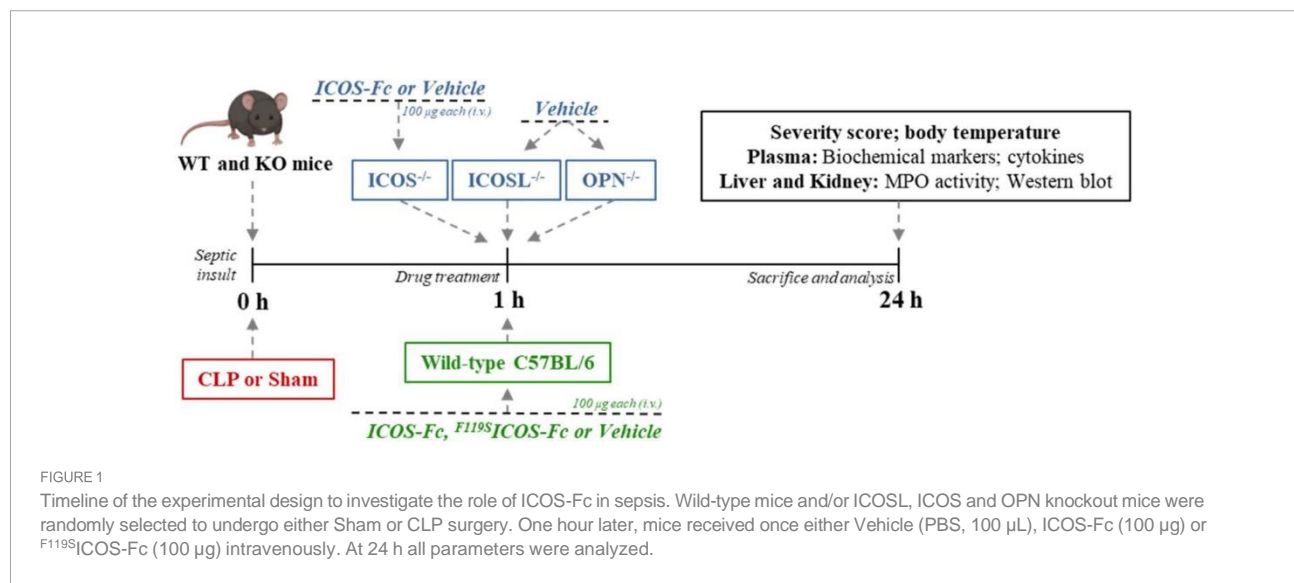
Twenty-four h after surgery all mice were anesthetized with isoflurane (3%) delivered in oxygen (0.4 L/min) and euthanized by cardiac exsanguination. Whole blood was withdrawn from each mouse in vials (EDTA 17.1 µM/mL) and plasma content was obtained after centrifugation (13,000 g, 10 min at R.T.). Organ samples (liver and kidney) were harvested and placed in cryotubes which were snap frozen in liquid nitrogen for storage at freezer -80°C. The samples were then analyzed in a blinded fashion (Figure 1).

### Biomarkers of organ injury and systemic inflammation

Plasma samples were used to measure systemic levels of aspartate aminotransferase (AST) (#7036) and alanine aminotransferase (ALT) (#7018) (as markers of hepatocellular injury), creatinine (#7075) and urea (#7144) (as markers of renal dysfunction) using colorimetric clinical assay kits (FAR Diagnostics, Verona, Italy) according to the manufacturer's instructions. Systemic cytokine levels were determined in plasma using the Luminex suspension bead-based multiplexed Bio-Plex Pro™ Mouse Cytokine Th17 Panel A 6-Plex (#M6000007NY) assay (Bio-Rad, Kabsketal, Germany). The cytokines (IL-1b, IL-6, TNF-a, IFN-g, IL-17 and IL-10) were measured following the manufacturer's instructions.

### Myeloperoxidase (MPO) activity analysis

MPO activity analysis was carried out in liver and kidney samples as previously described (29). Tissue samples (~100 mg) were homogenized (1:5 w-v) in 20 mM PBS (pH 7.4) and then centrifuged at 4°C (13,000 g, 10 min). Pellets were resuspended in



500 mL of hexadecyltrimethylammonium bromide buffer (0.5% HTAB in 50 mM PBS, pH 6.0). A second centrifugation at 4°C (13,000 g, 10 min) was performed and the supernatants (30 mL) were assessed for MPO activity by measuring spectrophotometrically (650 nm) the H<sub>2</sub>O<sub>2</sub>-dependent oxidation of 3,3',5,5'-tetramethylbenzidine (TMB). Bicinchoninic acid (BCA) protein assay (Pierce Biotechnology Inc., Rockford, IL, USA) was used to quantify the protein content in the final supernatant. MPO activity was expressed as optical density (O.D.) at 650 nm per mg of protein.

## Western blot analysis

Semi-quantitative immunoblot technique was carried out in hepatic and renal tissue samples as previously described (30). Total proteins were extracted from 50 mg of each tissue and the total content was quantified using BCA protein method following the manufacturer's instructions. Briefly, total proteins (50 µg/well) were separated by 8 and 10% sodium dodecyl sulphate-polyacrylamide gel electrophoresis (SDS-PAGE) and transferred to a polyvinylidene difluoride (PVDF) membrane, which was then blocked with 5% non-fat dry milk prepared in TBS-T buffer for 1 h at RT, followed by incubation with primary antibodies at the dilution 1:1000, rabbit anti-Thr<sup>180</sup>/anti-Tyr<sup>182</sup> p38 (Cell Signaling #9211); rabbit anti-total p38 (Cell Signaling #9212); mouse anti-NRLP3 (Adipogen- AG- 20B-0014-C100); rabbit anti-Caspase-1 (Cell Signaling #24232); rabbit anti-Tyr<sup>397</sup> FAK (Cell Signaling #3283); rabbit anti-total FAK (Cell Signaling #3285). The membranes were then incubated with a secondary antibody conjugated with

horseradish peroxidase (HRP) at the dilution 1:10000 for 1 h at RT (anti-mouse or anti-rabbit, Cell Signaling #7076 and #7074, respectively). Afterwards, the membranes were stripped and incubated with rabbit anti-β-actin (Cell Signaling #4970). Immune complexes were visualized by chemiluminescence and the densitometric analysis was performed using Bio-Rad Image Lab Software 6.0.1. Results were normalized to sham bands.

## Statistical analysis and data presentation

Sample size was determined on the basis of prior power calculations using G-Power 3.1<sup>TM</sup> software (31). Data are expressed as dot plots (for each mouse) and as mean ± S.E.M of 9 mice per group. Shapiro-Wilk and Bartlett tests were used to verify data distribution and the homogeneity of variances, respectively. The statistical analysis was performed by one-way ANOVA, followed by Bonferroni's *post-hoc* test. Data not normally distributed, a non-parametric statistical analysis was applied through Kruskal-Wallis followed by Dunn's *post hoc*-test as indicated in the figure legends. Statistical significance was set at P < 0.05. Statistical analysis was performed using GraphPad Prism<sup>®</sup> software version 7.05 (San Diego, California, USA).

## Materials

Unless otherwise stated, all reagents were purchased from the Sigma-Aldrich Company Ltd. (St. Louis, Missouri, USA).

## Results

### ICOS-Fc-mediated immunomodulation attenuates clinical status and organ injury/dysfunction triggered by sepsis

Sepsis was induced by CLP in WT mice treated with vehicle, ICOS-Fc or  $F^{119S}$ ICOS-Fc (unable to bind ICOSL) and clinical scores and body temperature were recorded after 24 h. Moreover, sepsis was induced in mice deficient for ICOS, ICOSL, or OPN to assess the role the endogenous molecules of the ICOS/ICOSL/OPN system. Finally, a group of ICOS-deficient mice received ICOS-Fc treatment to evaluate the effect of the drug in the absence of the endogenous ICOS.

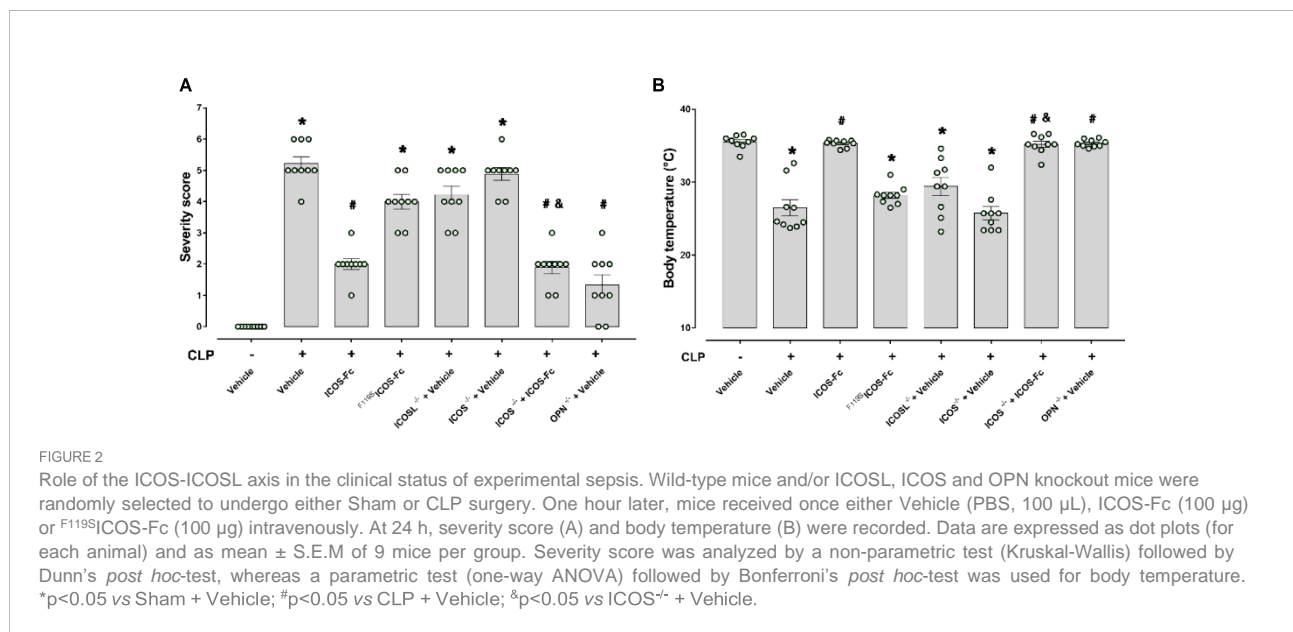
Results showed that, as expected, CLP-induced sepsis in WT mice led to a higher clinical severity score (Figure 2A) when compared to Sham WT mice, which was also associated with lower body temperature (Figure 2B). Intriguingly, treatment with ICOS-Fc improved both clinical score and hypothermia in WT septic mice, whereas treatment with  $F^{119S}$ ICOS-Fc had no effect (Figures 2A, B). Analysis of CLP knockout mice showed that ICOS $^{-/-}$  and ICOSL $^{-/-}$  mice showed similar clinical scores and decreased body temperatures as WT mice, whereas OPN $^{-/-}$  mice developed milder sepsis, with lower clinical scores and higher body temperature than WT mice. In ICOS $^{-/-}$  mice, treatment with ICOS-Fc induced similar positive effects as in WT mice (Figures 2A, B).

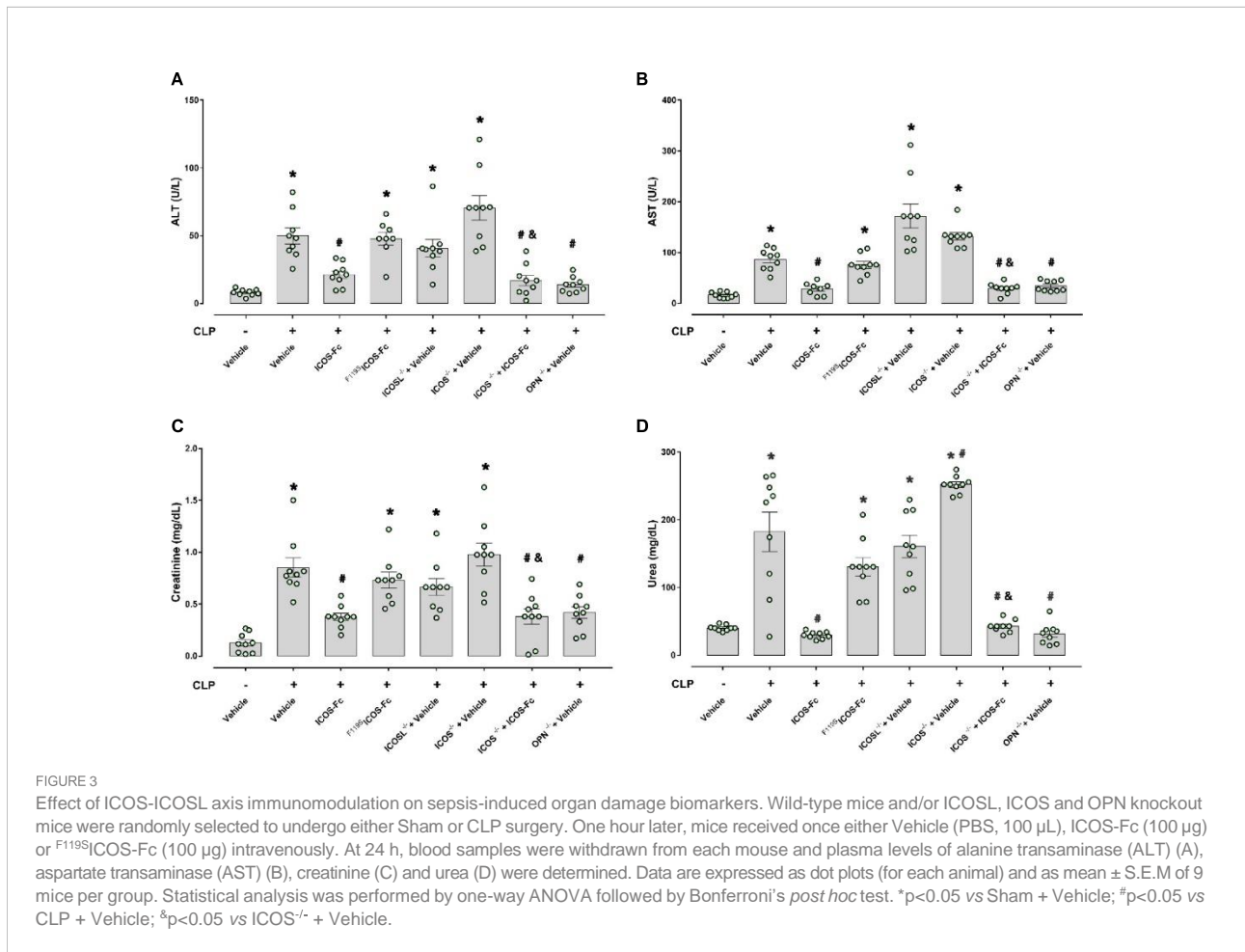
To investigate organ injury or dysfunction, plasma levels of ALT, AST, creatinine and urea were evaluated in these mice. Figure 3 shows that results mirrored those shown in Fig.2: CLP-

induced sepsis caused striking increase of ALT, AST, creatinine and urea levels in WT type mice, and these levels were decreased by treatment with ICOS-Fc, but not  $F^{119S}$ ICOS-Fc. Levels of these markers were increased also in CLP ICOS $^{-/-}$  and ICOSL $^{-/-}$  mice and urea levels were even higher in ICOS $^{-/-}$  than in WT mice. In CLP ICOS $^{-/-}$  mice, treatment with ICOS-Fc significantly decreased all these markers. In CLP OPN $^{-/-}$  mice, levels of these markers were significantly lower than in CLP WT mice.

### ICOS-Fc administration modulates experimental sepsis-induced cytokine storm

The 6 cytokines were measured systemically in plasma samples by using a multiplex array. Figure 4 shows that, in WT mice, CLP-induced sepsis led to a cytokine storm with significant increase of levels of IL-1b, IL-6, IL-10, TNF-a, IFN-g and a slight not significant increase of IL-17 compared to Sham mice. Administration of ICOS-Fc to WT CLP mice induced a significant decrease of IL-1b and TNF-a, whereas  $F^{119S}$ ICOS-Fc had no effect. Levels of IL-1b, IL-6, IL-10, TNF-a, and IFN-g were also increased in CLP ICOS $^{-/-}$  and ICOSL $^{-/-}$  mice at levels similar to those observed in CLP WT mice. Moreover, CLP ICOSL $^{-/-}$  mice showed higher levels of IL-17 than Sham mice, and CLP ICOS $^{-/-}$  mice displayed higher levels of TNF-a and, especially, IL-10 than CLP WT mice. The CLP ICOS $^{-/-}$  mice treated with ICOS-Fc significantly decreased levels of IL-1b, IL-6 and IL-10 compared to the untreated counterparts. In CLP OPN $^{-/-}$  mice, the increase of these cytokines was in general





moderate, with levels of IL-6, IL-10, TNF- $\alpha$  and IFN- $\gamma$  higher than in Sham mice, and levels of IL-1b and IL-6 lower than in CLP WT mice.

### ICOS-Fc treatment reduces sepsis-induced increase in MPO activity in the kidney

MPO activity was assessed in the liver and kidney, as an indirect biomarker of leukocyte tissue infiltration (Figure 5). When compared to Sham mice, CLP WT mice had increased MPO activity in both liver and kidney samples, and MPO activity was significantly decreased by ICOS-Fc (but not  $F^{119S}$ ICOS-Fc treatment) in the kidney, but not in the liver. In the liver, MPO activity was similarly increased also in CLP ICOS $^{-/-}$ , ICOSL $^{-/-}$ , and OPN $^{-/-}$  mice, and it was not modified by ICOS-Fc treatment in CLP ICOS $^{-/-}$  mice. In the kidney, MPO activity was increased in CLP ICOS $^{-/-}$  and ICOSL $^{-/-}$  mice, and treatment with ICOS-Fc decreased MPO activity in CLP ICOS $^{-/-}$  mice. By contrast, CLP OPN $^{-/-}$  mice showed lower MPO levels in the kidney than CLP WT mice.

### ICOS-Fc treatment reduces local FAK/p38 signalling and NLRP3 inflammasome activation in septic mice

In order to better elucidate the molecular mechanism underlying the beneficial effects evoked by ICOS-Fc administration, we focused on WT mice investigating the changes in some signaling cascades, previously documented to be affected by the ICOS-ICOSL axis and, at the same time, known to exert key role in sepsis pathogenesis. Western blot analysis showed that CLP mice showed significant increase of the phosphorylation of FAK at Tyr $^{397}$  and p38 MAPK at Thr $^{180}$ /Tyr $^{182}$  in both hepatic (Figures 6A, C) and renal (Figures 6B, D) tissues, when compared to Sham mice. Interestingly, mice treatment with ICOS-Fc significantly attenuated the degree of phosphorylation of FAK/p38 axis in both tissues, thus suggesting reduced activation of these signaling pathways (Figures 6A–D).

We then assessed the activation of the inflammasome, by evaluating the expression of NLRP3 and cleaved caspase-1 in both liver and kidney samples (Figures 6E–H). Results showed that, in both tissues, CLP-induced sepsis significantly increased both

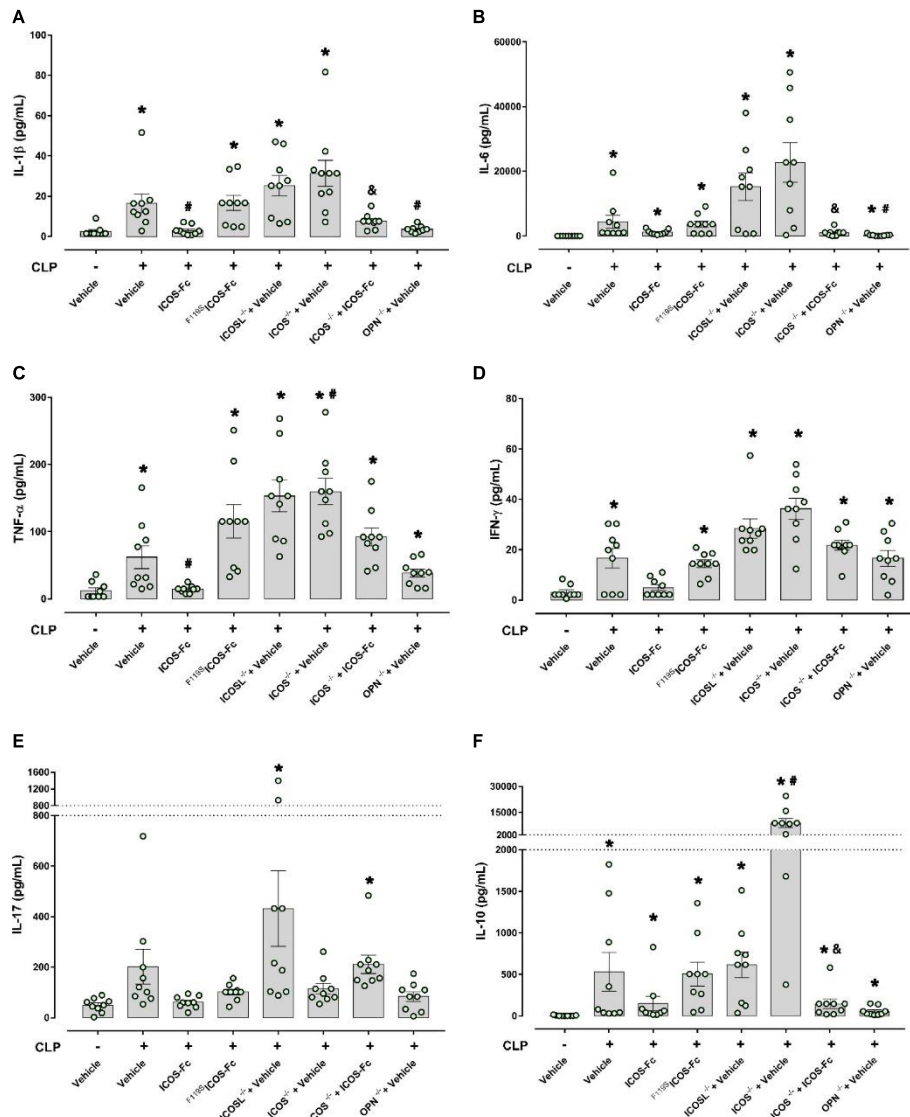


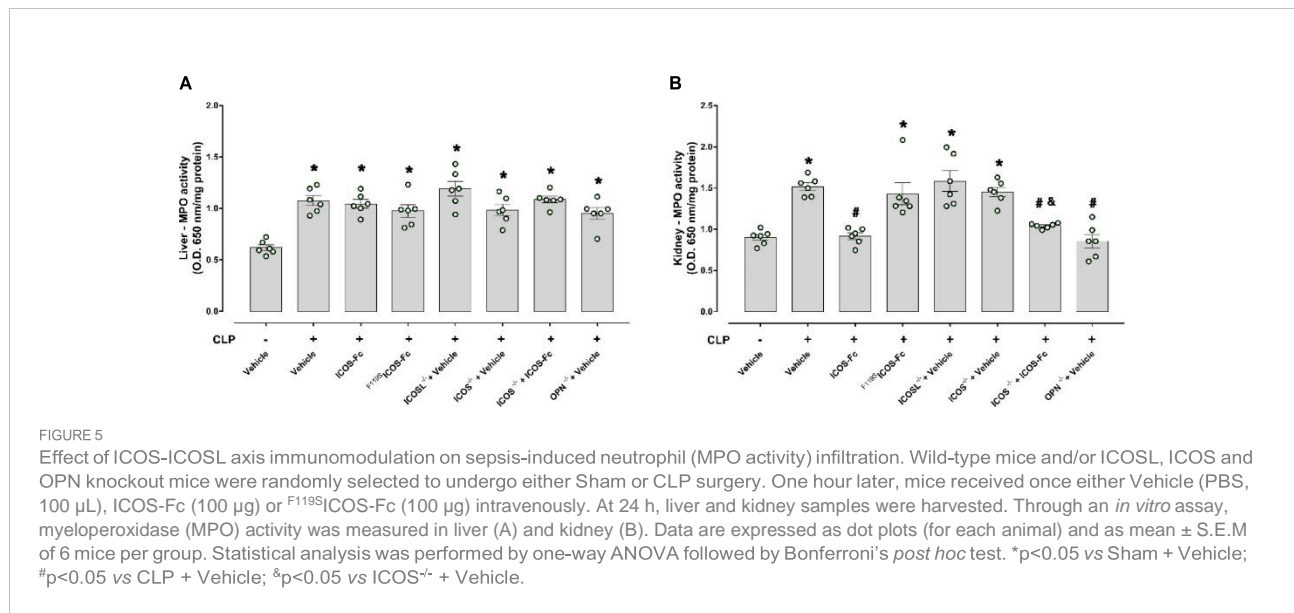
**FIGURE 4** Effect of ICOS-ICOSL axis immunomodulation on systemic cytokines during experimental sepsis. Wild-type mice and/or ICOSL, ICOS and OPN knockout mice were randomly selected to undergo either Sham or CLP surgery. One hour later, mice received once either Vehicle (PBS, 100  $\mu$ L), ICOS-Fc (100  $\mu$ g) or <sup>F119S</sup>ICOS-Fc (100  $\mu$ g) intravenously. At 24 h, blood samples were withdrawn from each mouse and plasma levels of IL-1 $\beta$  (A), IL-6 (B), TNF- $\alpha$  (C), IFN- $\gamma$  (D), IL-17 (E) and IL-10 (F) were determined. Data are expressed as dot plots (for each animal) and as mean  $\pm$  S.E.M. of 9 mice per group. Statistical analysis was performed by one-way ANOVA followed by Bonferroni's *post hoc* test. \* $p < 0.05$  vs Sham + Vehicle; # $p < 0.05$  vs CLP + Vehicle; & $p < 0.05$  vs ICOS<sup>-/-</sup> + Vehicle.

molecules, and the increase was inhibited by mice treatment with ICOS-Fc (Figures 6E–H).

## Discussion

Currently, most research on sepsis is focused on blocking the initial hyperinflammation, which in turn has resulted in promising outcomes. However, recent reports showed that

both pro- and anti-inflammatory responses occur immediately and simultaneously after the onset of sepsis and most patients who survive this initial hyperinflammatory phase develop an immunosuppressive phase that can progress to late deaths (1, 32 and 33). Among the main causes of death in this immunosuppressive phase, the failure to control a primary infection and/or secondary hospital-acquired infections stands out (34). In the present study we report for the first time



that ICOS-ICOSL axis may play a role in regulation of uncontrolled inflammation and organ injury induced by sepsis and that treatment of septic mice with ICOS-Fc may represent a novel immunomodulatory pharmacological approach that can simultaneously counteract both sepsis-induced hyperinflammation and immunosuppression.

These findings were obtained by evoking polymicrobial sepsis in either WT mice and knockout mice for ICOS, ICOSL and OPN genes. As expected, severe sepsis (score  $\geq 3$ ) was observed in vehicle-treated septic mice, suggesting potential late deaths, since the clinical scoring system is used as a surrogate marker of mortality. This detrimental effect was also associated with low body temperature ( $\sim 27^{\circ}\text{C}$ ), as similarly, hypothermia is another surrogate marker of mortality, as a  $5^{\circ}\text{C}$  decrease over time or  $<30^{\circ}\text{C}$  has also been shown to predict death in CLP-induced septic mice (35). Moreover, septic mice showed liver and kidney damage, displayed by increase of plasma AST/ALT and creatinine/urea levels, respectively, which is in line with the notion that sepsis can cause multiple organ failure including hepatocellular injury and renal dysfunction.

Intriguingly, treatment with ICOS-Fc substantially ameliorated the clinical picture by significantly decreasing all these parameters of sepsis. The effect was specific since no protection was detected following administration of  $F^{119S}$ ICOS-Fc (a mutated form of ICOS-Fc carrying a phenylalanine-to-serine substitution at position 119).

Theoretically, the protective activity of ICOS-Fc might be ascribed to a twofold mechanism, i.e. on the one hand to the inhibition of the endogenous ICOS activity and, on the other hand, to triggering of the endogenous ICOSL. However, the effectiveness of ICOS-Fc not only in WT mice but also in ICOS $^{-/-}$

mice, lacking the endogenous ICOS, strongly suggest that the main protective effect on sepsis is due to triggering of ICOSL, which is in line with previous works showing that ICOSL triggering by ICOS-Fc elicits several anti-inflammatory activities both *in vitro* and *in vivo* (13, 15, 16, 19).

These results are in keeping also with recent findings showing that ICOS-Fc protects against liver damage through a shift of pro-inflammatory monocyte-derived macrophages to an anti-inflammatory phenotype (20). In parallel, the direct renoprotective effect triggered by ICOS-Fc treatment is supported by a recent study showing a key role of ICOSL in preventing early kidney disease, possibly through a selective binding to podocyte  $\alpha\text{v}\beta 3$  integrin, in which ICOSL serves as an  $\alpha\text{v}\beta 3$ -selective antagonist that maintains adequate glomerular filtration (36).

The use of knockout mice highlighted that, in sepsis, a key role may be played by OPN as all the above septic parameters were significantly decreased in OPN $^{-/-}$  mice, so that OPN deficiency mirrored the effect of ICOS-Fc in WT mice. This finding is in line with data showing that, in humans, OPN levels are increased in sepsis (37) and OPN might be involved in the sepsis pathogenesis, possibly by supporting IL-6 secretion (38). Moreover, several reports showed that ICOS-Fc inhibits several proinflammatory activities of OPN *in vitro* and *in vivo* (16, 37, 39 and 40). Our findings are in keeping also with recent data showing that macrophage-derived OPN promotes glomerular injury in an experimental model of inflammatory and progressive kidney disease (41). OPN is a heavily phosphorylated extracellular protein, expressed and secreted by several cell types, including macrophages,



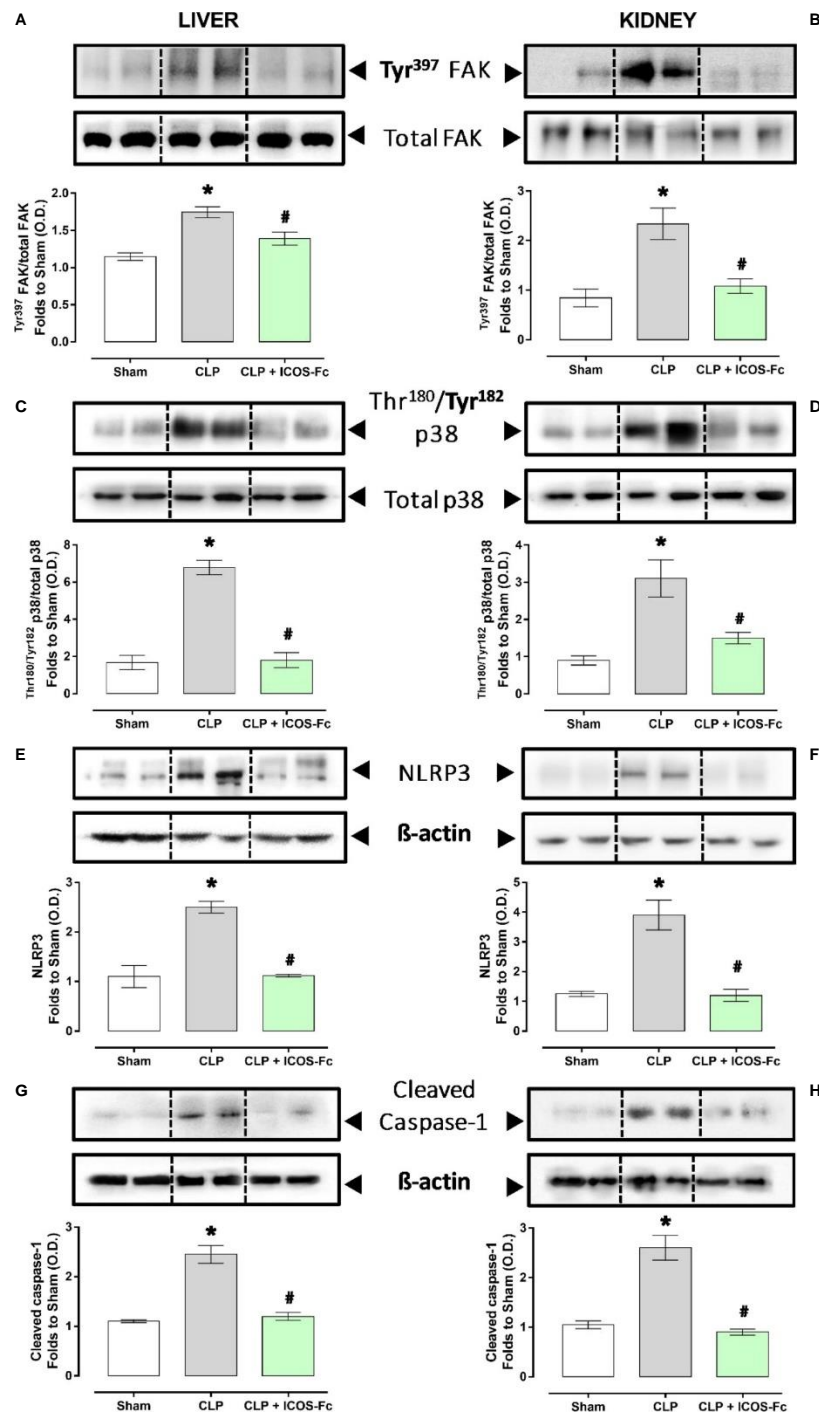


FIGURE 6

Effect of ICOS-ICOSL axis immunomodulation on tissue inflammatory pathways during experimental sepsis. Wild-type mice and/or ICOSL, ICOS and OPN knockout mice were randomly selected to undergo either Sham or CLP surgery. One hour later, mice received once either Vehicle (PBS, 100  $\mu$ L), ICOS-Fc (100  $\mu$ g) or <sup>F119S</sup>ICOS-Fc (100  $\mu$ g) intravenously. At 24 h, liver and kidney samples were harvested, and total proteins were extracted from them. Western blotting analysis for phosphorylation of Tyr<sup>397</sup> on FAK in the liver (A) and kidney (B) were normalized to total FAK; Phosphorylation of Thr<sup>180</sup>/Tyr<sup>182</sup> on p38 in the liver (C) and kidney (D) were normalized to total p38; NLRP3 expression in the liver (E) and kidney (F) were corrected against  $\beta$ -actin and normalized using the Sham related bands; Cleaved caspase-1 expression in the liver (G) and kidney (H) were corrected against  $\beta$ -actin and normalized using the Sham related bands. Densitometric analysis of the bands are expressed as relative optical density (O.D.). Data are expressed as dot plots (for each animal) and as mean  $\pm$  S.E.M of 4-5 mice per group. Statistical analysis was performed by one-way ANOVA followed by Bonferroni's *post hoc* test. \* $p < 0.05$  vs Sham + Vehicle; # $p < 0.05$  vs CLP + Vehicle.

endothelial cells, dendritic cells and T-cells. It can act as a cytokine mediating several biological functions, including cell migration, adhesion, activation of inflammatory cells, and modulation of T cell activation supporting differentiation of proinflammatory type 1 (Th1) and type 17 (Th17) Th cells (42).

Analysis of plasmatic cytokines showed that, in all mouse strains, sepsis was accompanied by increase of IL-1b, IL-6, IL-10, TNF-a and IFN-g. Moreover, increase of TNF-a and, especially, IL-10 was particularly striking in ICOS<sup>-/-</sup> mice, which may point out that ICOS deficiency causes a dysregulation of activation of M1 and M2 macrophages. However, treatment with ICOS-Fc significantly decreased IL-1b and TNF-a in WT mice and IL-1b, IL-6 and IL-10 in ICOS<sup>-/-</sup> mice indicating that ICOS-Fc substantially downmodulates the cytokine storm in sepsis. In OPN<sup>-/-</sup> mice, increase of these cytokines was in general moderate, with a significant decrease of IL-1b and IL-6, in line with the mild sepsis developed by these mice.

Among the main inflammatory pathways activated during sepsis, we report a local (liver and kidney) overactivation of the FAK and p38 MAPK pathways in CLP mice. Previously, we have shown that the FAK pathway mediates inflammation through p38 MAPK and that this inflammatory axis plays a role in exacerbating inflammation (28). Activation of this axis promotes increased expression/secretion of pro-inflammatory cytokines such as TNF-a, IL-6, IL-1b and IL-17, which in turn contribute to the cytokine storm and multiple organ failure (MOF) associated with sepsis (43). Intriguingly, treatment of septic mice with ICOS-Fc significantly attenuated FAK and p38 MAPK phosphorylation, thus reducing their activation during septic insult, with a following impact on the development of the above-mentioned cytokine storm. These findings are in accordance with previous studies focused on tumor cell migration, whose treatment with ICOS-Fc reduces FAK and p38 MAPK activation both *in vitro* and *in vivo* (15, 19). As we and other have recently shown, FAK activation may also affect the overexpression and activation of another peculiar inflammatory pathway, NLRP3 inflammasome complex (28, 44). Thus, we wondered here whether ICOS-Fc could also infer with this cross-talk mechanism linking FAK to

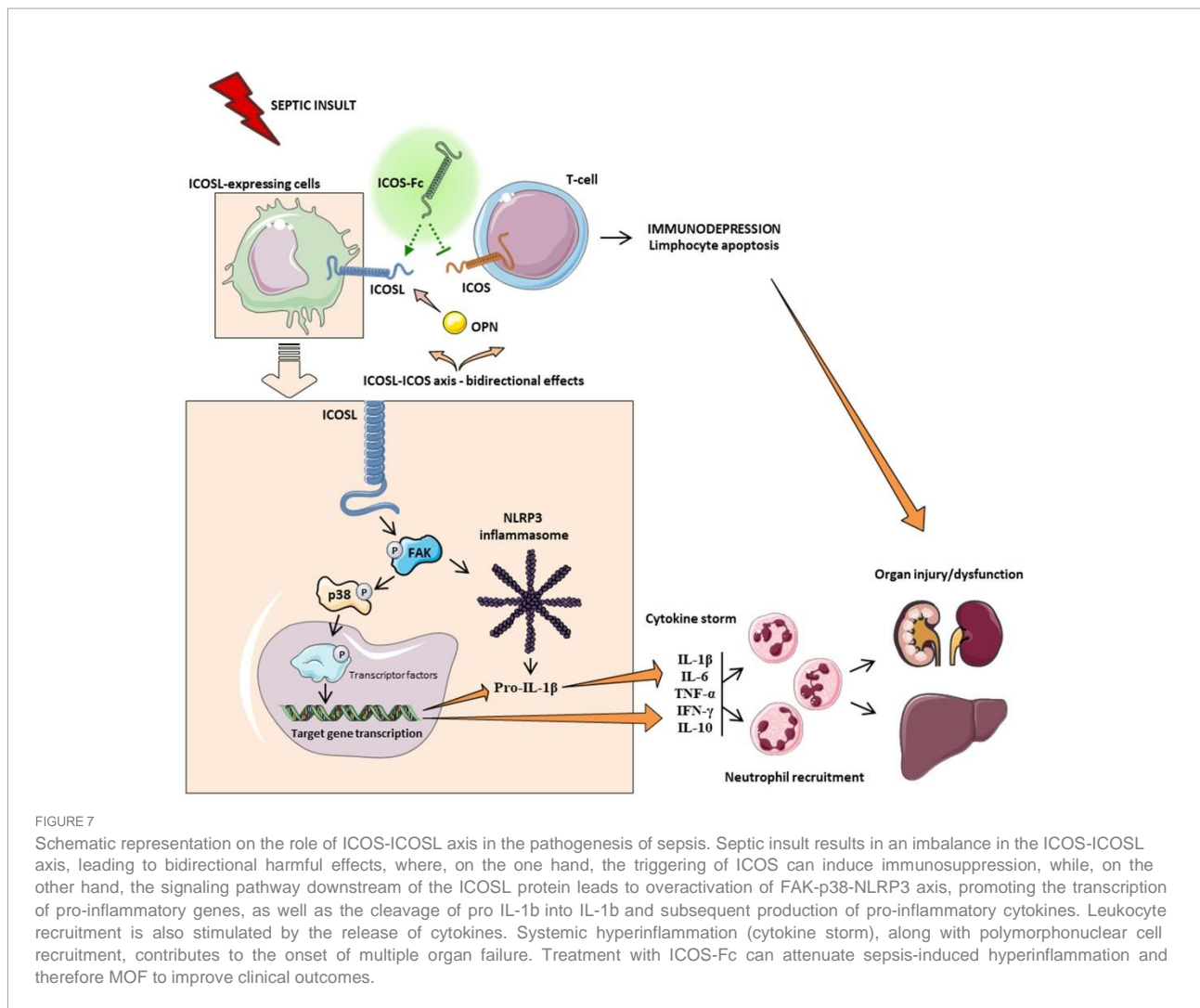
NLRP3 activation within the septic context. We report here that experimental sepsis led to an overactivation of the NLRP3 complex and consequent activation of its downstream mediator caspase-1, which were significantly reduced by treatment with ICOS-Fc, thus leading to reduced systemic release of IL-1b. In addition to the impact on the aforementioned inflammatory pathways, ICOS-Fc administration seems to directly affect leukocyte migration in CLP mice, as documented by the changes in MPO activity, a well-known biomarker of neutrophil infiltration, in both liver

and kidney homogenates (45). Specifically, we documented that the sepsis-induced increase in MPO activity in renal tissues, was significantly counteracted by ICOS-Fc treatment. This effect, on the other hand, was absent when CLP mice were treated with F119S-ICOS-Fc. Intriguingly, increased MPO activity was recorded in liver homogenates from septic mice, regardless of drug treatment or genetic intervention, when compared to Sham mice. Despite ICOS-Fc has been shown to reduce the migration of polymorphonuclear cells into inflamed tissues (15), these discrepant events observed in liver and kidney tissue may be the result of different levels of ICOSL expression. This finding corroborates a previous study reporting that hepatocytes did not express ICOSL, when compare to other organs, such as the kidney (46). Thus, suggesting that the hepatic protection induced by ICOS-Fc in septic mice is mainly due to a local and systemic resolution of inflammation rather than a reduction in leukocyte infiltration. A schematic representation summarizing the role of ICOS-ICOSL axis in the pathogenesis of sepsis and the protective effects of ICOS-Fc following sepsis-induced multiple organ failure is shown in Figure 7.

Despite the originality of our findings, we are aware of several limitations of our study, including the lack of extension of these findings to other important functional organs related to MOF during sepsis, such as the lungs and the cardiac tissue, along with the lack of analysis suggestive of the direct effect of ICOS-Fc treatment in preventing immunosuppression. Albeit the *in vivo* protocol described here is in accordance with the main recommendations provided by MQTiPSS consensus guidelines (27), we are not authorized to perform a survival study to assess the long-term effect of ICOS-Fc due to ethical reasons. Thus, further studies are needed to extend the clinical relevance of our findings as well as to gain a better insight into the safety profile of the proposed drug treatment.

## Conclusions

In conclusion, we demonstrate here, for the first time, that the ICOS-ICOSL axis plays a crucial role in the development of systemic inflammation and organ damage induced by a clinically relevant sepsis model. These findings were confirmed by an exacerbation of septic injury in mice knockout for the ICOS and ICOSL genes. Interestingly, we also documented its druggability by showing protection when ICOS-Fc, a recombinant protein which act as an antagonist of ICOS and an agonist of ICOSL, was administered during sepsis. The beneficial effects of this innovative pharmacological approach are likely due to a potential cross-talk mechanisms involving the FAK-p38-NLRP3 inflammasome axis. A greater



understanding of the molecular basis of ICOS-Fc-mediated effects is needed to harness its actions as a potentially powerful immunomodulatory tool for counteracting inflammation and organ injury in sepsis.

## Data availability statement

The raw data supporting the conclusions of this article will be made available by the authors, without undue reservation.

## Ethics statement

The animal study was reviewed and approved by Ethical committee OPBA University of Turin and Italian Ministry of Health, Italy.

## Author contributions

GA, CD, UD, and MC conceived and designed the experiments. GA, IS, EA, CM, RM, EP, GE, DC, and NC performed the experiments. GA, EA, CM, RM, IB, EB, CG, NC, MA, DF, CT, CC, CD, UD, and MC analyzed the data. GA, CD, UD, CT, and MC, writing - review and editing. All authors have read and agreed to the published version of the manuscript.

## Funding

The Università degli Studi di Torino has supported and funded this work (Ricerca Locale 2020 and 2021) and by the Associazione Italiana Ricerca sul Cancro (IG20714), Milan Italy.

## Acknowledgments

Parts of the **Figure 7** were drawn by using pictures from Servier Medical Art. Servier Medical Art by Servier is licensed

under a Creative Commons Attribution 3.0 Unported License (<https://creativecommons.org/licenses/by/3.0/>).

## Conflict of interest

The authors declare that the research was conducted in the absence of any commercial or financial relationships that could be construed as a potential conflict of interest.

## References

- Hotchkiss RS, Monneret G, Payen D. Sepsis-induced immunosuppression: From cellular dysfunctions to immunotherapy. *Nat Rev Immunol* (2013) 13:862–74. doi: 10.1038/nri3552
- Rudd KE, Johnson SC, Agesa KM, Shackelford KA, Tsoi D, Kievlan DR, et al. Global, regional, and national sepsis incidence and mortality, 1990 – 2017 : analysis for the global burden of disease study. *Lancet* (2020) 395:200–11. doi: 10.1016/S0140-6736(19)32989-7
- Hutloff A, Dittrich AM, Beier KC, Eljaschewitsch B, Kraft R, Anagnostopoulos I, et al. ICOS is an inducible T-cell co-stimulator structurally and functionally related to CD28. *Nature* (1999) 100:263–6. doi: 10.1038/16717
- Yoshinaga SK, Whoriskey JS, Khare SD, Sarmiento U, Guo J, Horan T, et al. T-Cell co-stimulation through B7RP-1 and ICOS. *Nature* (1999) 1:827–32. doi: 10.1038/45582
- Swallow MM, Wallin JJ, Sha WC. B7h, a novel costimulatory homolog of B7.1 and B7.2, is induced by TNFa. *Immunity* (1999) 11:423–32. doi: 10.1016/s1074-7613(00)80117-x
- Möhle P, Hirschberger S, Hinske LC, Briegel J, Hübner M, Weis S, et al. MicroRNAs 143 and 150 in whole blood enable detection of T-cell immunoparalysis in sepsis. *Mol Med* (2018) 24:1–14. doi: 10.1186/s10020-018-0056-z
- Menéndez R, Méndez R, Almansa R, Ortega A, Alonso R, Suescun M, et al. Simultaneous depression of immunological synapse and endothelial injury is associated with organ dysfunction in community-acquired pneumonia. *J Clin Med* (2019) 8:1–10. doi: 10.3390/jcm8091404
- Burmeister Y, Lischke T, Dahler AC, Mages HW, Lam K-P, Coyle AJ, et al. ICOS controls the pool size of effector-memory and regulatory T cells. *J Immunol* (2008) 180:774–82. doi: 10.4049/jimmunol.180.2.774
- Chen Q, Mo L, Cai X, Wei L, Xie Z, Li H, et al. ICOS signal facilitates Foxp3 transcription to favor suppressive function of regulatory T cells. *Int J Med Sci* (2018) 15:666–73. doi: 10.7150/ijms.23940
- Luan Y, Yin C, Qin Q, Dong N, Zhu X, Sheng Z. Effect of regulatory T cells on promoting apoptosis of T lymphocyte and its regulatory mechanism in sepsis. *J Interf Cytokine Res* (2015) 35:969–80. doi: 10.1089/jir.2014.0235
- Saito K, Wagatsuma T, Toyama H, Ejima Y, Hoshi K, Shibusawa M, et al. Sepsis is characterized by the increases in percentages of circulating CD4 + CD25 + regulatory T cells and plasma levels of soluble CD25. *J Exp Med* (2008) 216:61–8. doi: 10.1620/tjem.216.61
- Leng F, Liu J, Liu Z, Yin J, Qu H-P. Increased proportion of CD4 d CD25 d Foxp3 d regulatory T cells during early-stage sepsis in ICU patients. *J Microbiol Immunol Infect* (2013) 46:338–44. doi: 10.1016/j.jmii.2012.06.012
- Occhipinti S, Dianzani C, Chiochetti A, Boggio E, Clemente N, Gigliotti CL, et al. Triggering of B7h by the ICOS modulates maturation and migration of monocyte-derived dendritic cells. *J Immunol* (2013) 190:1125–34. doi: 10.4049/jimmunol.1201816
- Lund SA, Giachelli CM. The role of osteopontin in inflammatory processes. *J Cell Commun Signal* (2009) 3:311–22. doi: 10.1007/s12079-009-0068-0
- Dianzani C, Minelli R, Mesturini R, Chiochetti A, Barrera G, Boscolo S, et al. B7h triggering inhibits umbilical vascular endothelial cell adhesiveness to tumor cell lines and polymorphonuclear cells. *J Immunol* (2010) 185:3970–9. doi: 10.4049/jimmunol.0903269
- Raineri D, Dianzani C, Cappellano G, Maione F, Baldanzi G, Iacobucci I, et al. Osteopontin binds ICOSL promoting tumor metastasis. *Commun Biol* (2020) 3:1–15. doi: 10.1038/s42003-020-01333-1
- Di Niro R, Ziller F, Florian F, Crovella S, Stebel M, Bestagno M, et al. Construction of miniantibodies for the *in vivo* study of human autoimmune

## Publisher's note

All claims expressed in this article are solely those of the authors and do not necessarily represent those of their affiliated organizations, or those of the publisher, the editors and the reviewers. Any product that may be evaluated in this article, or claim that may be made by its manufacturer, is not guaranteed or endorsed by the publisher.

- diseases in animal models. *BMC Biotechnol* (2007) 7:1–10. doi: 10.1186/1472-6750-7-46
- Gigliotti CL, Boggio E, Clemente N, Shivakumar Y, Toth E, Sblattero D, et al. ICOS-ligand triggering impairs osteoclast differentiation and function *In vitro* and *In vivo*. *J Immunol* (2016) 197:3905–16. doi: 10.4049/jimmunol.1600424
- Dianzani C, Minelli R, Gigliotti CL, Occhipinti S, Giovarelli M, Conti LM, et al. B7h triggering inhibits the migration of tumor cell lines. *J Immunol* (2014) 192:4921–31. doi: 10.4049/jimmunol.1300587
- Ramavath NN, Gadipudi LL, Provera A, Gigliotti LC, Boggio E, Bozzola C, et al. Inducible T-cell costimulator mediates Lymphocyte/Macrophage interactions during liver repair. *Front Immunol* (2021) 12:786680. doi: 10.3389/fimmu.2021.786680
- Stoppa I, Gigliotti CL, Clemente N, Pantham D, Dianzani C, Monge C, et al. ICOSL stimulation by ICOS-fc accelerates cutaneous wound healing *In vivo*. *Int J Mol Sci* (2022) 23:1–12. doi: 10.3390/ijms23137363
- O'Sullivan AW, Wang JH, Redmond HP. NF- $\kappa$ B and P38 MAPK inhibition improve survival in endotoxin shock and in a cecal ligation and puncture model of sepsis in combination with antibiotic therapy. *J Surg Res* (2009) 152:46–53. doi: 10.1016/j.jss.2008.04.030
- Cornelius DC, Travis OK, Tramel RW, Borges-Rodríguez M, Baik CH, Greer M, et al. NLRP3 inflammasome inhibition attenuates sepsis-induced platelet activation and prevents multi-organ injury in cecal-ligation puncture. *PLoS One* (2020) 15:1–15. doi: 10.1371/journal.pone.0234039
- Lee S, Nakahira K, Dalli J, Siempos II, Norris PC, Colas RA, et al. NLRP3 inflammasome deficiency protects against microbial sepsis *via* increased lipoxin B4 synthesis. *Am J Respir Crit Care Med* (2017) 196:713–26. doi: 10.1164/rccm.201604-0892OC
- Chen X, Zhao Y, Wang X, Lin Y, Zhao W, Wu D, et al. FAK mediates LPS-induced in flammatory lung injury through interacting TAK1 and activating TAK1-NF  $\kappa$  b pathway. *Cell Death Differ* (2022) 13:1–12. doi: 10.1038/s41419-022-05046-7
- du Sert NP, Hurst V, Ahluwalia A, Alam S, Avey MT, Baker M, et al. The arrive guidelines 2.0: Updated guidelines for reporting animal research. *PLoS Biol* (2020) 18:1–12. doi: 10.1371/journal.pbio.3000410
- Osuchowski MF, Ayala A, Bahrami S, Bauer M, Boros M, Cavaillon J-M, et al. Minimum quality threshold in pre-clinical sepsis studies (mqtipss): An international expert consensus initiative for improvement of animal modeling in sepsis. *Shock* (2018) 50:377–80. doi: 10.1097/SHK.0000000000001212
- Alves GF, Aimaretti E, Einaudi G, Mastrocola R, Oliveira JG, Collotta D, et al. Pharmacological inhibition of FAK-Pyk2 pathway protects against organ damage and prolongs the survival of septic mice. *Front Immunol* (2022) 13:837180. doi: 10.3389/fimmu.2022.837180
- Kovalski V, Prestes AP, Oliveira JG, Alves GF, Colarites D, El Mattos J, et al. Protective role of cGMP in early sepsis. *Eur J Pharmacol* (2017) 807:174–81. doi: 10.1016/j.ejphar.2017.05.012
- Nandra KK, Collino M, Rogazzo M, Fantozzi R, Patel NSA, Thiemermann C. "Pharmacological preconditioning with erythropoietin attenuates the organ injury and dysfunction induced in a rat model of hemorrhagic shock." *DMM Dis Model Mech* (2013) 6:701–9. doi: 10.1242/dmm.011353
- Faul F, Erdfelder E, Lang A-G, Buchner A. G\*Power 3: A flexible statistical power analysis program for the social, behavioral, and biomedical sciences. *Behav Res Methods* (2007) 39:175–91. doi: 10.3758/bf03193146
- Tsirigotis P, Chondropoulos S, Gkirkas K, Meletiadiis J, Dimopoulou I. "Balanced control of both hyper and hypo-inflammatory phases as a new treatment paradigm in sepsis." *J Thorac Dis* (2016) 8:E312–6. doi: 10.21037/jtd.2016.03.47
- Boomer JS, To K, Chang KC, Takasu O, Osborne DF, Walton AH, et al. Immunosuppression in patients who die of sepsis and multiple organ failure. *J Am Med Assoc* (2011) 306:2594–605. doi: 10.1001/jama.2011.1829

34. Otto GP, Sossdorf M, Claus RA, Rödel J, Menge K, Reinhart K, et al. The late phase of sepsis is characterized by an increased microbiological burden and death rate. *Crit Care* (2011) 15:1–8. doi: 10.1186/cc10332
35. Mai SHC, Sharma N, Kwong AC, Dwivedi DJ, Khan M, Grin PM, et al. Body temperature and mouse scoring systems as surrogate markers of death in cecal ligation and puncture sepsis. *Intensive Care Med Exp* (2018) 6:1–14. doi: 10.1186/s40635-018-0184-3
36. Koh KH, Cao Y, Mangos S, Tardi NJ, Dande RR, Lee HW, et al. Nonimmune cell-derived ICOS ligand functions as a renoprotective  $\alpha\text{v}\beta 3$  integrin-selective antagonist. *J Clin Invest* (2019) 129:1713–26. doi: 10.1172/JCI123386
37. Castello LM, Baldrighi M, Molinari L, Salmi L, Cantaluppi V, Vaschetto R, et al. The role of osteopontin as a diagnostic and prognostic biomarker in sepsis and septic shock. *Cells* (2019) 8:1–12. doi: 10.3390/cells8020174
38. Uchibori T, Matsuda K, Shimodaira T, Sugano M, Uehara T, Honda T. IL-6 trans-signaling is another pathway to upregulate osteopontin. *Cytokine* (2017) 90:88–95. doi: 10.1016/j.cyt.2016.11.006
39. Hirano Y, Aziz M, Yang W-L, Wang Z, Zhou M, Ochani M, et al. Neutralization of osteopontin attenuates neutrophil migration in sepsis-induced acute lung injury. *Crit Care* (2015) 19:1–15. doi: 10.1186/s13054-015-0782-3
40. Fortis S, Khadaroo RG, Haitsma JJ, Zhang H. Osteopontin is associated with inflammation and mortality in a mouse model of polymicrobial sepsis. *Acta Anaesthesiol Scand* (2015) 59:170–5. doi: 10.1111/aas.12422
41. Trostel J, Truong LD, Roncal-Jimenez C, Miyazaki M, Miyazaki-Anzai S, Kuwabara M, et al. Disease different effects of global osteopontin and macrophage osteopontin in glomerular injury. *Am J Physiol - Ren Physiol* (2018) 315:F759–68. doi: 10.1152/ajprenal.00458.2017
42. Boggio E, Dianzani C, Gigliotti CL, Soluri MF, Clemente N, Cappellano G, et al. Thrombin cleavage of osteopontin modulates its activities in human cells *in vitro* and mouse experimental autoimmune encephalomyelitis *in vivo*. *J Immunol Res* (2016) 2016:1–13. doi: 10.1155/2016/9345495
43. Chaudhry H, Zhou J, Zhong Y, Ali MM, Mcguire F, Nagarkatti PS, et al. Role of cytokines as a double-edged sword in sepsis. *In Vivo (Brooklyn)* (2013) 27:669–84.
44. Chung IC, OuYang C-N, Yuan S-N, Li H-P, Chen J-T, Shieh H-R, et al. Pyk2 activates the NLRP3 inflammasome by directly phosphorylating ASC and contributes to inflammasome-dependent peritonitis. *Sci Rep* (2016) 6:1–13. doi: 10.1038/srep36214
45. Yu H, Liu Y, Wang M, Restrepo RJ, Wang D, Kalogeris TJ, et al. Myeloperoxidase instigates proinflammatory responses in a cecal ligation and puncture rat model of sepsis. *Am J Physiol - Hear Circ Physiol* (2020) 319:H705–21. doi: 10.1152/ajpheart.00440.2020
46. Wahl C, Bochtler P, Chen L, Schirmbeck R, Reimann J. B7-H1 on hepatocytes facilitates priming of specific CD8 T cells but limits the specific recall of primed responses. *Gastroenterology* (2008) 135:980–8. doi: 10.1053/j.gastro.2008.05.076

## Conclusions

The present thesis shows that ICOS-mediated triggering of ICOSL plays a role in the repair phase of inflammation and that boosting this triggering using ICOS-Fc might be exploited to reverse pathologic short circuits of inflammation such as those developing in sepsis and tumors. These short circuits may involve unbalance of the molecular and functional interactions between ICOS, OPN and ICOSL.

A key finding suggesting this possibility was that ICOS-Fc increases the physiologic angiogenesis of wound healing whereas it inhibits the pathologic angiogenesis of tumors. This discrepancy might be ascribed to involvement of different angiogenic mechanisms in the two setting and, possibly, to a differential involvement of OPN, participating to the ICOS/ICOSL/OPN network and playing an important role in tumor angiogenesis, compared to other angiogenic factors such as VEGF playing a key role in wound healing-associated angiogenesis.

In wound healing, triggering of ICOSL by instillation of ICOS-Fc into the wound bed favors tissue repair *in vivo*. These results extend those obtained by Maeda et al. [1] showing that wound healing is delayed in ICOS<sup>-/-</sup>, ICOSL<sup>-/-</sup>, or ICOS/ICOSL<sup>-/-</sup> mice, possibly due to defective production of IL-4, IL-10, and, especially, IL-6 at the wound site. Since this defective repair was overcome by adoptive transfer of wild-type T cells (expressing ICOS) in ICOS<sup>-/-</sup> but not ICOSL<sup>-/-</sup> mice, the healing defect in KO mice could be ascribed to the impaired development of T helper type 2 cells due to the lack of ICOS-mediated co-stimulation of T cells. Even though our findings confirm that wound healing is defective in mice lacking ICOS or ICOSL, the observation that ICOSL stimulation by ICOS-Fc is sufficient to accelerate the early phases of the healing process underscores the importance of ICOSL in ICOS/ICOSL mediated tissue repair. Indeed, enhanced wound healing in response to ICOS-Fc treatment is readily apparent in both wild-type and ICOS<sup>-/-</sup> mice, but not in mice lacking ICOSL, which indicates that this effect is not due to the inhibition of ICOS activity in T cells, but it is instead caused by ICOSL-mediated “reverse signaling” in other cell types. The fact that ICOS-Fc treatment is effective also in immunodeficient NSG mice confirms that T cells are not involved in ICOS-Fc-induced wound healing. Moreover, the lack of effect in ICOSL<sup>-/-</sup> mice rules out possible confounding effects due to the potential interaction of ICOS-Fc with Fc receptors. In conclusion, this work shows that ICOSL plays a key role in wound healing and that triggering of ICOSL by ICOS-Fc favors healing by increasing angiogenesis and the recruitment of fibroblasts and reparative

macrophages. Therefore, ICOS-Fc and other molecules capable of triggering ICOSL might be exploited to improve wound closure in patients with impaired tissue repair.

In sepsis, treatment with ICOS-Fc ameliorates the clinical picture and decreases organ damage. These findings were confirmed by exacerbation of septic injury in knockout mice for the ICOS and ICOSL genes. The beneficial effects of this innovative pharmacological approach are likely due to a potential cross-talk mechanisms involving the FAK-p38-NLRP3 inflammasome axis. A greater understanding of the molecular basis of ICOS-Fc-mediated effects is needed to harness its actions as a potentially powerful immunomodulatory tool for counteracting inflammation and organ injury in sepsis.

In multiple myeloma, ICOS and ICOSL are expressed on the tumor cells and sICOSL and sICOS serum levels correlate with several markers of tumour burden, and high serum levels of sICOS are an independent prognostic factor of shorter survival in patients with plasma cell disorders. However, no data indicate correlations of the osteolytic lesions. The possibility that ICOS/ICOSL signalling plays a role in MM development is supported by our *in vivo* experiments showing that treatment with ICOS-Fc significantly inhibits the growth of MOPC-21<sup>ICOSL</sup> tumours in mice. This effect may be due to inhibition of tumour angiogenesis, as documented by the decreased tumour microvessel density displayed by tumours from mice treated with ICOS-Fc. However, ICOS-Fc might also exert direct effects on myeloma cells by inhibiting their migration, since ICOS-Fc inhibits migration of ICOSL<sup>+</sup> myeloma cells. Moreover, ICOS-Fc might boost the anti-tumour immune response and overcome immune evasion, acting as an immune checkpoint antagonist, as suggested by our previous work on different tumour types [2,3] and several other works showing that inhibition of ICOS function on T cells impairs regulatory T-cell activity [4]. Given their ubiquitous distribution within the tumour microenvironment and neoplastic cell surface, ICOS and ICOSL may represent attractive therapeutic targets for MM [4].

In melanoma, we found that ICOS-Fc may be effective in combination therapies with cytostatic agents (TMZ), and a kinase inhibitor (SOR) when loaded in nanoemulsions used for total parenteral nutrition. Results showed that this therapy was effective in inhibiting the growth of mouse melanoma *in vivo* by exerting a potent anti-angiogenic effect and complex immunoregulatory activity. This combination approach allows to substantially decrease the drug dose needed to obtain a therapeutic effect. Use of ICOS-Fc is innovative since it works as both an immunostimulatory and antiangiogenic agent, and therefore would be optimally synergistic with the other drugs loaded in the nanoparticles. This approach might represent a potential

future tool that can merge immunotherapy, targeted therapy, and chemotherapy into one safe delivery vehicle to improve therapeutic efficacy, without increasing the incidence of the adverse side effects that are typical of combination therapies.

#### *Future Perspectives*

The work reported in this thesis may be supported with additional experiments with the aim to better understand the mechanisms activated by the ICOS/OPN/ICOSL system during the wound healing process. For this aim, the wound healing experiment performed on WT mice can be repeated by comparing mice KO for ICOS, OPN and ICOSL genes and dual KO mice (ICOS/OPN KO mice, ICOSL/OPN KO and ICOS/ICOSL KO) and comparing the effects of local treatment with ICOS-Fc or with OPN.

The *in vivo* experiments in multiple myeloma were quite preliminary and need to be improved using a more relevant model in which myeloma cells grow inside the bone marrow and induce the typical osteolytic lesions. These models should include the possibility to monitor the tumor growth and osteolytic lesions by *in vivo* imaging and to increase the bone-targeting ability of the drug-loaded nanoparticles.



## References

- 1- Maeda, S.; Fujimoto, M.; Matsushita, T.; Hamaguchi, Y.; Takehara, K.; Hasegawa, M. Inducible costimulator (ICOS) and ICOS ligand signaling has pivotal roles in skin wound healing via cytokine production. *Am. J. Pathol.* **2011**, 179, 2360–2369.
- 2- Clemente, N.; Boggio, E.; Gigliotti, L.C.; Raineri, D.; Ferrara, B.; Miglio, G.; Argenziano, M.; Chiocchetti, A.; Cappellano, G.; Trotta, F.; et al. Immunotherapy of experimental melanoma with ICOS-Fc loaded in biocompatible and biodegradable nanoparticles. *J. Control. Release* **2020**, 320, 112–124.
- 3- Iwata, R.; Lee, J.H.; Hayashi, M.; Dianzani, U.; Ofune, K.; Maruyama, M.; Oe, S.; Ito, T.; Hashiba, T.; Yoshimura, K.; Nonaka, M.; Nakano, Y.; Norian, L.; Nakano, I.; Asai, A. ICOSLG-mediated regulatory T-cell expansion and IL-10 production promote progression of glioblastoma. *Neuro Oncol*, **2020**; 22(3), 333–44.
- 4- Amatore, F.; Laurent, G. L.; Olive, D. Role of inducible co-stimulator (ICOS) in cancer immunotherapy. *Expert Opin Biol Ther.* **2020**, 20(2), 141–50.

## Acknowledgements

Three years and half ago I thought my academic studies were finished with my master's degree in medical biotechnologies, but I was wrong. That summer I had the opportunity to enter in a PhD program and by writing this part of my thesis I'm ending this chapter of my life. This is the end of a journey that made me a scientist, overstepping limits I was not even able to see at the beginning.

Here I want to thank my colleagues Elena, Luca and Deepika with whom I shared most of the time in laboratory; especially I want to thank Professor Umberto Dianzani that followed me during my whole PhD. I thank my tutors Professor Marisa Gariglio and Professor Emanuele Albano for their availability. I also thank all the students I had the pleasure to follow for their internship in our laboratory, and I wish them a bright future.

I thank my family, my parents Laura and Luca, my sister Licia and my girlfriend Ilaria for their support during these last 3 years.

*"All we have to decide is what to do with the time that is given us."*

*J.J.R. Tolkien.*